Review article **Doi:** 10.63823/2026040002

2D/2D S-Scheme Heterojunction Photocatalysts: Fundamentals, Engineering Modification Strategies, and Applications

Jungan Ding [a], Xinghua Wen[a], Ziyang Ke[a],Shijie Li[b*], Rongchen Shen[a*], Xiaobo Chen[c*],Xin Li[a*]

[a] Institute of Biomass Engineering, Key Laboratory for Biobased Materials and Energy of Ministry of Education, College of Materials and Energy, South China Agricultural University, Guangzhou 510642, China; [b] Key Laboratory of Health Risk Factors for Seafood of Zhejiang Province, National Engineering Research Center for Marine Aquaculture, College of Marine Science and Technology, Zhejiang Ocean University, Zhoushan 316022, China; [c] Department of Chemistry, University of Missouri-Kansas City, MO 64110, USA

Abstract Two-dimensional/two-dimensional (2D/2D) S-scheme heterojunctions have emerged as promising photocatalytic platforms due to their intimate face-to-face interfaces, large specific surface areas, shortened charge-migration pathways, and strong interfacial built-in electric fields. The S-scheme charge-transfer mechanism selectively recombines low-energy carriers while preserving highly reductive electrons and strongly oxidative holes, enabling efficient charge separation without compromising redox capability. This review summarizes recent progress in 2D/2D S-scheme heterojunction photocatalysts, focusing on charge-transfer mechanisms, band-alignment requirements, structural merits, and design principles. Representative construction strategies—including mixing-assisted assembly, surface chemical regulation, and in situ growth—are discussed, along with key characterization techniques for probing interfacial structures and validating S-scheme charge transfer, such as electron microscopy, X-ray photoelectron spectroscopy, Kelvin probe force microscopy, electron paramagnetic resonance, in

* Corresponding authors E-mail: lishijie@zjou.edu.cn(Shijie Li), shenrongchenscau@163.com (Rongchen Shen), chenxiaobo@umkc.edu(Xiaobo Chen), Xinli@scau.edu.cn(Xin Li)

Received: 30 Apr, 2026 Revised: 10 Jun, 2026 Accepted 3 July, 2026

situ irradiated XPS, transient spectroscopy, and density functional theory calculations. We further review recent modification strategies—including multidimensional heterointerface construction, interfacial bonding, elemental doping, defect engineering, cocatalyst engineering, single-atom regulation, interfacial strain and facet engineering—in terms of their effects on charge separation, redox activity, and surface reaction kinetics. Finally, applications in H_2 evolution, CO_2 reduction, pollutant degradation, and H_2O_2 production are summarized, and key challenges as well as future design directions are outlined.

Keywords: 2D/2D S-scheme heterojunction; photocatalysis; environmental purification; interfacial engineering; energy conversion

1. Introduction

With the rapid development of society and the increasing demand for sustainable energy, energy shortages and environmental pollution have become two pressing global challenges.[1,2] In this context, semiconductor photocatalysis has attracted considerable attention as a promising strategy for solar-energy conversion and environmental remediation.[2,3,4,5] This technology is not only capable of converting solar energy into utilizable fuels[6,7], but also achieves efficient pollutant degradation and waste reduction.[8,9] Owing to its dual potential in energy conversion and environmental purification, photocatalysis has emerged as an important frontier in contemporary research.[10,11]

The overall efficiency of semiconductor photocatalysis is governed by several key processes, including light harvesting, charge-carrier separation and transport, surface reaction kinetics, and the thermodynamic driving force for redox reactions.[1,12,13] However, single-component photocatalysts often fail to optimize these factors simultaneously. In particular, extending the light-absorption range generally requires a narrow band gap, whereas maintaining strong redox power demands a more negative conduction-band (CB) potential and a more positive valence-band (VB) potential, which are typically associated with a wider band gap.[14,15] In addition, the rapid recombination of photogenerated electrons and holes further limits charge utilization and overall photocatalytic efficiency.[16,17] Therefore, developing rational photocatalyst architectures that can simultaneously promote charge separation and preserve sufficient redox driving force remains a

central challenge in this field.[18,19,20]

Constructing semiconductor heterojunctions has been widely regarded as an effective strategy to overcome the intrinsic limitations of single-component photocatalysts.[11,21,22] Nevertheless, conventional heterojunction systems still suffer from several inherent drawbacks. Type-II heterojunctions can promote spatial charge separation, but this charge-transfer pathway usually occurs at the expense of redox capability.[23,24] Traditional Z-scheme heterojunctions can retain high-energy charge carriers for surface redox reactions; however, their practical implementation is frequently restricted by complicated structural design, possible interfacial transport barriers, and difficulties in unambiguously verifying the charge-transfer pathway.[25,26] These issues have stimulated the development of more advanced heterojunction models capable of integrating efficient charge separation with strong redox capacity.

In this context, S-scheme heterojunctions have emerged as an advanced charge-transfer model for high-efficiency photocatalysis.[27,28] By coupling a reduction photocatalyst with an oxidation photocatalyst, S-scheme systems provide a promising route to reconcile kinetically favorable charge separation with thermodynamically favorable redox reactions.[29,30] Since the performance of S-scheme systems is highly dependent on interfacial charge transfer, the structural configuration and interfacial quality of the coupled components are crucial for realizing their full photocatalytic potential. Accordingly, 2D/2D architectures have attracted increasing attention as ideal platforms for constructing S-scheme heterojunctions, because their extended face-to-face contact provides a favorable structural basis for strong interfacial coupling and efficient charge transfer.[31,32,33]

Despite these advantages, several critical challenges remain in the practical development of 2D/2D S-scheme heterojunction photocatalysts.[34,35] First, the controllable fabrication of stable, intimate, and low-defect 2D/2D interfacial structures remains a major bottleneck, thereby limiting interfacial charge transport and structural/catalytic stability. Second, definitive verification of the S-scheme charge-transfer mechanism remains challenging, because enhanced photocatalytic activity alone cannot provide direct evidence for the proposed charge-migration pathway. Third, the intrinsic relationships among material selection, interfacial configuration, built-in electric field, charge-transfer behavior, and photocatalytic performance have not yet been fully elucidated. Furthermore, generally accepted evaluation criteria and systematic design principles are still lacking, which hinders the further development of this emerging field.

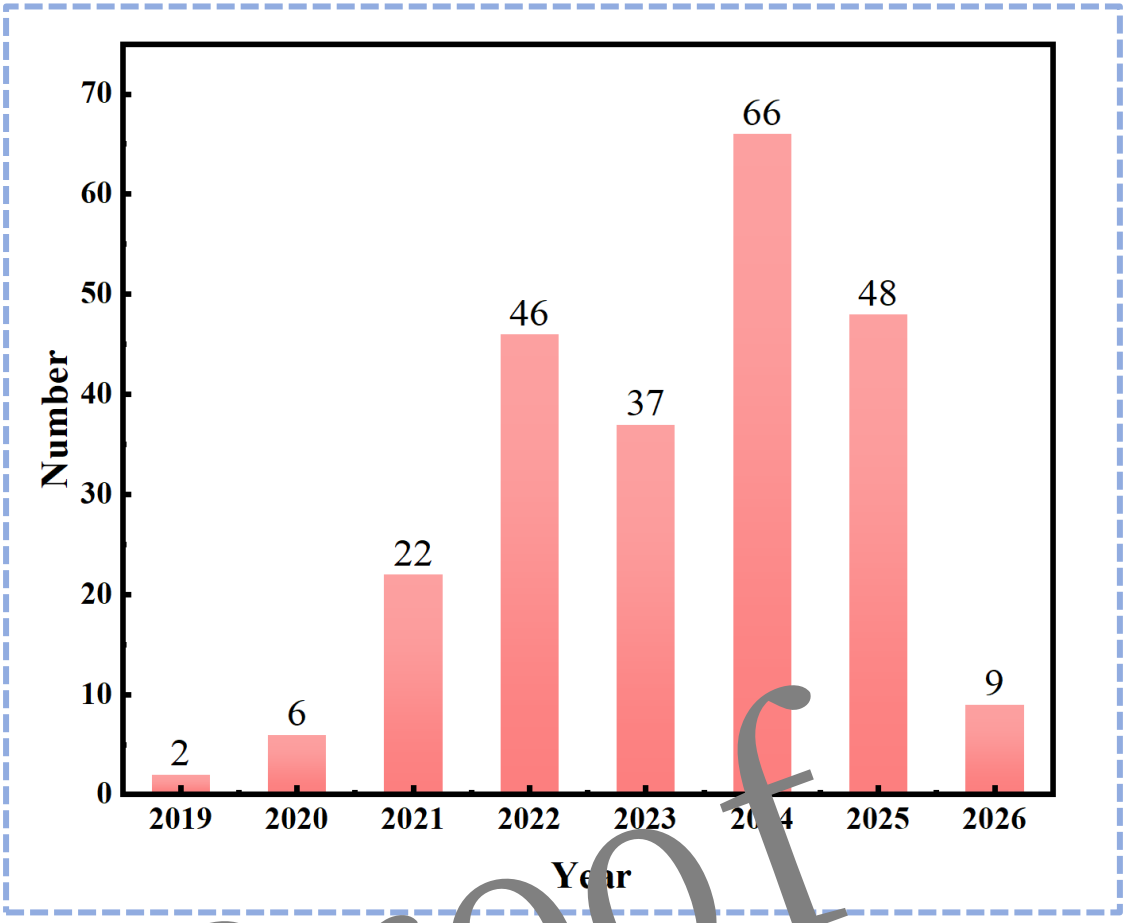

Fig 1. Number of publications recorded over the last decade with the Topic "2D/2D*or two-dimensional/two-dimensional*or nanosheet* and "S-scheme heterojunction* or step-scheme heterojunction*" (Only studies explicitly reporting 2D/2D S-scheme heterojunction photocatalytic systems were included after manual screening.) Source: Web of Science Core Collection (accessed on 5 June 2026）

In this review, recent advances in 2D/2D S-scheme heterojunction photocatalysts are systematically summarized, with particular emphasis on their design principles, interfacial construction, mechanism verification, performance regulation, and photocatalytic applications. The fundamental basis of 2D/2D S-scheme heterojunctions is first discussed, including their theoretical evolution, structural characteristics, charge-transfer mechanisms, design criteria, and representative material systems. Subsequently, synthetic strategies for constructing high-quality 2D/2D interfaces are summarized, followed by a discussion of key characterization techniques for identifying interfacial structures and verifying S-scheme charge-transfer pathways. Recent performance-enhancement strategies are then reviewed, with emphasis on their roles in regulating charge transport, redox ability, and surface reaction kinetics. Representative photocatalytic applications, including H_2 evolution, CO_2 reduction, pollutant degradation, and H_2O_2 production, are further highlighted. Finally, current challenges and future perspectives are

discussed to provide guidance for the rational design and further development of high-performance 2D/2D S-scheme heterojunction photocatalysts.

2. Fundamentals of S-scheme Heterojunctions

The rational design of 2D/2D S-scheme heterojunction photocatalysts requires a systematic understanding of photocatalytic fundamentals, interfacial charge-transfer mechanisms, structural characteristics, and material-selection principles. The photocatalytic performance of these systems is jointly governed by the intrinsic properties of the coupled semiconductors, band alignment, Fermi-level difference, interfacial contact, built-in electric field, and surface redox kinetics. Accordingly, this section summarizes the evolution from conventional heterojunctions to S-scheme systems, the S-scheme charge-transfer mechanism, the structural advantages of 2D/2D architectures, and the key criteria for OP/RP selection.

2.1 Mechanism of Heterogeneous Photocatalysis

Semiconductor photocatalysis generally proceeds through three fundamental steps[36]: light absorption, charge-carrier separation and migration, and surface redox reactions. First, when the incident photon energy is equal to or greater than the band gap of a semiconductor, electrons are excited from the valence band (VB) to the conduction band (CB), leaving holes in the VB. Second, the photogenerated electrons and holes are separated and migrate from the bulk to the surface or reactive sites; during this process, bulk or surface recombination may occur, leading to energy loss and reduced quantum efficiency. Third, the electrons and holes that reach the surface participate in reduction and oxidation reactions, respectively. Specifically, electrons can reduce electron acceptors adsorbed on or near the catalyst surface, such as protons, CO_2, O_2, or other reducible species, whereas holes can oxidize water, hydroxide ions, organic molecules, or pollutants.[12] Therefore, efficient photocatalysis requires sufficient light-harvesting ability, effective charge separation, rapid carrier transport, accessible surface active sites, favorable surface reaction kinetics, and appropriate band-edge potentials for the target redox reactions.[37]

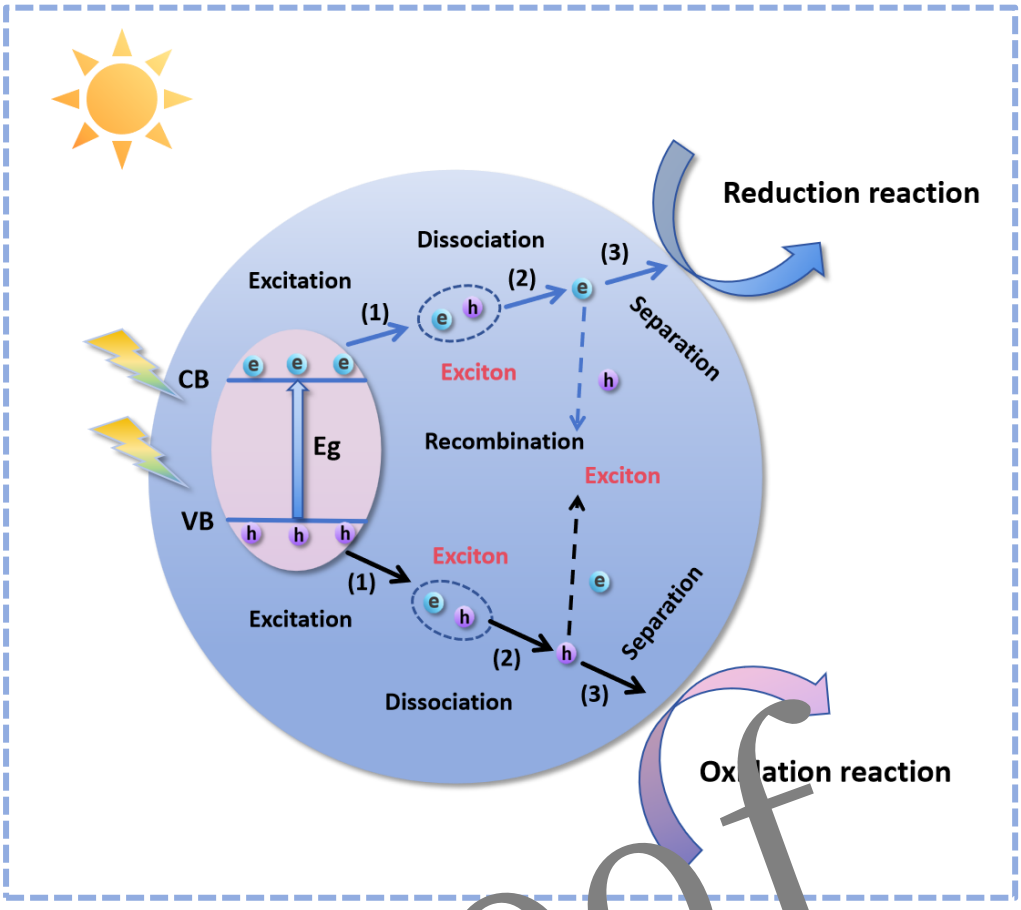

Fig 2. Schematic diagram of photocatalytic mechanism.

However, single component photocatalysts usually struggle to satisfy these requirements simultaneously. A narrow band gap can enhance light absorption but often compromises redox ability, whereas strong reduction and oxidation abilities generally require a sufficiently negative CB potential and a sufficiently positive VB potential, which are usually associated with a wider band gap.[14,38]Moreover, rapid recombination of photogenerated electrons and holes further limits charge utilization.[16] These intrinsic limitations have motivated the construction of semiconductor heterojunctions to improve charge separation and photocatalytic performance.

2.2 Evolution and Charge-transfer Mechanism of S-scheme Heterojunctions

Composite photocatalysts were initially interpreted mainly within the framework of the Type-II heterojunction model.[24] In a typical Type-II system, upon photoexcitation of both semiconductor components, photogenerated electrons migrate from the semiconductor with a more negative conduction-band potential to its counterpart with a less negative conduction-band potential, whereas holes transfer in the opposite direction, from the semiconductor with a more positive valence-band potential to that with a less positive valence-band potential.[37] Such a staggered band configuration promotes the spatial separation of electrons and holes and thereby suppresses

charge recombination from a kinetic perspective. However, from a thermodynamic viewpoint, this charge-transfer pathway drives electrons and holes to band positions with diminished reduction and oxidation potentials, respectively.[35] As a result, Type-II heterojunctions intrinsically suffer from a trade-off between efficient charge separation and strong redox capability.[39]

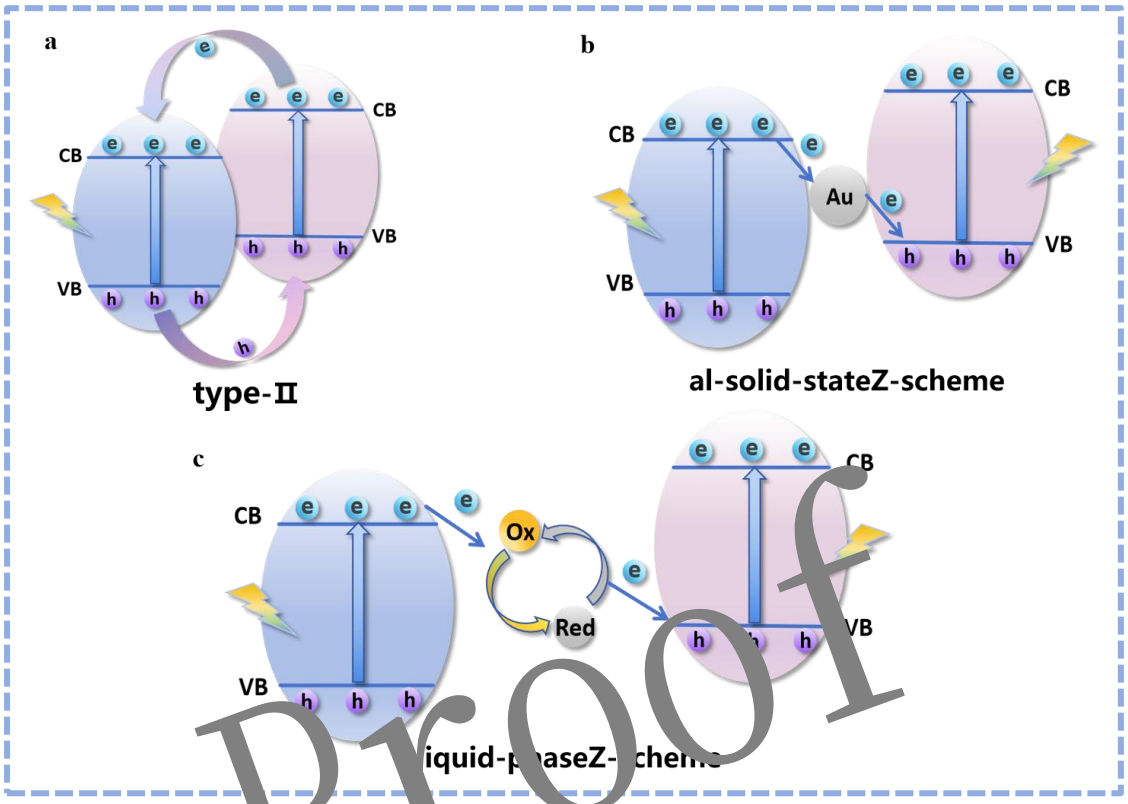

Fig 3. (a) type-II heterojunction (b) all-solid-state Z-scheme heterojunction (c) liquid-phase Z-scheme heterojunction.

To address this dilemma, liquid-phase and all-solid-state Z-scheme heterojunctions were developed to retain strongly reductive electrons and highly oxidative holes for surface redox reactions.[40,41] In principle, the Z-scheme configuration enables the recombination of relatively low-energy electrons and holes while preserving the most energetic charge carriers. Nevertheless, traditional Z-scheme systems remain limited by several factors, including their dependence on redox mediators, possible light-shielding effects, high interfacial charge-transport barriers, complicated structural design, and ambiguous interpretation of the charge-transfer pathway.[2,42] These limitations stimulated the development of a more rational heterojunction model capable of simultaneously achieving favorable charge-separation kinetics and retained redox thermodynamics.

In this context, Yu et al. proposed the S-scheme heterojunction concept in 2019.[27] An S-

scheme heterojunction is generally constructed by coupling a reduction photocatalyst (RP) with an oxidation photocatalyst (OP).[37] Typically, the RP possesses a higher Fermi level and a more negative conduction-band potential, whereas the OP exhibits a lower Fermi level and a more positive valence-band potential. This energetic asymmetry provides the fundamental prerequisite for the formation of an S-scheme charge-transfer pathway. Unlike the Type-II model, the S-scheme mechanism is not a simple downhill transfer of photogenerated carriers toward lower-energy band positions. Instead, it selectively removes thermodynamically less favorable charge carriers while retaining highly reductive electrons and strongly oxidative holes for photocatalytic reactions.[43,44]

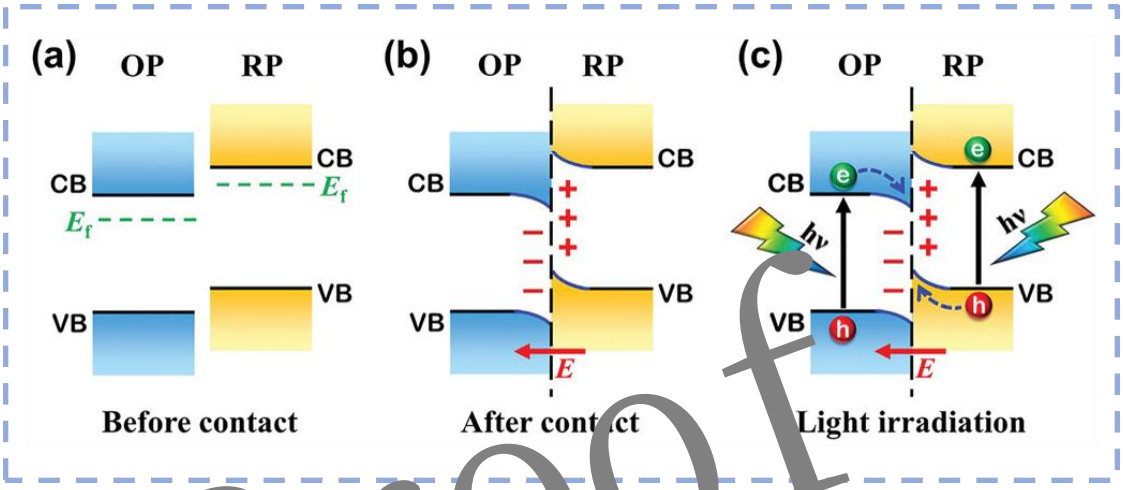

Fig 4. S-scheme heterojunction charge transfer mechanism.[45]

As schematically shown in Fig. 4, when the RP and OP come into intimate contact, electrons spontaneously transfer from the RP to the OP because of the higher Fermi level of the RP.[45] This interfacial electron redistribution continues until Fermi-level equilibration is reached, resulting in electron depletion and positive charge accumulation on the RP side, as well as electron enrichment and negative charge accumulation on the OP side.[46] Consequently, the energy bands of the RP bend upward, whereas those of the OP bend downward.[47] Meanwhile, an internal electric field directed from the RP to the OP is established across the heterointerface. Therefore, Fermi-level equilibration, interfacial charge redistribution, band bending, and internal electric-field formation collectively constitute the thermodynamic basis of the S-scheme charge-transfer mechanism.[48]

Under light irradiation, both the RP and OP generate electron–hole pairs. Driven by the internal electric field, interfacial electrostatic interaction, and band bending, electrons in the conduction band of the OP preferentially migrate toward the interface and recombine with holes in the valence band of the RP.[34] In contrast, the transfer of highly reductive electrons from the conduction band of the RP to the OP is suppressed, while the migration of strongly oxidative holes

from the valence band of the OP to the RP is also inhibited.[45] As a result, highly reductive electrons are retained in the conduction band of the RP, whereas strongly oxidative holes remain in the valence band of the OP.[49] This selective interfacial recombination pathway eliminates charge carriers with relatively weak redox ability and spatially separates the energetic electrons and holes required for surface reduction and oxidation reactions.[50,51]

Thus, the heterointerface is central to the S-scheme mechanism, governing charge redistribution, internal electric-field formation, directional carrier migration, and selective recombination of low-energy carriers. The requirement for intimate, clean, and strongly coupled interfaces makes 2D/2D architectures particularly suitable for constructing high-performance S-scheme photocatalysts.

2.3 Structural Advantages of 2D/2D Architectures

Since its proposal, the S-scheme heterojunction has attracted increasing attention and has been widely applied in various photocatalytic systems owing to its ability to integrate efficient charge separation with strong redox capability.[9,52] In particular, S-scheme heterojunctions based on two-dimensional (2D) materials are highly attractive because their large specific surface areas, ultrathin layered structures, and abundant exposed active sites favor interfacial charge transfer, photogenerated-carrier utilization, and surface redox reactions.[2,5] The large surface area of 2D materials promotes intimate contact between the oxidation photocatalyst and reduction photocatalyst, thereby facilitating interfacial charge redistribution, internal electric-field formation, and directional carrier migration.[54,55] Moreover, their ultrathin structure shortens the transport distance of photogenerated carriers to the surface or heterointerface, suppressing bulk recombination and improving charge-utilization efficiency.[56,57] These advantages make 2D materials suitable building blocks for constructing efficient S-scheme photocatalysts.[58]

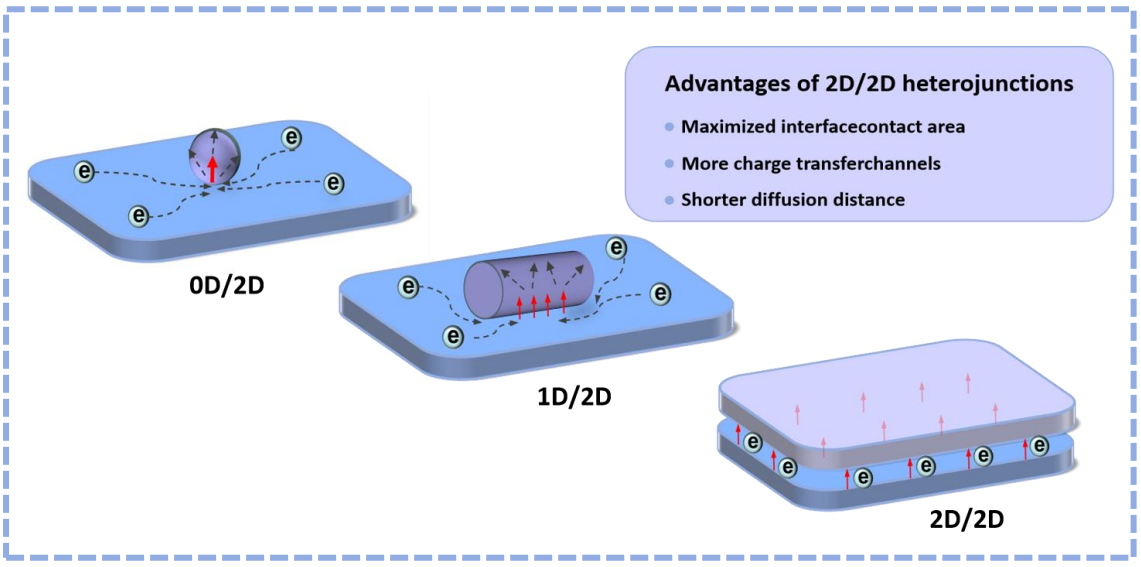

Fig 5. Schematic structure of 0D/2D, 1D/2D, and 2D/2D heterojunction.

S-scheme heterojunctions containing 2D components can generally be categorized into 0D/2D[59,60], 1D/2D[61,62], and 2D/2D[63,64] configurations, as shown in Fig5. Compared with point-contact 0D/2D and line-contact 1D/2D heterojunctions, 2D/2D architectures enable extended face-to-face coupling between two nanosheet components, thereby creating enlarged and continuous interfacial contact areas.[34,65] Such an interface facilitates Fermi level equilibration, interfacial charge redistribution, and internal electric-field formation, which are essential for S-scheme charge transfer. Furthermore, the face-to-face interface in 2D/2D heterojunctions provides abundant charge-transfer channels, reduces interfacial migration resistance, and shortens the carrier diffusion distance from the bulk phase to the interface.[2,66] These features promote directional charge migration, suppress nonselective recombination losses, and favor selective recombination of low-energy carriers at the interface. Consequently, 2D/2D architectures enable more efficient charge separation, improved light utilization, and enhanced synergistic effects within heterojunction systems.[48,67]

2.4 Design Principles of 2D/2D S-scheme Heterojunctions

Based on the above mechanistic and structural considerations, the rational design of 2D/2D S-scheme heterojunctions should focus on three key aspects: appropriate band alignment, high-quality interfacial coupling, and functional complementarity between the two components. In general, an S-scheme heterojunction is composed of a reduction photocatalyst (RP) and an oxidation photocatalyst (OP).[37] The conduction-band minimum and Fermi level of the RP should be higher than those of the OP, which represents the primary energetic criterion for establishing

an S-scheme charge-transfer pathway.[48] Once this requirement is met, the conductivity types of the two semiconductors are not strictly constrained,[45] allowing the construction of n–n, p–p, p–n, and n–p S-scheme heterojunctions.[68,69] This flexibility considerably broadens the material scope for designing 2D/2D S-scheme photocatalysts.

Functional complementarity between the RP and OP should also be considered during material selection.[70] The RP is expected to retain highly reductive electrons and mainly drive reduction reactions, such as H_2 evolution, CO_2 reduction, and N_2 fixation. In contrast, the OP should preserve strongly oxidative holes for oxidation reactions, including water oxidation, organic oxidation, and pollutant degradation.[71] Therefore, the selection of OP/RP pairs should not rely solely on band-edge positions, but should also consider light-harvesting ability, carrier mobility, surface catalytic activity, chemical stability, and compatibility with the target reaction.

2.5 Representative OP/RP Materials and Band-Structure Mapping

The practical implementation of these design criteria ultimately depends on the rational selection of semiconductor pairs with matched electronic structures and complementary redox functions. Among the relevant parameters, band-edge positions provide the most direct indication of whether a given OP/RP combination can establish the required energetic alignment, whereas surface chemistry, catalytic activity, and reaction compatibility determine its practical feasibility under specific photocatalytic conditions. Therefore, a systematic comparison of representative OP and RP photocatalysts in terms of their band structures is essential for guiding the rational construction of 2D/2D S-scheme heterojunctions.

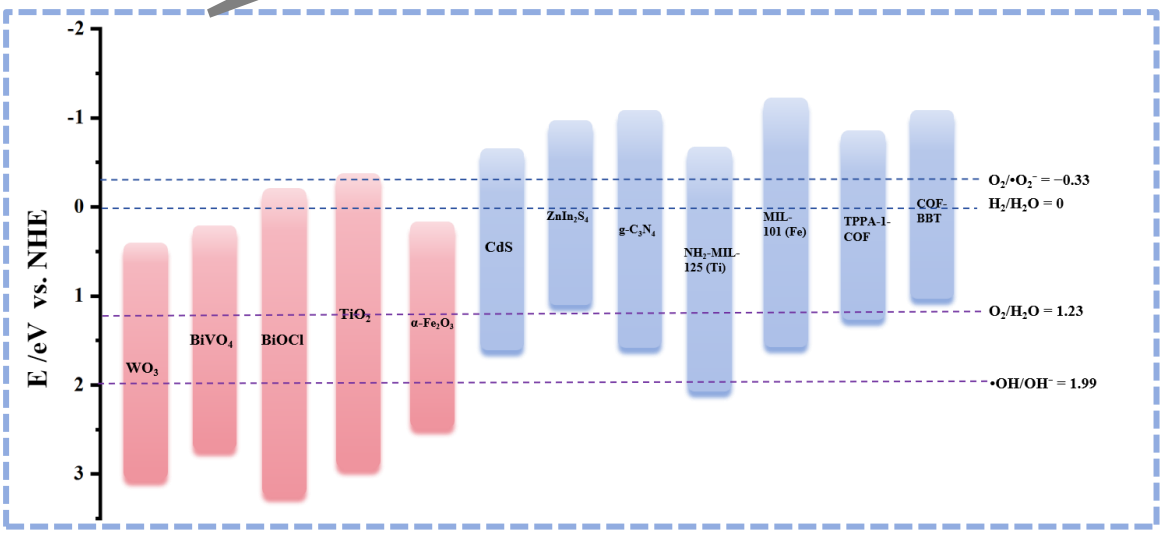

Fig 6. Band structures of various photocatalysts referenced to normal hydrogen electrode (NHE). The values are compiled from representative reports[72,73,74] and are shown for schematic comparison. Actual band positions may vary with pH, crystal phase, exposed facets, defects, dopants, and measurement methods.

Based on these principles, a broad range of semiconductors have been employed to construct S-scheme heterojunctions, ranging from conventional metal oxides, such as TiO_2 and WO_3,[75,76] to emerging semiconductor platforms, including C_3N_4,[77] metal–organic frameworks (MOFs),[78] covalent organic frameworks (COFs),[79] and perovskites. From a functional perspective, materials with relatively positive valence-band potentials, such as WO_3, $BiVO_4$, TiO_2, BiOCl, α-Fe_2O_3, are commonly considered as OP candidates because they are favorable for generating strongly oxidative holes. By contrast, materials with relatively negative conduction-band potentials, such as CdS, $ZnIn_2S_4$, g-C_3N_4, C_3N_5, and selected MOFs or COFs, are generally suitable as RP candidates because they can retain highly reductive electrons. [72,74,80] Nevertheless, the role of a given semiconductor as an OP or RP is not absolute, but depends on its band position relative to its counterpart, Fermi-level difference, interfacial configuration, and reaction environment.

3. Interfacial Construction Strategies for 2D/2D S-scheme Heterojunctions

Constructing high-quality 2D/2D interfaces is a prerequisite for achieving efficient S-scheme photocatalytic performance.[34] The interfacial coupling strength between two 2D materials directly affects charge-transfer efficiency, interfacial stability, and overall catalytic activity. According to the dominant interfacial formation mode, the stage at which the interface is generated, and the resulting interfacial coupling strength, the commonly used construction strategies for 2D/2D S-scheme heterojunctions can be classified into three categories: mixing-assisted assembly, surface chemical regulation and bonding, and in situ growth.

3.1 Mixing-Assisted Assembly

Mixing-assisted assembly represents one of the most fundamental and widely employed approaches for constructing 2D/2D heterostructures. In this strategy, two preformed 2D components are integrated through post-synthetic processes such as stirring, sonication, grinding, mechanical blending, or dispersion processing.[81,82] The formation of 2D/2D heterointerfaces primarily depends on the processing conditions and the intrinsic physicochemical properties of the constituent materials. During the mixing process, external physical forces facilitate the dispersion, exfoliation, and spatial proximity of the two 2D components, thereby increasing the probability of interfacial contact. The subsequent evolution of such contact into an effective heterointerface is largely governed by inherent intercomponent interactions, including electrostatic attraction, van der Waals forces, surface-energy matching, hydrophilic/hydrophobic interactions, hydrogen bonding, and π–π stacking interactions.[83,84] In this context, “self-assembly” should not be considered an independent synthesis route separate from mixing-assisted assembly, but rather an

interaction-driven interfacial organization process occurring during post-synthetic mixing. Thus, mixing-assisted assembly can be understood as a broad operational strategy, whereas self-assembly describes the interfacial driving force that enhances the directionality, intimacy, and stability of contact in certain systems.

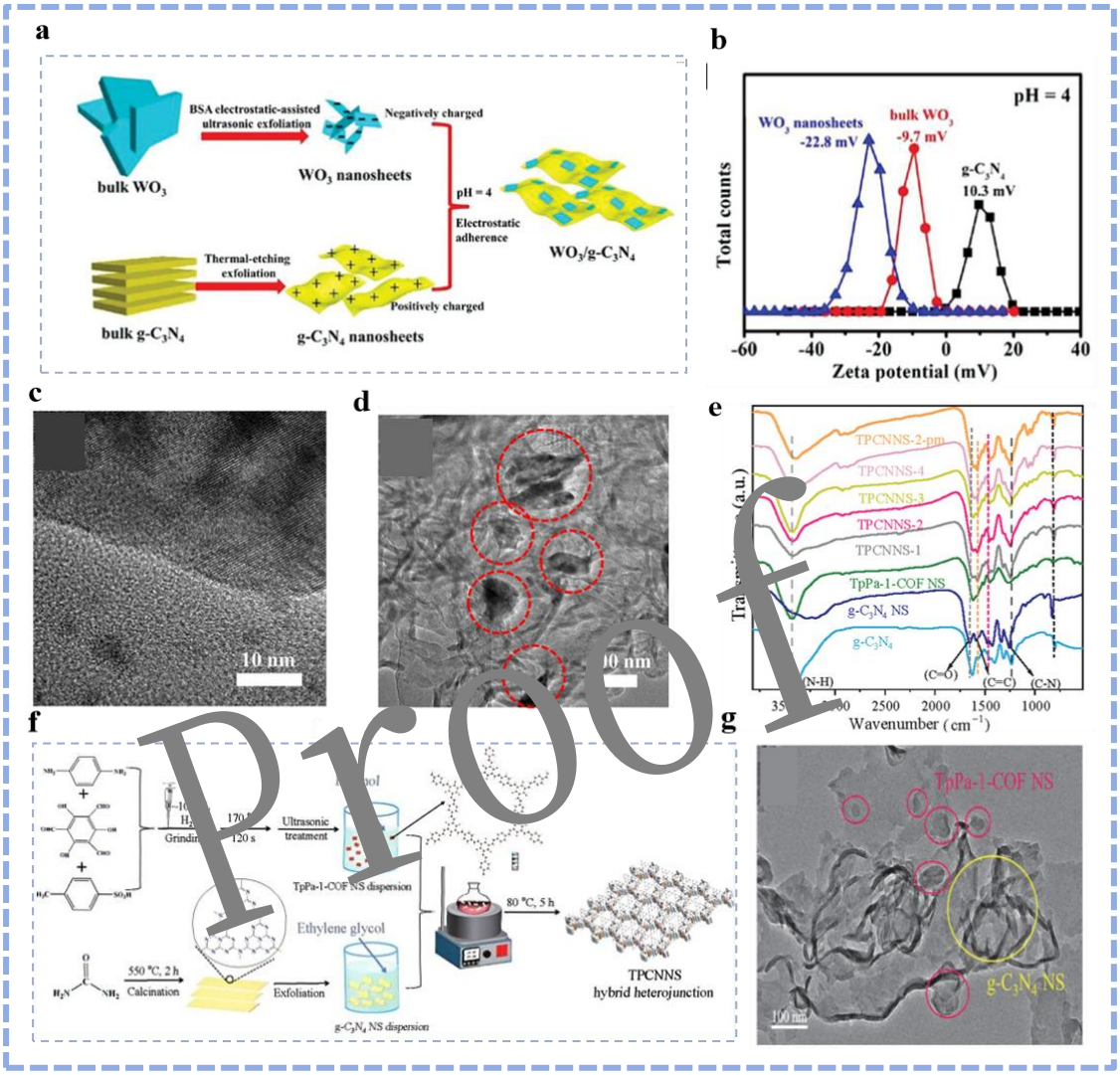

Fig 7. (a)The formation schematic diagram of 2D/2D WO_3/g-C_3N_4 heterojunctions by Coulomb electrostatic interaction. (b) Zeta potentials of bulk WO_3, WO_3 nanosheets and g-C_3N_4 at pH = 4. (c, d). HRTEM and TEM images of 15%WO_3/g-C_3N_4 samples. [27] (e) FT-IR spectra of TpPa-1-COF/g-C_3N_4 system. (f) Preparation of TpPa-1-COF/g-C_3N_4 NS (TPCNNS) hybrid heterojunction. (g) TEM images of TPCNNS-2.[85]

WO_3/g-C_3N_4[27] is a representative example of electrostatic interaction-assisted mixing assembly. By tuning the pH of the suspension, Fu et al. induced opposite zeta potentials (Fig7.b) on WO_3 and g-C_3N_4, thereby enabling electrostatic attraction to serve as the primary driving force for large-area face-to-face stacking between the two ultrathin nanosheets. This strategy led to the construction of a composite heterostructure with intimate interfacial contact. The TpPa-1-COF/g-C_3N_4[85] system further extends this strategy to the field of all-organic semiconductors, where

interfacial assembly mainly relies on π–π stacking interactions between two-dimensional organic frameworks. TEM (Fig7.g) morphological observations and FT-IR (Fig7.e) characterization confirmed that the two components were effectively integrated while preserving the structural integrity of their respective frameworks, thus providing a structural basis for the subsequent establishment of an S-scheme charge-transfer pathway.

3.2 Interfacial Construction via Surface Chemical Regulation

In contrast to mixing strategies, which largely rely on the inherent surface properties of the constituent materials, interfacial engineering based on surface chemical regulation provides a more powerful platform for rational interface design. By means of surface functionalization, incorporation of specific functional groups, elemental doping, and modulation of the local electronic structure, the surface reactivity and interfacial interaction behavior of materials can be deliberately tailored.[86,87,88] Consequently, heterointerface formation shifts from passive compatibility between components to directed assembly governed by predesigned interfacial interactions. This evolution enables interfacial regulation to move beyond the adjustment of external assembly conditions toward the precise control of intrinsic interfacial driving forces, thereby substantially enhancing the directionality, stability, and electronic coupling of heterointerfaces.[89]

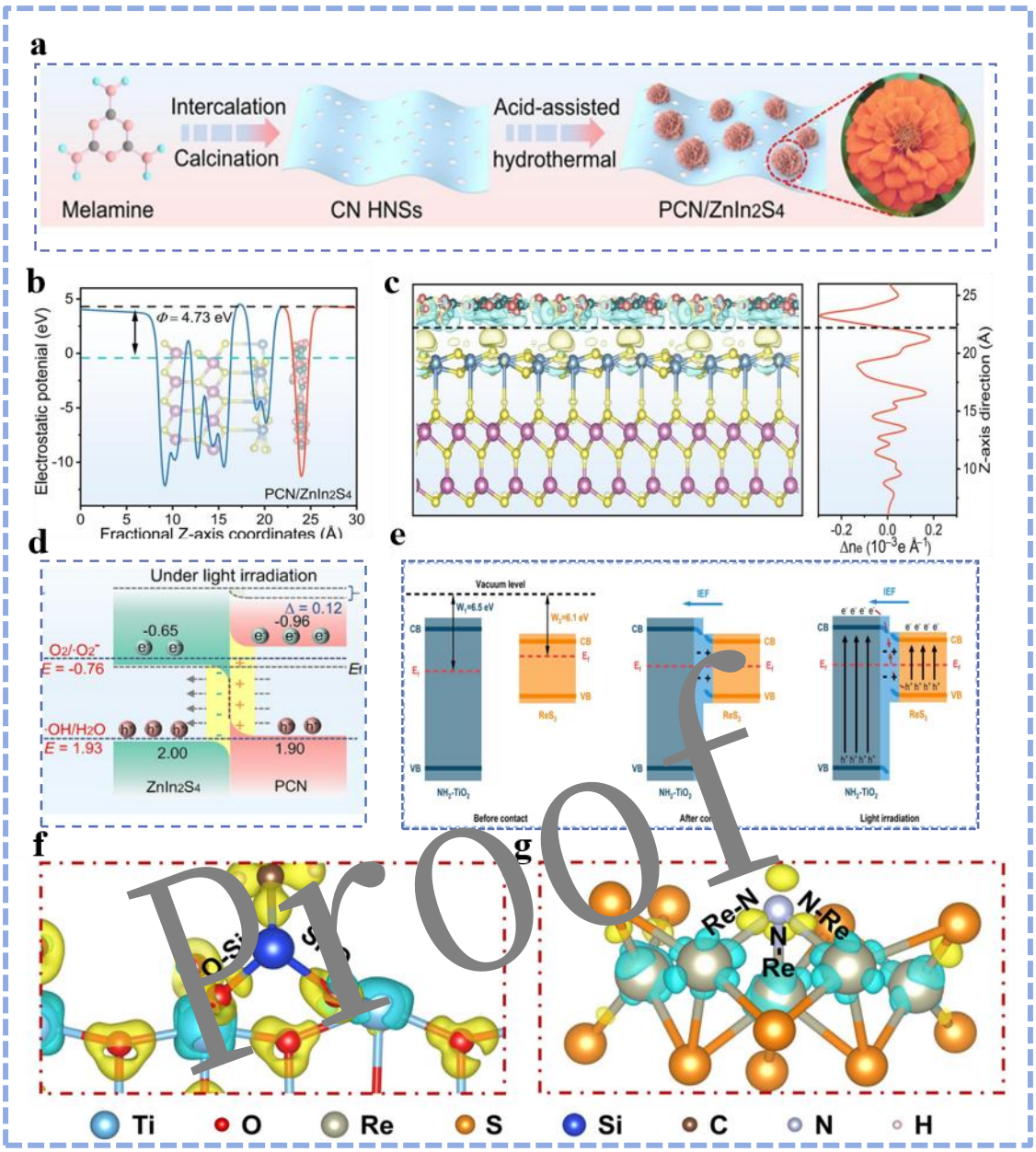

Fig 8. (a) Schematic illustration of the synthetic process of the PCN/$ZnIn_2S_4$ heterojunction. (b) Structure model of PCN/$ZnIn_2S_4$ heterojunction. (c) Calculated charge density difference and planar-averaged charge density difference for PCN/$ZnIn_2S_4$ heterojunction. (d) Schematic illustration of the formation of the PCN/$ZnIn_2S_4$ heterojunction.[90] (e) The molecular-connected heterojunction charge transfer mechanism of NH_2-TiO_2/ReS_2. (f, g) Charge density differences at the Si (f) and N (g) sites of NH_2-TiO_2/ReS_2.[88]

In recent studies, Chen et al.[86] constructed a two-dimensional/two-dimensional (2D/2D) porous graphitic carbon nitride (Pg-C_3N_4)/CdS-diethylenetriamine (DETA) organic–inorganic composite photocatalytic system. The introduction of DETA groups onto CdS nanosheets simultaneously modulated their crystal growth behavior and electronic band structure, while imparting a positively charged surface. These changes promoted intimate interfacial contact with Pg-C_3N_4 nanosheets and facilitated the formation of an S-scheme heterojunction. The resulting

built-in electric field drives the recombination of electrons in the conduction band of CdS with holes in the valence band of Pg-C_3N_4, thereby preserving strongly reducing electrons and oxidizing holes on opposite sides of the interface. This charge-transfer pathway effectively suppresses electron–hole recombination and substantially enhances photocatalytic H_2 evolution. Similarly, the NH_2-TiO_2/ReS_2[88] system exemplifies this strategy. Functionalization of the TiO_2 surface with APTMS reverses its surface charge from negative to positive, thereby enabling efficient assembly with negatively charged ReS_2 through electrostatic attraction. More importantly, APTMS serves not only as a surface charge regulator but also as a molecular bridge between the two phases, strengthening the interfacial interaction from simple electrostatic adsorption to more stable bridge-mediated coupling. Differential charge density analysis (Fig8.f, g) further reveals pronounced charge redistribution at the Si and N sites of the NH_2-TiO_2/ReS_2 interface, corroborating the formation of Si–O and Re–N bridging interactions and the markedly enhanced interfacial coupling. This case demonstrates that surface chemical regulation can actively tailor surface properties and interfacial affinity, allowing components with inherently weak assembly tendencies to form stable and strongly coupled heterojunctions.

Furthermore, in the protonated g-C_3N_4/$ZnIn_2S_4$[90] system, surface chemical regulation enables the synergistic optimization of both interfacial structure and electronic behavior through a protonation strategy. Under acidic conditions, protonated CN–H^+ species are generated on the surface of g-C_3N_4, which modify the local charge distribution (Fig8.b, c) and provide coordination sites for the oriented growth of $ZnIn_2S_4$. As a result, a 2D/2D heterostructure with intimate interfacial contact is established. Meanwhile, the built-in electric field at the interface promotes charge separation and migration, while the optimized interfacial electronic structure lowers the reaction energy barrier, collectively leading to markedly improved photocatalytic CO_2 reduction performance. This system underscores that surface chemical regulation can simultaneously tailor interfacial binding configurations, growth behavior, and electronic structure, thereby enabling the synergistic design of heterojunction structure and function.

3.3 In Situ Growth-Dominated Interfacial Construction

Unlike mixing or surface chemical modification, which primarily improve interfacial contact after the individual components have already formed, in situ growth-driven interfacial engineering moves the regulation of heterointerfaces to the nucleation and growth stages of the constituent materials.[46] In this strategy, one two-dimensional material typically serves as a substrate or structure-directing scaffold, while the other component is generated directly on its surface through

heterogeneous nucleation, followed by subsequent growth or lateral spreading.[48] As a result, the heterointerface is constructed synchronously with material formation.[89] Compared with post-synthetic hybridization, this strategy is more conducive to the formation of large-area, continuous, and intimate interfacial contact, thereby minimizing random stacking, local lattice or structural mismatch, and poor interfacial integration.[91] Therefore, the significance of in situ growth lies not merely in establishing physical contact, but more importantly in enhancing interfacial continuity, strengthening interfacial coupling, and synergistically optimizing the electronic structure through regulation of the nucleation and growth processes.

CdS/g-C_3N_4[92] system is a representative example of a 2D/2D S-scheme heterointerface constructed via in situ growth. In this system, g-C_3N_4 acts as a two-dimensional substrate and provides a reactive surface for CdS formation under hydrothermal conditions. Studies have shown that Cd^{2+} ions can accumulate on the surface of g-C_3N_4 and subsequently react with the generated S^{2-} species, leading to the in situ growth of CdS nanosheets and the formation of an intimate heterointerface. Compared with routes in which the two components are synthesized separately and then physically combined, the interface in this system is established concurrently with material generation, generally resulting in higher interfacial continuity. This example clearly demonstrates the essential characteristic of the in situ growth strategy: the heterointerface originates from the in situ generation of the second phase rather than from post-synthetic physical assembly.

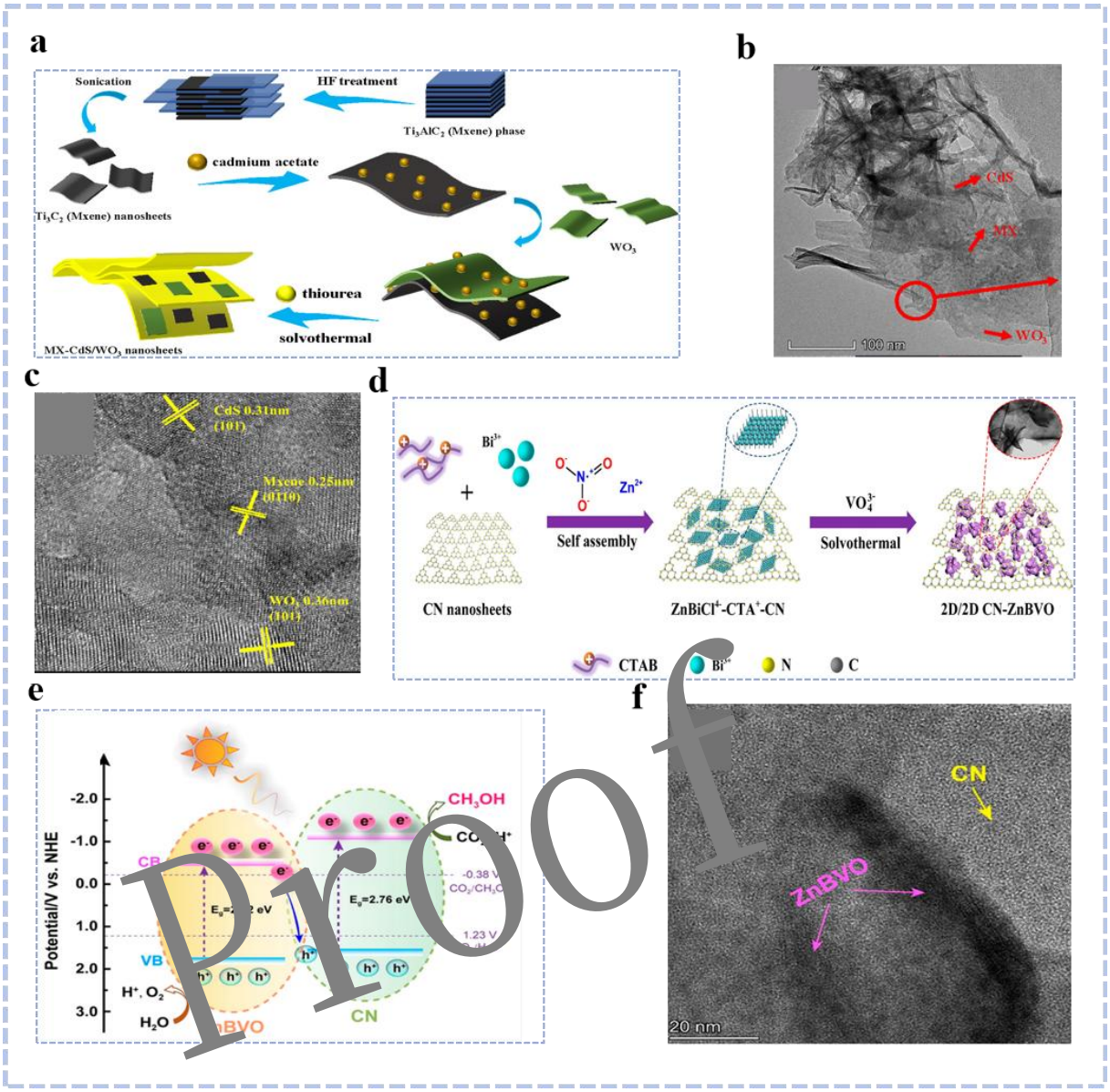

Fig 9. (a) Schematic of the fabrication of MX-CdS/WO_3 composites. (b) TEM images of MX-CdS/WO_3 (c) HRTEM image of MX-CdS/WO_3.[93] (d) Schematic diagram for the fabrication route of CN-ZnBVO. (e) Illustration of the proposed photocatalytic CO_2 reduction mechanism of the CN-ZnBVO-3 heterojunctions. (f) high-resolution TEM images of CN-ZnBVO-3.[94]

On this basis, the g-C_3N_4—ZnBVO (CN–ZnBVO)[94] system further illustrates the importance of nucleation control in the in situ growth process. In this system, CN nanosheets act as the two-dimensional substrate, whereas ZnBVO is formed under solvothermal conditions, with its nucleation and growth mediated by the CTAB surfactant. The study suggests that CTAB facilitates the formation of charged intermediates, such as $BiCl^{4-}$–CTA^{+}, which provide favorable nucleation sites and thereby promote the heterogeneous nucleation of ZnBVO on the CN surface, followed by the growth of ZnBVO nanostructures. As a result, ZnBVO nanosheets are firmly anchored onto the CN surface, yielding a 2D/2D heterostructure with intimate interfacial contact, as shown in the TEM

image in Fig9.f. In contrast to the CdS/g-C_3N_4 system, this example more clearly reflects the regulation of nucleation through manipulation of the reaction environment, particularly the surfactant and precursor species, thereby improving interfacial uniformity and interfacial integration.

To further illustrate the potential for the synergistic construction of multiple interfaces, the MX-CdS/WO_3[93]system represents a more sophisticated example. In this system, two-dimensional WO_3 and Ti_3C_2 MXene nanosheets serve as a composite substrate, on which CdS nanostructures are subsequently grown in situ via a hydrothermal process, resulting in a hierarchical 2D/2D/2D multi-interfacial architecture, as shown in the TEM image in Fig9.b, c. Within this configuration, an S-scheme heterojunction is established between CdS and WO_3, generating an internal electric field that facilitates directional charge separation, while an ohmic contact is formed between CdS and MXene, providing a low-resistance pathway for electron transport. The simultaneous formation of multiple interfaces within a single growth process enables the integration of distinct interfacial functions, thereby markedly enhancing charge separation and transport efficiency. This system demonstrates that the value of in situ growth extends beyond the construction of a single high-quality interface; more importantly, it enables the synergistic integration of multiple components, multiple interfaces, and multiple functions during material formation.

4. Mechanistic Characterization of 2D/2D S-Scheme Heterojunctions

A detailed understanding of directional interfacial charge transport is essential for validating the photocatalytic mechanism of 2D/2D S-scheme heterojunctions. To establish a robust mechanistic framework, this section summarizes multidimensional characterization strategies, including structural analysis of interfacial architectures, band-alignment evaluation, and dynamic tracking of charge-transfer processes. These approaches provide critical experimental evidence for identifying S-scheme charge-transfer pathways and assessing interfacial coupling strength in 2D/2D systems.

4.1 Structural Characterization of Interfacial Architectures

The formation of an atomically intimate and continuous heterointerface is a prerequisite for efficient interfacial charge recombination in S-scheme systems. High-quality face-to-face contact enlarges the effective interfacial area, improves active-site accessibility, and shortens both exciton diffusion distances and charge-carrier migration pathways, thereby reducing interfacial contact resistance.[46,95,96] Therefore, direct visualization of the geometric contact, interlayer stacking configuration, and spatial distribution of each component is essential for clarifying microscopic

reaction mechanisms and verifying the establishment of S-scheme charge-transfer channels.

4.1.1 Lattice structure

Transmission electron microscopy (TEM) and related techniques are powerful tools for resolving interfacial morphology and atomic arrangements in heterojunctions. They enable direct visualization of lattice-fringe continuity, crystallographic orientation relationships, and interfacial structural coherence at the atomic scale.[97] However, because electron-scattering contrast and beam sensitivity vary substantially among different material systems, characterization strategies should be adapted to sample crystallinity, scattering behavior, and structural stability under electron irradiation.[98]

For highly crystalline systems with long-range order, TEM-based analysis should focus on identifying lattice matching, possible epitaxial relationships, and moiré fringes arising from lattice mismatch. Such information helps exclude interfacial amorphous layers, high-density dislocations, and other structural defects that may serve as charge-recombination centers.[63,99,100] By contrast, weakly scattering systems often exhibit extremely low mass–thickness contrast in conventional bright-field TEM images, making interface identification difficult.[98] In these cases, high-angle annular dark-field scanning TEM (HAADF-STEM) can enhance interfacial contrast through Z-contrast imaging. For beam-sensitive organic or hybrid interfaces, cryogenic electron microscopy (Cryo-EM) offers an advanced alternative by preserving native molecular configurations under near-intrinsic solvated or dispersed states.[101] This strategy effectively reduces beam-induced damage and morphological distortion, enabling high-resolution imaging of fragile organic–organic interfaces down to the sub-angstrom scale.

4.1.2 Three-dimensional surface topography and interlayer structure

TEM images are two-dimensional projections of three-dimensional structures and therefore provide limited information along the out-of-plane direction. In this context, atomic force microscopy (AFM), with its sub-angstrom vertical resolution, is particularly useful for characterizing the surface topography and interlayer stacking features of 2D/2D heterojunctions.[102] Height-profile analysis enables quantitative determination of the absolute thickness of ultrathin nanosheets. By comparing the thickness increment in heterojunction regions with those of the individual components,[103] AFM can verify whether a compact and ordered face-to-face stacking configuration has formed between different nanosheets.[104] This evidence helps distinguish genuine 2D/2D interfacial integration from simple physical mixing or nonspecific aggregation.

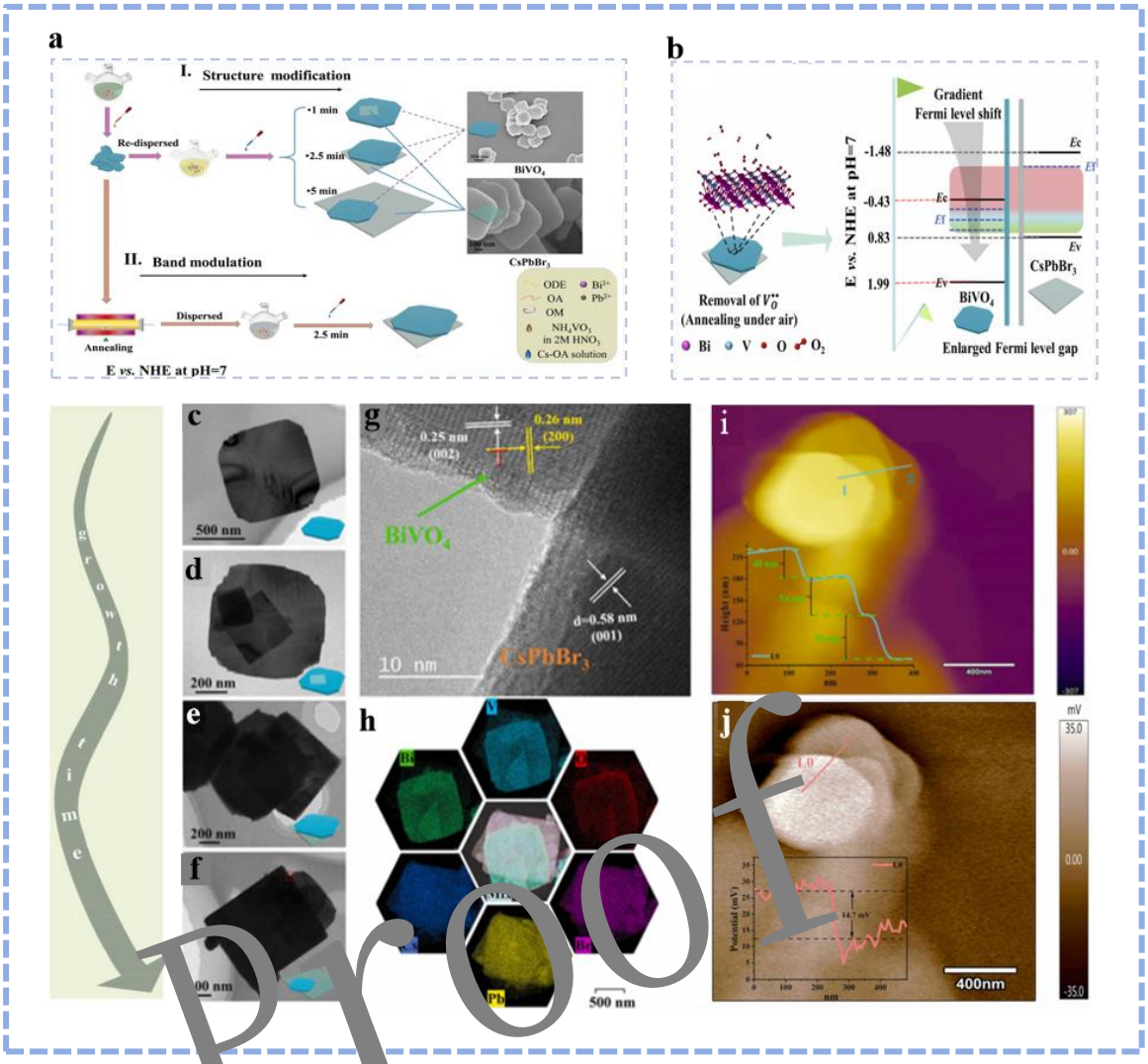

Fig 10. (a) Schematic illustration of the $BiVO_4/CsPbBr_3$ heterojunction (b) Illustration of the enlarged Fermi level gap between $BiVO_4$ and $CsPbBr_3$ from regulation towards $BiVO_4$ NSs. (c), BC1(d), BC2 (e) and BC3 (f, g). The corresponding insets illustrate the structural evolution along with the reaction time and HRTEM from the red dotted areas in f; (h) Elemental mapping images for Bi, V, O, Cs, Pb, Br and the Mixed for BC2; (i)AFM of BC2 (Inset in g is the height cutaway view from position 1 to position 2, the thicknesses of these nanosheets are 40, 54 and 59 nm, corresponding to $CsPbBr_3$, $BiVO_4$ and $BiVO_4$, respectively.); (j) Atomic force microscopy images with potential mode (KPFM) for BC2 under dark condition (Inset in j is the potential cutaway view of marked L_0, and the potential difference between $BiVO_4$ and $CsPbBr_3$ NSs is 14.7 mV).[105]

For example, TEM (Fig10.d-f) characterization has demonstrated a face-to-face vertically stacked architecture in a $BiVO_4/CsPbBr_3$ heterojunction.[105] he quasi-square $BiVO_4$ nanosheets, featuring well-defined two-dimensional surfaces, act as growth templates for $CsPbBr_3$. Benefiting from its high surface energy, $CsPbBr_3$ preferentially nucleates on the $BiVO_4$ surface to reduce the overall interfacial energy, resulting in intimate interfacial coupling and improved size uniformity of the $CsPbBr_3$ nanosheets. HRTEM (Fig10.g) images further show a sharp heterointerface with clear lattice fringes corresponding to the $BiVO_4$ (200) / (002) and $CsPbBr_3$ (001) planes, indicative of an

ordered crystalline interface. EDS (Fig10.h) elemental mapping further verifies the coexistence and spatial distribution of Bi, V, O, Cs, Pb, and Br in BC2. AFM height profiling (Fig10.i) and surface-potential mapping (Fig10.j) further verify the layered structure and interfacial electronic redistribution, respectively, providing complementary evidence for the successful formation of the 2D/2D S-scheme heterojunction.

4.2 Chemical nature of interfacial interactions

The intimate contact revealed by microscopic imaging provides the physical basis for S-scheme charge-transfer channels, while chemical interactions at the interface create effective pathways for charge migration across the junction.[106] Whether arising from noncovalent interactions or robust chemical bonding, identifying interfacial interactions beyond simple physical mixing is essential for reducing interfacial contact resistance and promoting efficient S-scheme charge transfer.[107,108]

4.2.1 Identifying bonding motifs via vibrational spectroscopy

Fourier transform infrared spectroscopy (FT-IR) is widely used to probe local chemical environments and monitor the evolution of surface functional groups during heterojunction assembly.[109,110] In 2D/2D heterojunctions, interfacial coupling can perturb the vibrational modes of specific chemical bonds, and the resulting spectral changes provide insight into the nature and strength of interfacial interactions. For noncovalently assembled systems, such as those involving π–π stacking or hydrogen bonding, the preservation of framework-related bands together with subtle red- or blue-shifts of key functional groups is generally regarded as evidence of effective interfacial coupling.[111,112]

For example, Zhang et al.[55] used FT-IR (Fig9.b) spectroscopy to investigate the chemical structure and assembly mode of a BiOI/porphyrin-based coordination polymer composite. The BiOI@PCP samples retained the characteristic BiOI features, including the Bi–O vibration at 490 cm^{-1} and the surface hydroxyl band. After Zn^{2+}coordination, a new band appeared at approximately 1000 cm^{-1}, which was assigned to skeletal vibrations of the pyrrolic ring in Zn–porphyrin. These results confirm successful Zn^{2+} coordination and indicate the formation of chemically linked interfacial structures.

4.2.2 Static redistribution of electron density

Interfacial interactions are often accompanied by charge redistribution across the interface. X-ray photoelectron spectroscopy (XPS), by detecting binding-energy shifts of core-level electrons,

provides direct evidence for changes in local electron density.[46,106] Typically, shifts toward higher binding energy suggest reduced local electron density, weakened electron screening, and increased effective nuclear charge. Therefore, XPS binding-energy shifts can be used to infer the direction and degree of interfacial charge transfer, offering strong evidence for electronic coupling between components and helping to distinguish genuine heterojunction formation from simple physical mixing.[113,114]

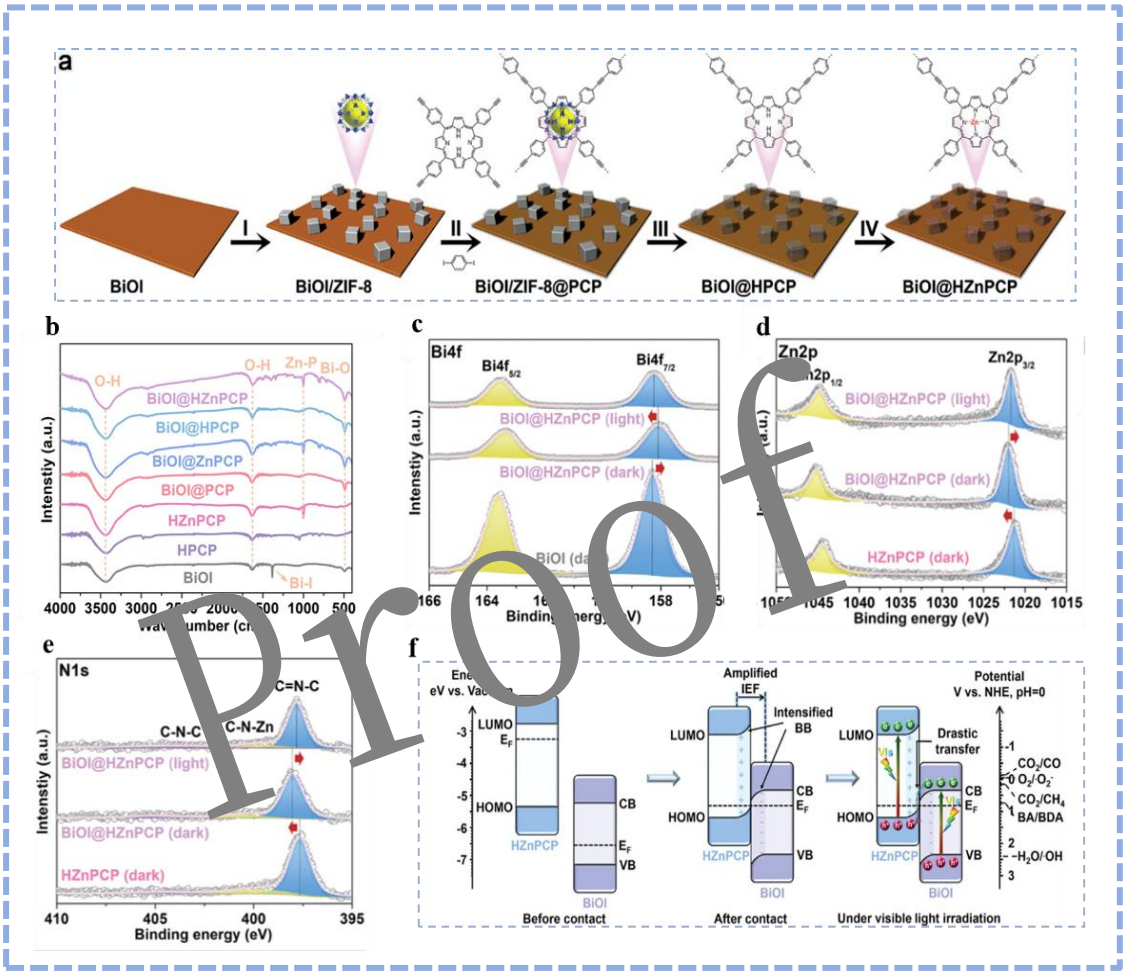

Fig 11. (a)BiOIv@HZnPCP schematic illustrating the synthetic procedue. (b)FTIR spectra of BiOI@HZnPCP and reference samples. (c-e) high-resolution XPS spectra: c) Bi4f, d) Zn2p, and e) N1s.[55]

In the BiOI@HZnPCP heterojunction studied by Zhang et al[55]. XPS analysis showed opposite binding-energy shifts for the two components. The Bi 4f (Fig11.c) peak of BiOI shifted toward lower binding energies, while the Zn 2p (Fig11.d), N 1s (Fig11.e), peaks of HZnPCP shifted toward higher binding energies. These shifts indicate directional electron transfer from HZnPCP to BiOI and the establishment of an interfacial built-in electric field. Compared with the Zn-free BiOI@HPCP sample, BiOI@HZnPCP exhibited larger binding-energy shifts, suggesting that the Zn center enhances interfacial charge redistribution. Thus, although Zn does not alter the direction of charge transfer,

it can function as an electron-transport center that promotes electron delocalization and strengthens interfacial electronic coupling.

4.3 Band Alignment and Interfacial Electric Field

In S-scheme photocatalytic systems, the interfacial built-in electric field (IEF) provides the thermodynamic driving force for the directional migration of photogenerated charge carriers and enables selective recombination of low-energy carriers at the interface. Therefore, quantitatively determining the band structures, Fermi-level positions, and IEF direction is essential for validating the S-scheme charge-transfer mechanism.[102]

4.3.1 Visualization and direction determination of the IEF

Kelvin probe force microscopy (KPFM), an advanced AFM-based technique, is widely used to visualize the IEF and determine its direction at heterojunction interfaces.[115] By measuring the contact potential difference between a conductive tip and the sample surface, KPFM maps the spatial distribution of surface potential and work-function variations. According to the principle of Fermi-level equilibration, when two components come into contact, electrons spontaneously diffuse from the component with a lower work function, corresponding to a higher Fermi level, to that with a higher work function, corresponding to a lower Fermi level, until thermodynamic equilibrium is reached. This charge redistribution generates a directional interfacial potential gradient, providing the thermodynamic basis for directional charge transfer in S-scheme systems.[104,116]

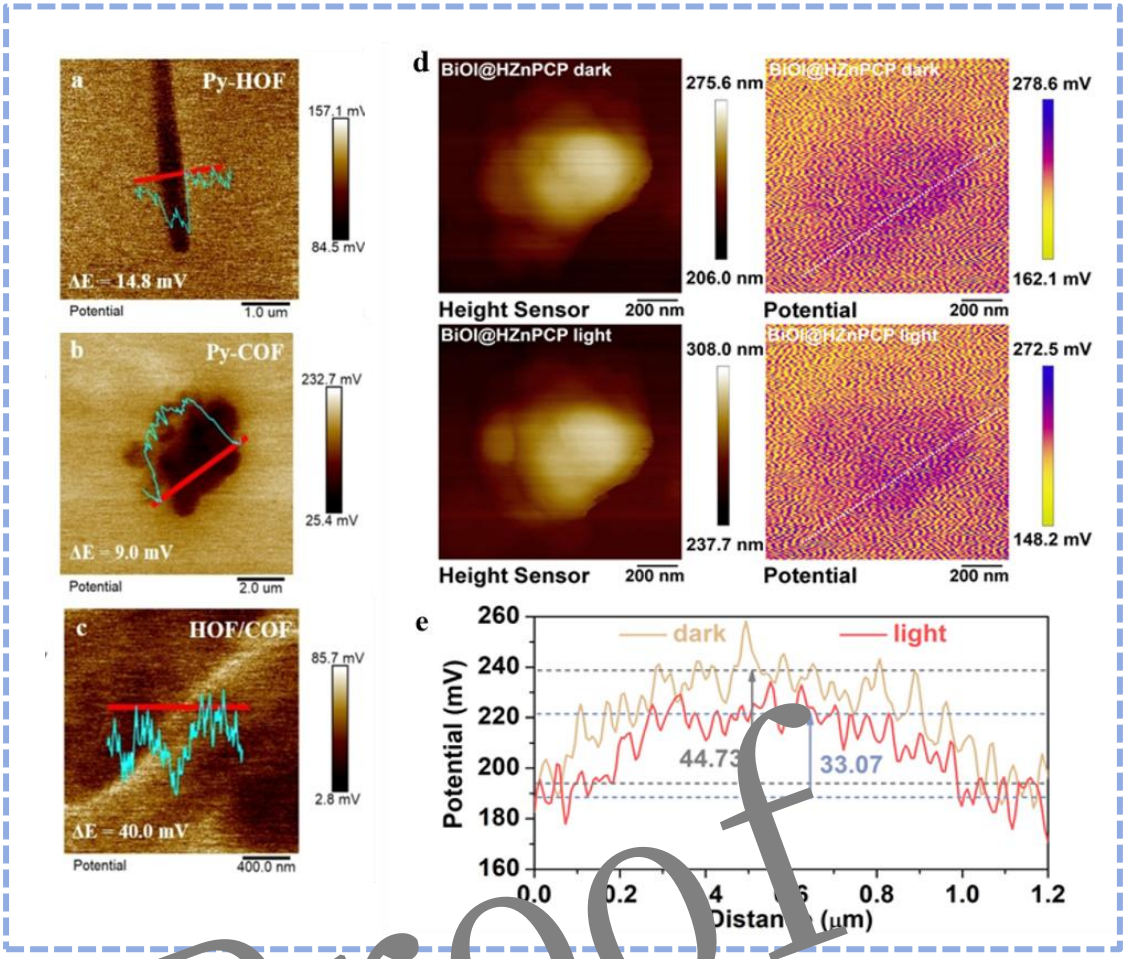

Fig 12. Surface potentials of (a) Py-HOF, (b) Py-COF and (c) HOF/COF[117] (d-e) KPFM of BiOI@HZnPCP: (d) atomic force microscopy images (left) and corresponding surface potential distributions (right) in darkness and under light irradiation; (e) surface potential curves along the line in darkness and under light irradiation.[55]

KPFM enables both qualitative visualization of the interfacial built-in electric field (IEF) and quantitative assessment of its magnitude and light-induced response. For field-strength quantification, recent studies on all-organic HOF/COF heterojunctions[117] offer a representative example. KPFM (Fig12.a-c) measurements showed that the surface potential difference across the HOF/COF heterojunction reached 40.0 mV, markedly higher than those of pristine Py-HOF (14.8 mV) and Py-COF (9.0 mV). This enhanced potential difference indicates a strengthened IEF, which provides a thermodynamic driving force for efficient charge separation and transport. T Furthermore, light-assisted KPFM, which maps surface photovoltage, enables the monitoring of light-induced charge redistribution. Taking BiOI@HZnPCP as an example[55] (Fig12.d, e), the surface potential under dark conditions was 44.73 mV higher than that of the substrate. Upon light irradiation, the surface potential decreased markedly to 33.07 mV, with no obvious morphological change. This negative potential shift indicates directional transfer of photogenerated electrons from the inner BiOI core to the outer ZnPCP surface under the driving effect of the IEF. Overall,

KPFM provides strong evidence for the establishment of the thermodynamic driving force in S-scheme heterojunctions by correlating static surface-potential differences with light-induced potential variations.

4.3.2 Theoretical simulations as auxiliary validation

As an important complement to experimental characterization, density functional theory (DFT) calculations provide atomic-level insights into interfacial charge transfer and the formation of built-in electric fields in 2D/2D S-scheme heterojunctions.[34] Through structural optimization of heterojunction models and calculations of differential charge density and planar-averaged electrostatic potential, charge redistribution upon interfacial contact can be systematically evaluated.[118] Differential charge density maps visualize charge accumulation and depletion at the interface, reflecting pronounced electronic coupling between the two components.[119] Meanwhile, planar-averaged electrostatic potential profiles reveal interfacial potential reconstruction and a pronounced potential gradient, providing theoretical evidence for the formation of a built-in electric field.[120] When combined with quantitative charge-transfer analysis, these simulations further demonstrate that the built-in electric field can drive directional migration of photogenerated charge carriers, promote the recombination of low-energy electrons and holes, and retain high-energy carriers with strong redox potentials, consistent with the characteristic charge-transfer pathway of S-scheme heterojunctions.[4]

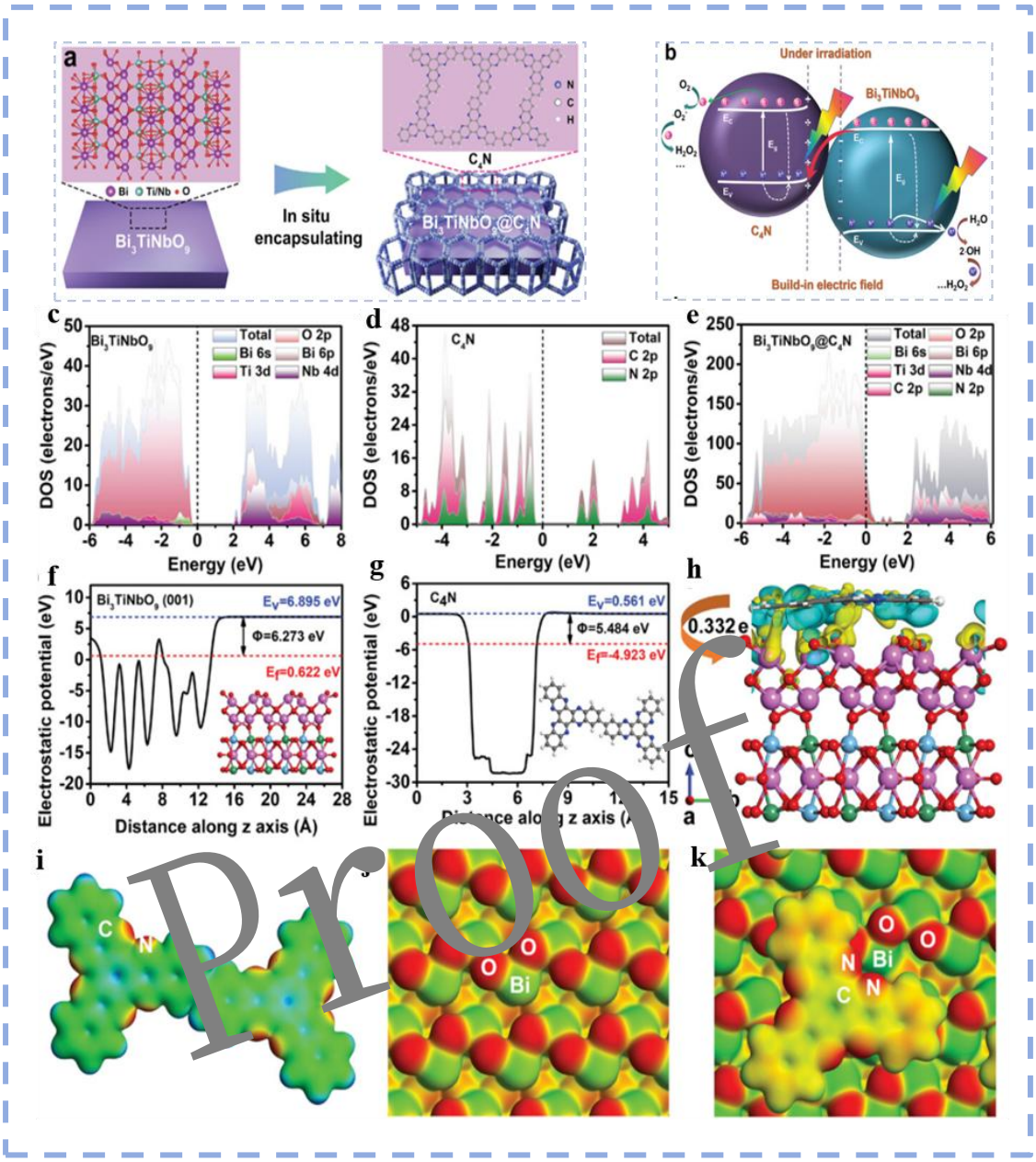

Fig 13. (a) Scheme illustration for the synthesis process of the $Bi_3TiNbO_9@C_4N$ heterojunction. (b) Schematic illustration of the artificial photosynthesis process of H_2O_2 and the photoinduced carriers transfer mechanism over the $Bi_3TiNbO_9@C_4N$. (c–e) The calculated PDOS results of the Bi_3TiNbO_9, C_4N, and $Bi_3TiNbO_9@C_4N$ heterojunction. (f, g) The calculated work function (Φ) of the Bi_3TiNbO_9 and C_4N, respectively. (h) The charge density difference of the $Bi_3TiNbO_9@C_4N$ heterojunction. (i–k) The electron density isosurface of the C_4N, Bi_3TiNbO_9 and $Bi_3TiNbO_9@C_4N$ surfaces, respectively.[22]

For example, Teng et al.[22] used DFT calculations to clarify the interfacial electronic structure of a $Bi_3TiNbO_9@C_4N$ 2D/2D S-scheme heterojunction. As shown in Fig13.a, the *in-situ* encapsulation strategy enables intimate coupling between Bi_3TiNbO_9 and C_4N, providing a structural basis for interfacial charge transfer. The PDOS results in Fig13.c–e indicate that heterojunction formation modifies the electronic-state distribution near the Fermi level,

suggesting strong electronic coupling between the two components. Work-function calculations further show that C_4N possesses a higher Fermi level than Bi_3TiNbO_9, which drives spontaneous electron migration from C_4N to Bi_3TiNbO_9 upon contact and induces an interfacial built-in electric field. This charge redistribution is further supported by the charge-density difference and electron-density isosurface analyses in Fig13.h–k, where obvious interfacial electron rearrangement and a transferred charge of 0.332 e are observed. Under irradiation, the built-in electric field and band bending promote S-scheme charge transfer, retaining electrons with strong reduction ability for O_2 reduction and holes with strong oxidation ability for water oxidation. Consequently, the Bi_3TiNbO_9@C_4N heterojunction provides a favorable electronic configuration for artificial photosynthetic H_2O_2 production.

4.4 Kinetic Evidence for S-scheme Charge Transfer

Although the above structural analyses and thermodynamic characterizations can establish the interfacial basis and internal electric field driving force for S-scheme charge transfer, they are not sufficient to fully determine the actual carrier migration pathway under photoexcitation. Direct kinetic evidence is therefore essential for clarifying how photogenerated charges are generated, transferred, recombined, and spatially retained during photocatalysis. In situ spectroscopic techniques and ultrafast time-resolved measurements provide powerful tools for monitoring carrier migration pathways and lifetimes under working conditions, thereby offering critical evidence for verifying the S-scheme charge-transfer mechanism.

4.4.1 Monitoring electron flow under in situ illumination

Among the currently available characterization techniques, in situ irradiated X-ray photoelectron spectroscopy (ISI-XPS) is widely regarded as one of the most direct and persuasive approaches for probing light-induced interfacial charge migration[121]. This technique relies on the high sensitivity of core-level binding energies to the local electron density. In general, electron accumulation enhances electronic shielding and shifts the corresponding core-level peaks toward lower binding energies, whereas electron depletion weakens the shielding effect and leads to positive binding-energy shifts.[114,122]. Therefore, by comparing the XPS spectra of individual components and their heterojunctions under dark and illuminated conditions, ISI-XPS can track the light-induced evolution of electron-rich and electron-deficient regions during photocatalysis.

A convincing ISI-XPS analysis should distinguish between interfacial charge redistribution in the dark and photoinduced carrier migration under illumination. In the dark, binding-energy shifts relative to the pristine components mainly reflect Fermi-level equilibration, interfacial electron

redistribution, and the formation direction of the built-in electric field. Upon illumination, the reversible shifts of characteristic core levels provide direct information on the migration direction of photogenerated carriers.[122] For an S-scheme heterojunction, the built-in electric field drives the selective recombination of low-energy electrons and holes at the interface, while preserving strongly reductive electrons and strongly oxidative holes on different components.[123] This light-induced charge-transfer pattern is fundamentally different from that expected for a conventional type-II heterojunction, and therefore provides strong evidence for an S-scheme pathway.[114]

Recent studies on COF-based organic/inorganic S-scheme heterojunctions have further demonstrated the diagnostic capability of ISI-XPS. Representative systems, including CYANO–COF/$ZnIn_2S_4$ [124] and COF/ $Mn_{0.2}Cd_{0.8}S$[125], exhibit reversible light-induced binding-energy shifts, confirming that ISI-XPS can sensitively probe interfacial electron redistribution under photocatalytic conditions. When combined with complementary techniques such as electron paramagnetic resonance (EPR), Kelvin probe force microscopy (KPFM), and femtosecond transient absorption spectroscopy (fs-TAS), ISI-XPS provides a robust criterion for distinguishing S-scheme charge transfer from conventional type-II mechanisms.

This approach is particularly informative for 2D/2D S-scheme heterojunctions, where intimate face-to-face interfaces can strengthen orbital coupling and accelerate interfacial charge migration. For example, in a 2D/2D BN-$g-C_3N_4$/C_3N_5 S-scheme heterojunction (Fig14.e), interfacial B–O bonds function as direct charge-transfer channels.[126] In situ irradiated B 1s XPS (Fig14.f) showed that the B–O-related peak shifted toward higher binding energy under illumination and returned to its initial position after the light was switched off, whereas the O 1s peak exhibited the opposite shift behavior. These reversible spectral changes indicate light-induced electron migration through interfacial B–O bonds, supporting an S-scheme pathway in which charge carriers with weaker redox ability recombine at the interface, while those with stronger redox ability are preserved for overall water splitting. A similar conclusion was obtained for the 2D/2D COF-316/ TpBpy-COF[127] nanosheet heterojunction (Fig14.a). Under illumination, the pyridinic N signal of TpBpy-COF shifted negatively, whereas the –CN signal of COF-316 shifted positively, indicating electron migration from COF-316 to TpBpy-COF (Fig14.b). These opposite light-induced XPS shifts provide direct evidence for the formation of a 2D/2D S-scheme charge-transfer channel.

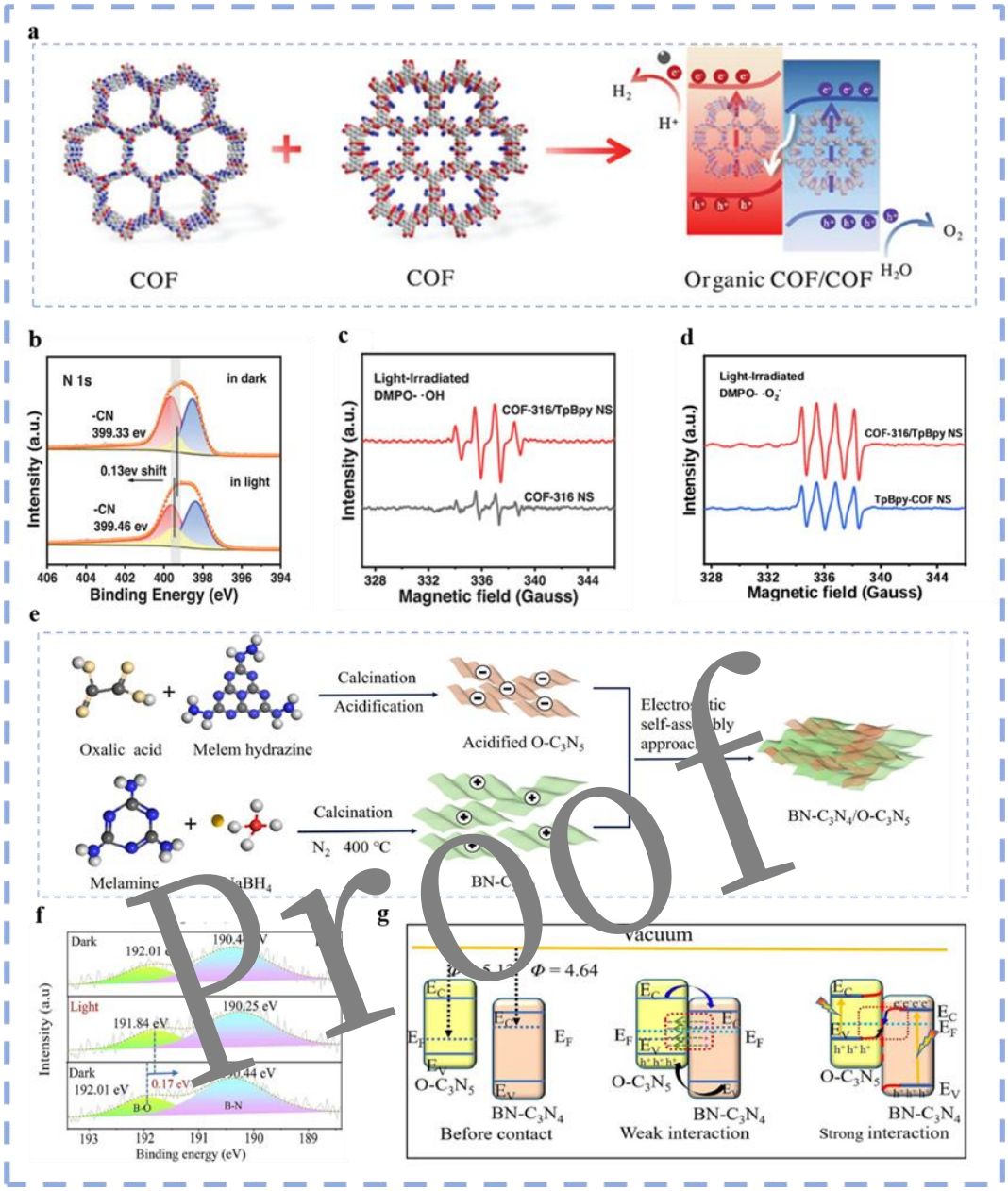

Fig 14. (a) Schematic illustration of COF/COF heterojunction for overall water splitting.(b)The XPS spectra of COF-316/TpBpy-COF NS in dark and in light.(c)DMPO spin-trapping EPR spectra of COF-316 NS and COF-316/TpBpy-COF NS with light irradiation.(d) DMPO spin-trapping EPR spectra of TpBpy-COF NS and COF-316/TpBpy-COF NS with light irradiation.[127] (e) Schematic of the synthesis of BN-C_3N_4/O-C_3N_5. (f) In-situ B 1s XPS spectra of BN-C_3N_4/O-C_3N_5. (g) Simulation of band bending and electron transfer of BN-C_3N_4/O-C_3N_5.[126]

4.4.2 Indirect verification of redox capability

Electron paramagnetic resonance (EPR) spectroscopy cannot independently determine the charge-transfer route, but it provides important supporting evidence by identifying the reactive species generated during photocatalysis. In S-scheme heterojunctions, the built-in electric field and selective recombination of low-energy carriers allow the preservation of electrons and holes with

strong redox potentials. Thus, the simultaneous enhancement of DMPO-•O_2^- and DMPO-•OH signals usually suggests that the heterojunction retains sufficient reduction and oxidation ability, which is more compatible with an S-scheme pathway than with a conventional type-II mechanism.[46,128]

For example, Luan et al.[127] used DMPO-assisted EPR measurements (Fig14.c,d) to examine ROS generation over COF-316/TpBpy-COF under visible-light irradiation. The composite showed much stronger DMPO-•O_2^- and DMPO-•OH signals than either single COF component, indicating enhanced carrier utilization and preserved redox capacity. These results suggest that photogenerated electrons can reduce O_2 to •O_2^-, while holes can oxidize H_2O/OH^- to •OH. When combined with in situ XPS evidence, the EPR results support the assignment of an S-scheme-dominated charge-transfer mechanism in the COF-316/TpBpy-COF heterojunction.

4.4.3 Ultrafast carrier dynamics

Femtosecond transient absorption spectroscopy (fs-TAS) is a powerful technique for resolving ultrafast carrier dynamics in photocatalytic heterojunctions on femtosecond-to-nanosecond timescales. By monitoring transient signals such as ground-state bleaching (GSB), excited-state absorption (ESA), and their decay kinetics, fs-TAS can provide kinetic evidence for interfacial charge transfer and carrier recombination pathways.[129] In S-scheme heterojunctions, the built-in electric field and band bending promote selective interfacial recombination between low-energy electrons and holes, while preserving high-energy carriers with strong redox potentials. Therefore, variations in transient spectral features and lifetime components, rather than simple acceleration or retardation of decay alone, should be analyzed together with complementary evidence to identify an S-scheme charge-transfer pathway.[130,131]

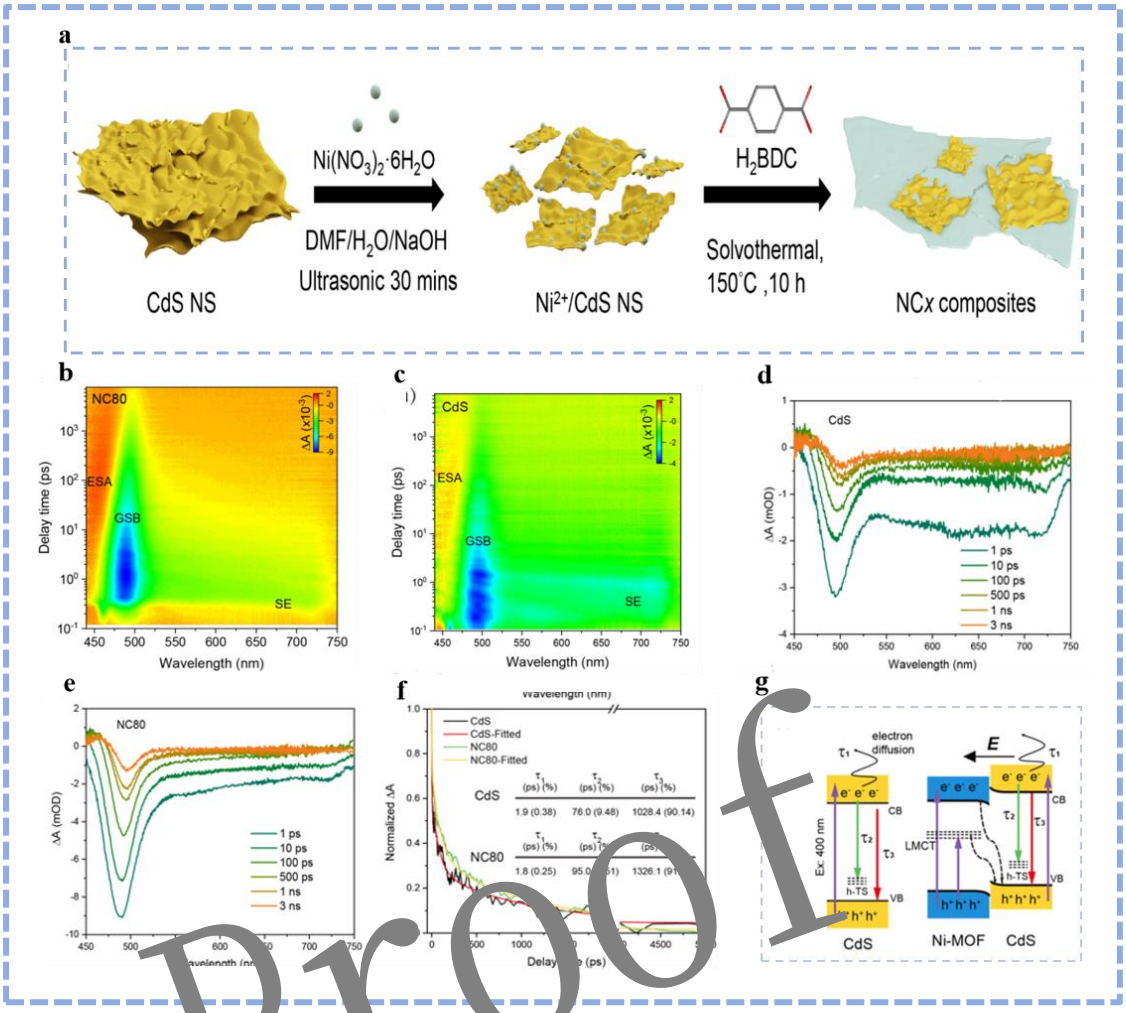

Fig 15. (a) Schematic of the synthesis of NCx composites. (b, c) Fs-TA spectra of (b) CdS (c) and NC80 composite under 400 nm excitation. (d, e) TA spectral signals of (d) CdS and (e) NC80 composite on nanosecond timescales. (g) Corresponding fitted decay kinetics curves for CdS and NC80 at 500 nm. (i) Mechanisms underlying the photoexcited dynamics in CdS (left) and NC80 composite (right).[132]

For example, Liu et al.[132] used fs-TAS to investigate ultrafast charge dynamics in a Ni-MOF/CdS heterojunction. As shown in Fig15.b–e, the fs-TA maps and transient spectra of NC80 exhibit characteristic CdS-related ground-state bleaching, excited-state absorption, and stimulated-emission features, with the GSB signal mainly assigned to photogenerated electrons. Compared with pristine CdS, NC80 shows prolonged carrier lifetimes in the fitted decay kinetics monitored at 500 nm (Fig15.h), indicating the retention of long-lived electrons on CdS after heterojunction formation. Meanwhile, the weakened Ni-MOF-related transient features and the proposed carrier-dynamics scheme (Fig15.i) suggest rapid interfacial recombination between electrons in Ni-MOF and holes in CdS. Together with XPS and TRPL analyses, these results support an S-scheme charge-transfer pathway, in which low-energy carriers are selectively recombined at the interface while

high-energy electrons are preserved on CdS for subsequent redox reactions.

In summary, although both S-scheme and type-II heterojunctions can promote spatial charge separation, their charge-transfer consequences are fundamentally different. In a type-II heterojunction, photogenerated electrons and holes are transferred to relatively low-energy band positions, resulting in weakened thermodynamic driving forces for surface redox reactions. In contrast, an S-scheme heterojunction selectively recombines low-energy carriers at the interface while retaining highly reductive electrons and strongly oxidative holes. Therefore, a convincing distinction between S-scheme and type-II mechanisms requires a mutually consistent evidence chain. Structural and spectroscopic characterizations should first confirm the formation of an intimate heterointerface. Band-structure and work-function analyses should then establish the RP/OP configuration, Fermi-level equilibration, band bending, and the built-in electric field. Interfacial charge redistribution can be further supported by dark-state XPS, KPFM, and related electronic-structure analyses. More importantly, in situ irradiated XPS and time-resolved spectroscopies are needed to track photoinduced charge migration and carrier lifetime evolution, thereby determining whether low-energy carriers recombine through an S-scheme pathway or follow a conventional type-II transfer route. EPR detection of reactive species provides complementary evidence for retained redox ability, particularly when both $\bullet O_2^-$ and •OH are generated under conditions where a type-II pathway would be thermodynamically unfavorable. Thus, an S-scheme assignment is reliable only when interfacial structure, band alignment, built-in electric field, light-induced charge migration, and preserved redox capability are mutually supported.

4.5 Reaction-induced dynamic evolution of photocatalytic heterointerfaces

Most discussions of S-scheme heterojunctions rely on static band structures, work-function differences, and interfacial configurations. However, under photocatalytic conditions, the active heterointerface may undergo dynamic electronic evolution induced by light irradiation, charge accumulation, reactant adsorption, intermediate formation, defect activation, and local reaction environments. Such evolution can alter band bending, built-in electric fields, interfacial recombination channels, and surface reaction kinetics.[133] Therefore, S-scheme heterointerfaces should be regarded as reaction-responsive charge-transfer regions rather than fixed contact boundaries.

A representative example is the BN-C_3N_4/O-C_3N_5 S-scheme heterojunction[126] reported by Cui et al., in which interfacial B–O bonds act as direct electron-transfer bridges between two carbon

nitride components. In situ irradiated XPS revealed reversible binding-energy shifts of B–O-related signals under illumination, indicating dynamic modulation of the electronic state at the bonded interface. Together with fs-TA and DFT analyses, these results suggest that B–O bonding channels can reduce the interfacial charge-transfer barrier, shorten the migration distance, and facilitate selective S-scheme recombination of low-energy carriers, while preserving carriers with strong redox potentials for overall water splitting. Notably, post-reaction XRD and FTIR spectra showed negligible changes, suggesting that the chemically bonded interface can sustain dynamic charge transfer without obvious structural degradation.

Dynamic interfacial charge redistribution has also been observed in tandem heterojunction systems. In GDY-Cu/WO_3, the WO_3/GDY S-scheme junction and the GDY-Cu ohmic contact establish coupled charge-transfer channels.[73] Under illumination, in situ XPS showed a negative shift of the C 1s binding energy and a positive shift of the W_{4f} binding energy, suggesting directional electron migration from WO_3 to GDY through the S-scheme pathway. Meanwhile, the GDY-Cu ohmic interface provides an additional electron-extraction route toward reduction sites. This system indicates that photocatalytic heterointerfaces can undergo light-induced electronic reconfiguration, in which multiple interfacial electric fields cooperate to regulate charge flow, carrier extraction, and surface redox reactions.

In summary, the catalytic performance of S-scheme heterojunctions is governed by both the initially constructed interface and its dynamic evolution under reaction conditions. Future studies on 2D/2D S-scheme photocatalysts should integrate in situ/operando XPS, in situ FTIR spectroscopy, EPR, KPFM, time-resolved spectroscopy, isotope-labeling experiments, and theoretical simulations to distinguish reversible electronic polarization, bond-assisted charge migration, defect activation, adsorbate-induced interfacial changes, and irreversible structural degradation. Such systematic analysis is essential for establishing a reliable structure–evolution–charge-transfer–activity relationship in 2D/2D S-scheme photocatalysts.

5. Engineering Modification Strategies for 2D/2D S-Scheme Heterojunctions

With a clearer understanding of the construction principles, charge-transfer mechanisms, and characterization methods of 2D/2D S-scheme heterojunctions, increasing attention has shifted from heterojunction fabrication to interfacial performance optimization. Although face-to-face 2D/2D contact can enlarge the interfacial contact area, shorten carrier migration pathways, and strengthen the built-in electric field, the practical photocatalytic performance of these systems remains constrained by interfacial resistance, discontinuous charge transport, sluggish mass

transfer, insufficient active sites, and limited structural stability. Therefore, precise modulation of interfacial structures, charge dynamics, and surface-active sites is essential for overcoming these bottlenecks.

Current optimization strategies mainly involve multidimensional heterointerface engineering, interfacial chemical bonding, element doping, defect engineering, cocatalyst modification, and single-atom regulation. These strategies contribute to enhanced charge transport, stronger interfacial coupling, optimized band and electronic structures, improved reactant activation, and more efficient surface charge utilization. In essence, their shared objective is to translate the intrinsic charge-separation advantage of S-scheme heterojunctions into accelerated surface reaction kinetics and improved photocatalytic performance.

5.1 Construction of multidimensional heterointerface.

Conventional 2D/2D S-scheme heterojunctions primarily rely on a single face-to-face contact interface to achieve charge separation and selective recombination.[91,134] However, under complex reaction conditions or high carrier fluxes, a single interface is often required to simultaneously mediate light absorption, charge migration, interfacial recombination, and surface reactions, which may intensify local carrier recombination and limit charge-transport efficiency. Therefore, introducing a third component to construct multidimensional heterointerfaces has emerged as an effective strategy to overcome the charge-transport limitations of single-interface systems.[135,136]

The key to multidimensional heterointerface design lies in functional partitioning and multichannel charge management. By incorporating conductive layers, cocatalytic components, light-harvesting units, or interfacial modulation layers, cascade band structures and additional charge-migration pathways can be established beyond the original RP/OP S-scheme interface. This design facilitates the directional recombination of low-energy charge carriers while preserving highly reductive electrons on the RP and highly oxidative holes on the OP.[93] Compared with single 2D/2D interfaces, multidimensional heterostructures can simultaneously promote charge separation, alleviate interfacial transport pressure, and improve structural stability and adaptability under complex reaction environments.

For example, multidimensional heterointerface construction provides an effective route to overcoming the charge-transport bottleneck in single 2D/2D S-scheme interfaces. A representative case is the 2D/2D/0D $TiO_2/C_3N_4/Ti_3C_2$ MXene system,[136] in which 2D TiO_2 and ultrathin C_3N_4 form a tightly coupled S-scheme heterointerface (Fig16.d), enabling the selective recombination of low-energy carriers while retaining strong redox capability. Meanwhile, Ti_3C_2 MXene quantum dots

anchored on the C_3N_4 surface act as electron acceptors and transport channels, accelerating electron extraction and migration from the C_3N_4 conduction band and thereby promoting multielectron CO_2 reduction (Fig16.f). This example demonstrates that the incorporation of conductive cocatalytic components can effectively decouple charge separation from electron transport, thereby improving interfacial charge utilization and photocatalytic reaction efficiency.

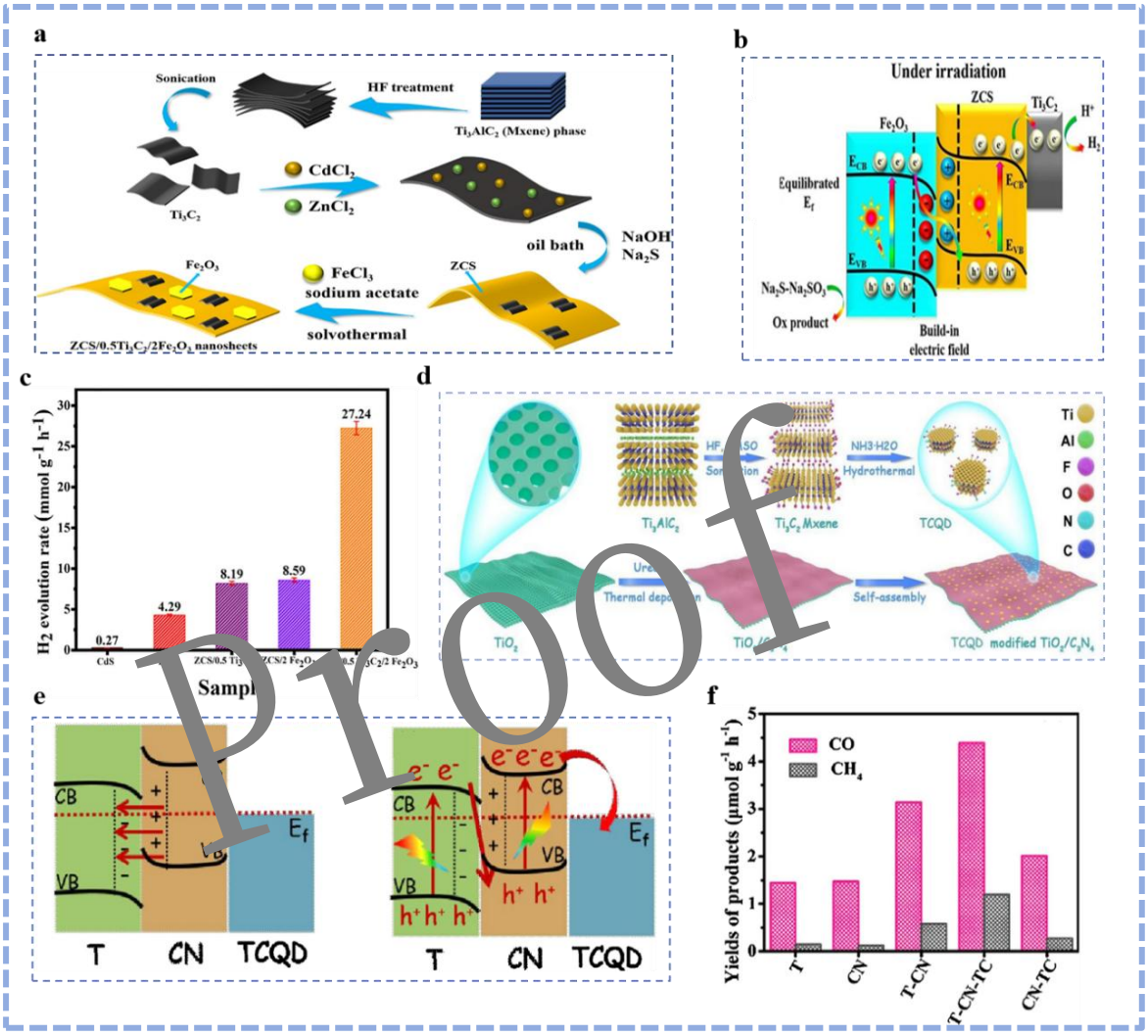

Fig 16. (a) Schematic diagram of the fabrication of $ZCS/_{0.5}Ti_3C_2/2Fe_2O_3$ composites. (b) The S-scheme heterojunction of $ZCS/_{0.5}$ $Ti_3C_2/2Fe_2O_3$ after contact upon irradiation, charge migration and separation and photocatalytic hydrogen evolution. (c) Comparison of optimal ratio hydrogen.[135] (d) Schematic of the synthesis of ultrathin TCQD anchored TiO_2/C_3N_4 core–shell nanosheets. (e) The S-scheme heterojunction of $TiO_2/C_3N_4/Ti_3C_2$ quantum dots after contact and after contact upon irradiation and charge migration and separation. (f) Photocatalytic CO_2 reduction performance of the prepared samples after irradiation for 1 h.[136]

Similarly, the cascaded 2D-coupled $Ti_3C_2/Zn_{0.7}Cd_{0.3}S/Fe_2O_3$ heterojunction (Fig16.a) further highlights the merits of multi-interface synergy.[135] In this architecture, the $Zn_{0.7}Cd_{0.3}S/Fe_2O_3$ S-scheme interface establishes a built-in electric field and preserves charge carriers with strong redox

potentials, whereas metallic Ti_3C_2 MXene forms an ohmic contact with $Zn_{0.7}Cd_{0.3}S$, offering a low-resistance channel for rapid electron transport and additional active sites for hydrogen evolution (Fig16.b). The optimized ternary composite therefore delivers substantially improved H_2-evolution activity (Fig16.c), demonstrating that the coupling of S-scheme and ohmic interfaces can synergistically enhance charge separation, interfacial transport, and surface reaction efficiency.

These findings suggest that multidimensional 2D/2D-based S-scheme heterostructures should be developed through function-oriented interface engineering rather than simple component stacking. In such systems, S-scheme interfaces maintain strong redox capability and promote selective charge separation, conductive components such as MXene accelerate electron extraction and transport, and cocatalytic or active-site interfaces facilitate surface reactions. Accordingly, future efforts should focus on coordinated band alignment, work-function matching, intimate interfacial coupling, and directional charge migration to construct well-defined multi-interface S-scheme photocatalysts.

5.2 Interfacial Bonding Engineering.

Interfacial quality is crucial for determining the charge-transfer efficiency and structural stability of 2D/2D S-scheme heterojunctions.[137] Although face-to-face contact enlarges the interfacial area, interfaces assembled therein through van der Waals interactions, electrostatic adsorption, or physical mixing often exhibit weak coupling, high charge-transfer resistance, and insufficient structural stability. In S-scheme heterojunctions, the interface serves as both the region for built-in electric field formation and charge redistribution and the pathway for selective recombination of low-energy carriers while retaining charge carriers with strong redox potentials.[138,139] Thus, constructing chemically coupled interfaces through interfacial bonding, molecular bridging, or ligand-assisted assembly is essential for improving 2D/2D S-scheme systems. Interfacial bonding motifs, such as Mg–N, Ti–O–Si, and N–Re linkages, can establish direct atomic-scale connections across heterointerfaces, thereby enhancing interfacial coupling and promoting localized charge redistribution. These effects reduce interfacial charge-transfer resistance, regulate the work-function difference and built-in electric field, and ultimately promote S-scheme charge-transfer dynamics.[88,140]

For example, in the 2D/2D MgO/g-C_3N_4 S-scheme heterojunction,[140] MgO nanosheets were uniformly grown on the surface of g-C_3N_4 through an *in-situ* growth process, leading to the formation of Mg–N interfacial bonds. XPS (Fig17.d) confirmed the presence of Mg–N bonding in the MgO/g-C_3N_4 composite, whereas such bonding was absent in the physically mixed counterpart.

Meanwhile, the Mg–N bonds promoted the generation of oxygen vacancies in MgO. DFT calculations (Fig17.f) further revealed that Mg–N bonding and oxygen vacancies jointly facilitated interfacial charge migration from the perspective of electronic structure. As a result, the MgO/g-C_3N_4 system achieved a RhB photo-Fenton degradation efficiency of 80.01%, demonstrating that interfacial Mg–N bonding can synergistically enhance charge migration and catalytic reaction activity.

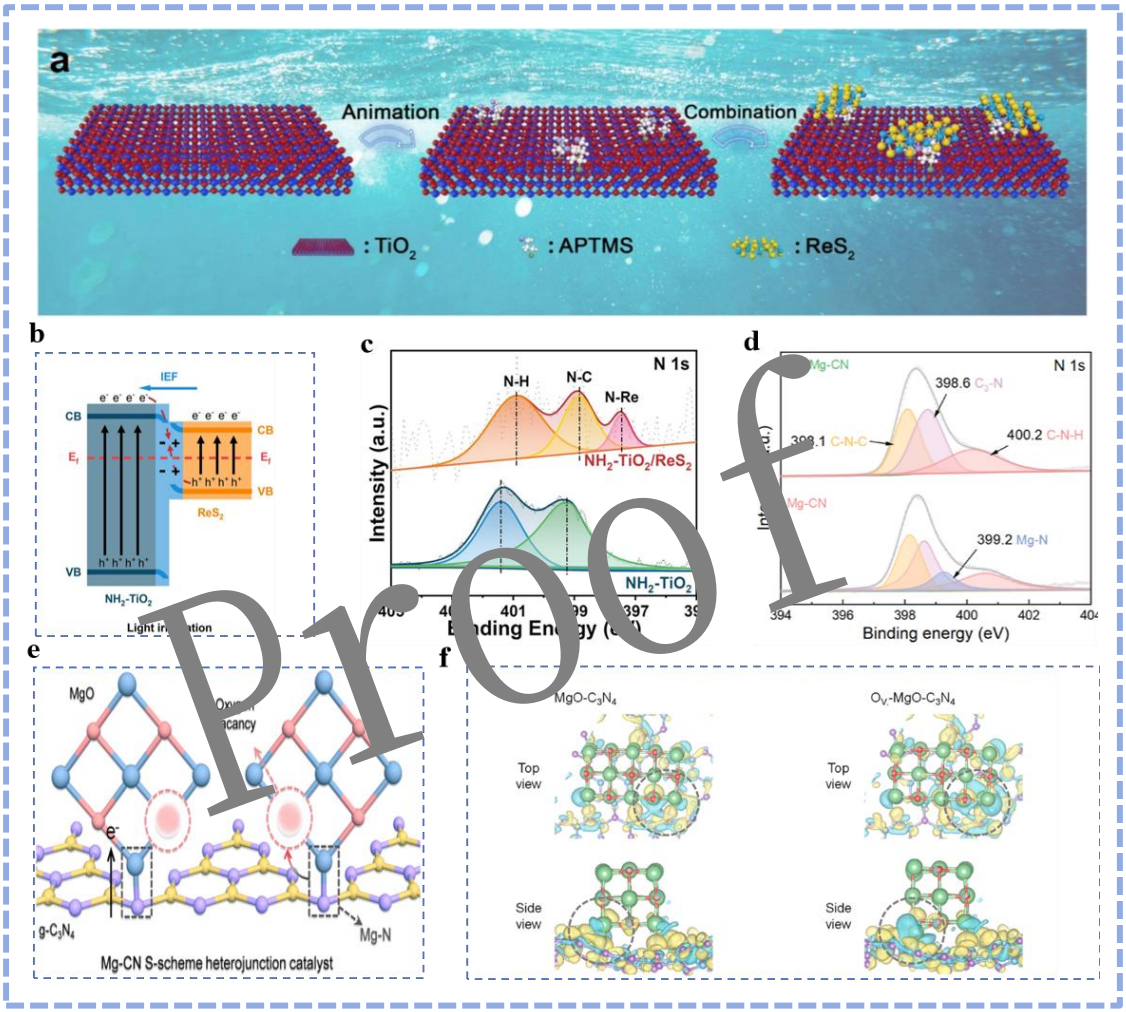

Fig 17. (a) Synthetic process of NH_2-TiO_2/ReS_2 photocatalysts. (b) The molecular-connected heterojunction charge transfer mechanism of NH_2-TiO_2/ReS_2. (c) High-resolution XPS of N_{1s}.[88] (d) High-resolution XPS spectra for N_{1s}. (e) Graphical Abstract of MgO/g-C_3N_4 System. (f) differential charge density of MgO–C_3N_4 and O_V-MgO-C_3N_4.[140]

A representative molecularly bridged system is the 2D/2D NH_2-TiO_2/ReS_2 S-scheme heterojunction.[88]In this system, APTMS was used to introduce amino groups onto the TiO_2 surface, creating a molecular bridge between TiO_2 and ReS_2 (Fig17.a). XPS (Fig17.c) analysis verified the formation of Ti–O–Si and N–Re interfacial linkages, and charge-density-difference calculations further revealed pronounced electron redistribution between APTMS and ReS_2. Such molecularly

mediated interfacial coupling lowered the charge-transfer resistance and modulated the work function of TiO_2, thereby shifting TiO_2/ReS_2 from type-I band alignment to an S-scheme charge-transfer pathway. As a result, NH_2-TiO_2/ReS_2 delivered markedly enhanced H_2 evolution activity and favorable cycling stability.

Collectively, these examples suggest that interfacial chemical bonding plays a role beyond simple structural reinforcement. By integrating structural connection, electronic coupling, built-in electric field modulation, and directional carrier migration, interfacial bonding can substantially improve charge separation, interfacial transport kinetics, and structural robustness in 2D/2D S-scheme heterojunctions. Accordingly, interfacial bonding engineering represents an important strategy for the rational design of high-performance 2D/2D S-scheme photocatalysts.

5.3 Element Doping

Elemental doping represents an effective atomic-level strategy for enhancing the photocatalytic performance of 2D/2D S-scheme heterojunctions.[141] By incorporating metal or nonmetal dopants into the semiconductor lattice, key electronic properties, including the work function, Fermi level, band gap, defect states, and local charge distribution, can be effectively modulated. These electronic-structure changes can further influence band bending, the built-in electric field, and the directional migration of photogenerated carriers at the heterointerface.[139] For S-scheme heterojunctions, the primary role of elemental doping is to optimize band alignment and interfacial charge transfer, while simultaneously regulating the adsorption/desorption behavior of reaction intermediates. This enables the preserved high-energy electrons and holes to participate more efficiently in surface redox reactions.[141]

A representative case is the 2D/2D $SnNb_2O_6$/Ni-doped $ZnIn_2S_4$ (Fig18.a) S-scheme heterojunction.[142] DOS analysis (Fig18.b, c) shows that pristine $ZnIn_2S_4$ (ZIS) has a clear band gap and limited electronic states near the Fermi level, whereas Ni-doped ZIS exhibits dopant-induced defect states close to the Fermi level. These Ni-related states reconstruct the electronic structure of ZIS, narrow the effective band gap, and provide additional pathways for photoinduced charge excitation and transfer. Meanwhile, Ni doping modulates the local electronic environment of ZIS, thereby improving its surface HER kinetics. After coupling with $SnNb_2O_6$ (SNO), the work-function difference between Ni-doped ZIS and SNO drives electron transfer from Ni-doped ZIS to SNO, resulting in the formation of a built-in electric field. Under illumination, this field facilitates the preferential recombination of low-energy electrons in SNO with holes in Ni-doped ZIS, while retaining highly reductive electrons in Ni-doped ZIS for H_2 evolution. This example highlights that

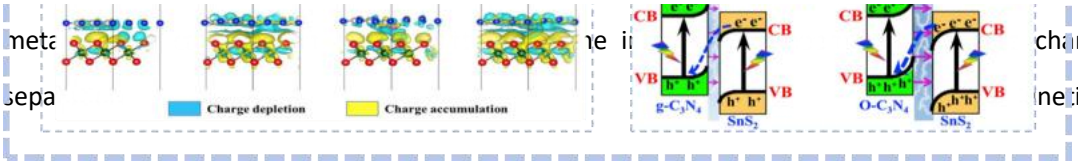

Fig 18. (a) Synthesis of SNO/Ni-ZIS S-Scheme Heterojunction Photocatalysts (b) DOS profiles of (b) ZIS and (c) Ni-ZIS. (d) Charge transfer process in SNO/Ni-ZIS S-scheme heterojunction.[142] (e) Charge density difference of the composite systems. The isosurface value is 0.0002 e A^{-3}. (f) Electron transfer caused by different Fermi levels. Photocatalytic mechanism of S-scheme g-C_3N_4/SnS_2 and O–C_3N_4/SnS_2 heterojunctions.[141]

Another representative example involves nonmetal-doped g-C_3N_4/MS_2 (M = Sn or Zr) 2D/2D S-scheme heterojunctions.[141] DFT calculations (Fig18.e) revealed that O or S doping lowered the work function and upshifted the Fermi level of g-C_3N_4, thereby increasing the Fermi-level offset relative to SnS_2/ZrS_2. This enlarged Fermi-level difference promoted interfacial electron transfer, as reflected by the increase in Bader charge transfer (Fig18.f) from 0.015–0.049 e to 0.179–0.243 e. Meanwhile, the built-in electric field was enhanced from 1.32×10^9–2.80×10^9 V m^{-1} to 4.98×10^9–7.11×10^9 V m^{-1}. Such a strengthened internal field promoted the selective recombination of low-energy carriers while retaining high-energy electrons and holes for surface redox reactions. Experimentally, the H_2 evolution rate of O-doped g-C_3N_4/SnS_2 increased from 38 to 154 μmol/g/h, further confirming that nonmetal doping can amplify the built-in field-driven charge separation in S-scheme heterojunctions.[141]

Collectively, these cases indicate that elemental doping goes beyond simple compositional modification and serves as an atomic-level strategy for tuning electronic structure, defect states, built-in electric fields, and surface adsorption behavior in S-scheme heterojunctions. Ni doping mainly improves the reductive capability and H_2 adsorption/desorption kinetics of $ZnIn_2S_4$, whereas O or S doping upshifts the Fermi level of g-C_3N_4 and strengthens interfacial electron transfer. In this regard, elemental doping provides an effective route to couple band-structure modulation, built-in electric field enhancement, charge-separation optimization, and surface reaction kinetics regulation, thereby improving the photocatalytic performance of 2D/2D S-scheme systems

5.4 Defect Engineering

Defect engineering represents an important atomic-level approach for improving the photocatalytic performance of 2D/2D S-scheme heterojunctions. Rather than merely increasing the density of active sites, controlled vacancy formation can modulate the local electronic structure, thereby enhancing light absorption, interfacial charge migration, and reactant adsorption/activation.[143] In S-scheme heterojunctions, surface vacancies can cooperate with the

built-in electric field to promote the selective recombination of low-energy carriers at the interface, while preserving high-energy electrons or holes for surface redox reactions.[144] [145] This coupling enables the simultaneous optimization of charge separation, surface activation, and product selectivity.

A representative case is the Br-vacancy-engineered $H_2WO_4/Cs_2AgBiBr_6$ (HWO/CABB) 2D/2D S-scheme heterojunction.[145] Zhou et al. constructed a strongly coupled HWO/CABB interface via acid cleavage of Bi_2WO_6 followed by in situ epitaxial growth of $Cs_2AgBiBr_6$ (Fig19.a). The obtained heterostructure featured surface Br vacancies together with Bi–O/Ag–O interfacial linkages. EPR (Fig19.b) and elemental ratio analyses confirmed the presence of Br vacancies, while interfacial bonding and charge redistribution supported the formation of an S-scheme charge-transfer pathway. DFT (Fig19.d) calculations revealed that Br vacancies strengthened CO_2 adsorption/activation, reduced the formation barriers of COOH and CHO, and promoted multi-electron CO_2 reduction toward CH_4. Notably, the barrier for CHO* formation was lower than that for CO desorption, favoring further hydrogenation toward CH_4 rather than CO release (Fig19.e). As a result, HWO/CABB delivered a CH_4 production rate of 22.6 μmol/g/h with a CH_4 selectivity of 86.1%, demonstrating the effectiveness of Br-vacancy engineering in optimizing CO_2 activation and intermediate conversion pathways.

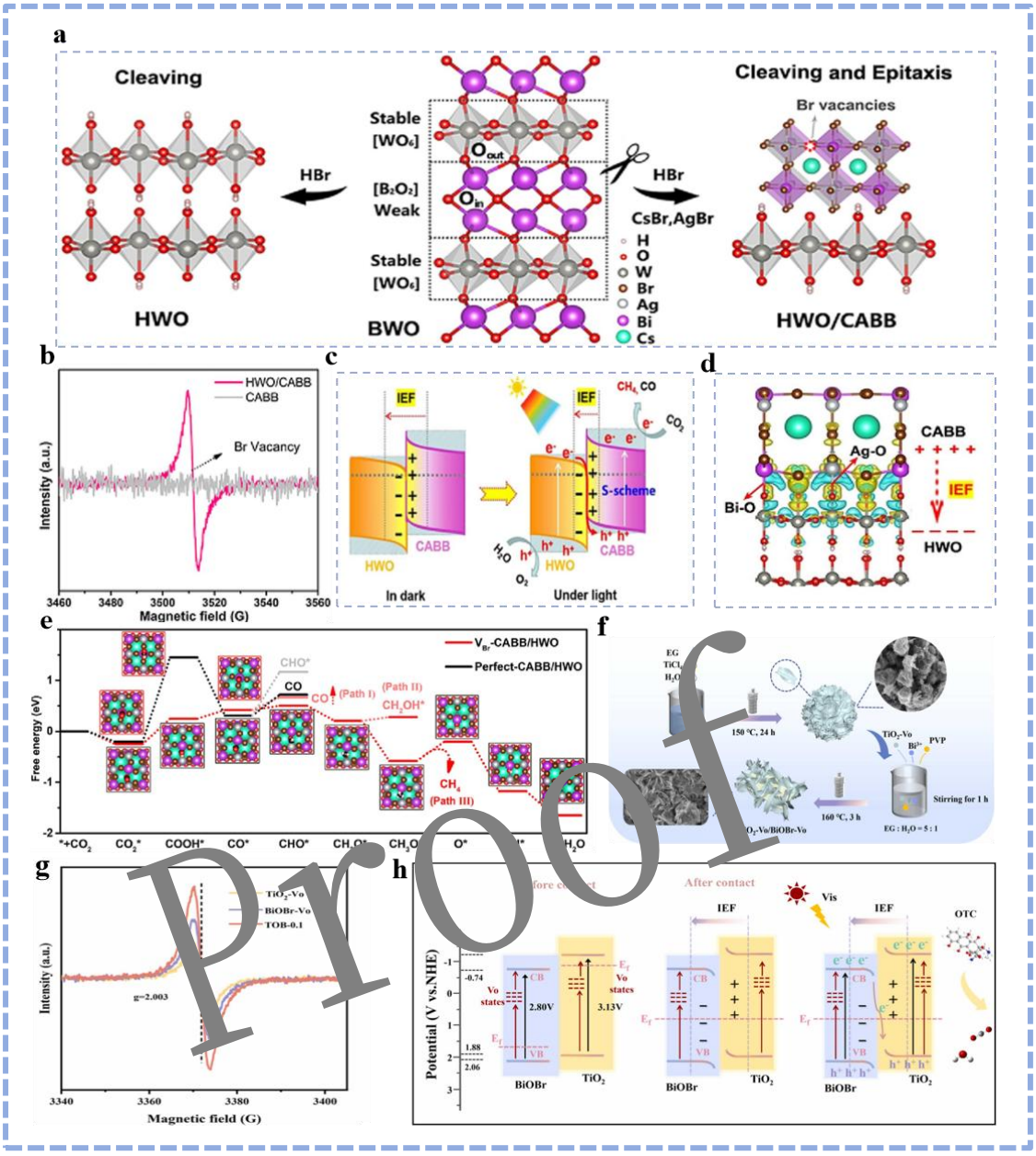

Fig 19. (a) Schematic illustration of the conversion process from 2D BWO NS to 2D/2D HWO/CABB heterojunction. (b) low-temperature EPR spectra of CABB and HWO/CABB. (c) Proposed charge transfer mechanism for the HWO/CABB heterojunction under dark and light. (d) electron density redistribution at the interface between HWO and CABB in HWO/CABB. (e) Free energy diagrams of CO_2 photoreduction to CH_4 for HWO/CABB (with and without V_{Br}).[145] (f) Schematic illustration of the fabrication procedure for 2D/2D TiO_2-Vo/BiOBr-Vo. (g) EPR spectra of the samples. (h) Schematic diagram of charge transfer mechanism in the TOB-0.1 heterostructure for OTC removal under visible-light illumination.[146]

Another representative example is the dual-oxygen-vacancy-engineered TiO_2-Vo/BiOBr-Vo (Fig19.f) 2D/2D S-scheme heterojunction.[146] Tian et al. introduced oxygen vacancies into both TiO_2 and BiOBr, with abundant vacancies in TOB-0.1 confirmed by EPR (Fig19.g). These vacancy-induced defect states broadened visible-light absorption. Upon interfacial contact, the Fermi-level

difference between TiO_2-Vo and BiOBr-Vo generated a built-in electric field, driving S-scheme charge transfer while preserving high-energy electrons and holes for photocatalytic reactions (Fig19.h). The oxytetracycline degradation rate constant reached 0.030 min^{-1}, which was 3.75 and 1.76 times those of TiO_2-Vo and BiOBr-Vo, respectively. Trapping and ESR results confirmed h^+ and $\bullet O_2^-$ as the main reactive species, indicating that oxygen vacancies enhance pollutant degradation by improving light absorption, charge separation, and reactive oxygen species generation.

Collectively, defect engineering provides an effective route to tailor the interfacial electronic structure and surface reaction microenvironment of 2D/2D S-scheme heterojunctions. Vacancies can serve as atomic-scale regulatory centers that bridge S-scheme interfacial charge migration with surface catalytic processes. Therefore, rational defect engineering can integrate electronic-structure modulation, interfacial charge-transfer regulation, and surface-reaction optimization, offering a versatile strategy for improving the photocatalytic performance of 2D/2D S-scheme systems.

5.5 Interfacial Cocatalyst Engineering

S-scheme heterojunctions enable the selective recombination of low-energy carriers through built-in electric fields and band bending, while preserving highly reducing electrons and strongly oxidizing holes for surface redox reactions. Nevertheless, efficient charge separation can be converted into enhanced catalytic performance only if these energetic carriers are effectively extracted and consumed at reactive surface sites. Therefore, incorporating cocatalysts into 2D/2D S-scheme heterojunctions represents an effective strategy to improve charge utilization, reduce reaction barriers, and modulate product selectivity. In general, cocatalysts serve as charge-carrier trapping centers, surface active sites, and interfacial charge-transfer mediators.[147,148]

A representative example is the Ag/AgO-modified 2D/2D g-C_3N_4/$Ni_3V_2O_8$ S-scheme heterojunction. [149] In this heterostructure, g-C_3N_4 and $Ni_3V_2O_8$ establish a 2D/2D p–n S-scheme interface, while Ag/AgO nanoparticles act as cocatalysts to facilitate carrier trapping/extraction, suppress charge recombination, enhance visible-light harvesting, and provide surface catalytic sites. Consequently, the optimized composite achieved ciprofloxacin and amoxicillin removal efficiencies of 58.8% and 62.1%, respectively, with $\bullet O_2^-$ and h^+ identified as the dominant reactive species. This result demonstrates that Ag/AgO enhances pollutant degradation by integrating interfacial charge separation with reactive-species generation.

Non-noble-metal cocatalysts can also promote S-scheme H_2 evolution. Hua et al.[87] constructed a Ni_2P-modified 2D/2D $SnNb_2O_6$/CdS-D S-scheme heterojunction (Fig20.e), where

$SnNb_2O_6$ (SNO) and CdS-D formed the 2D/2D S-scheme interface and Ni_2P served as the HER cocatalyst. [87] Ni_2P loading increased the H_2-evolution rate from 7808 to 11992 μmol/g/h. XPS and DFT analyses revealed a CdS-D → SNO → Ni_2P charge-transfer pathway, indicating that Ni_2P functioned as both an electron-accumulation center and a HER active site. Thus, Ni_2P accelerated electron extraction and promoted surface H_2-evolution kinetics.

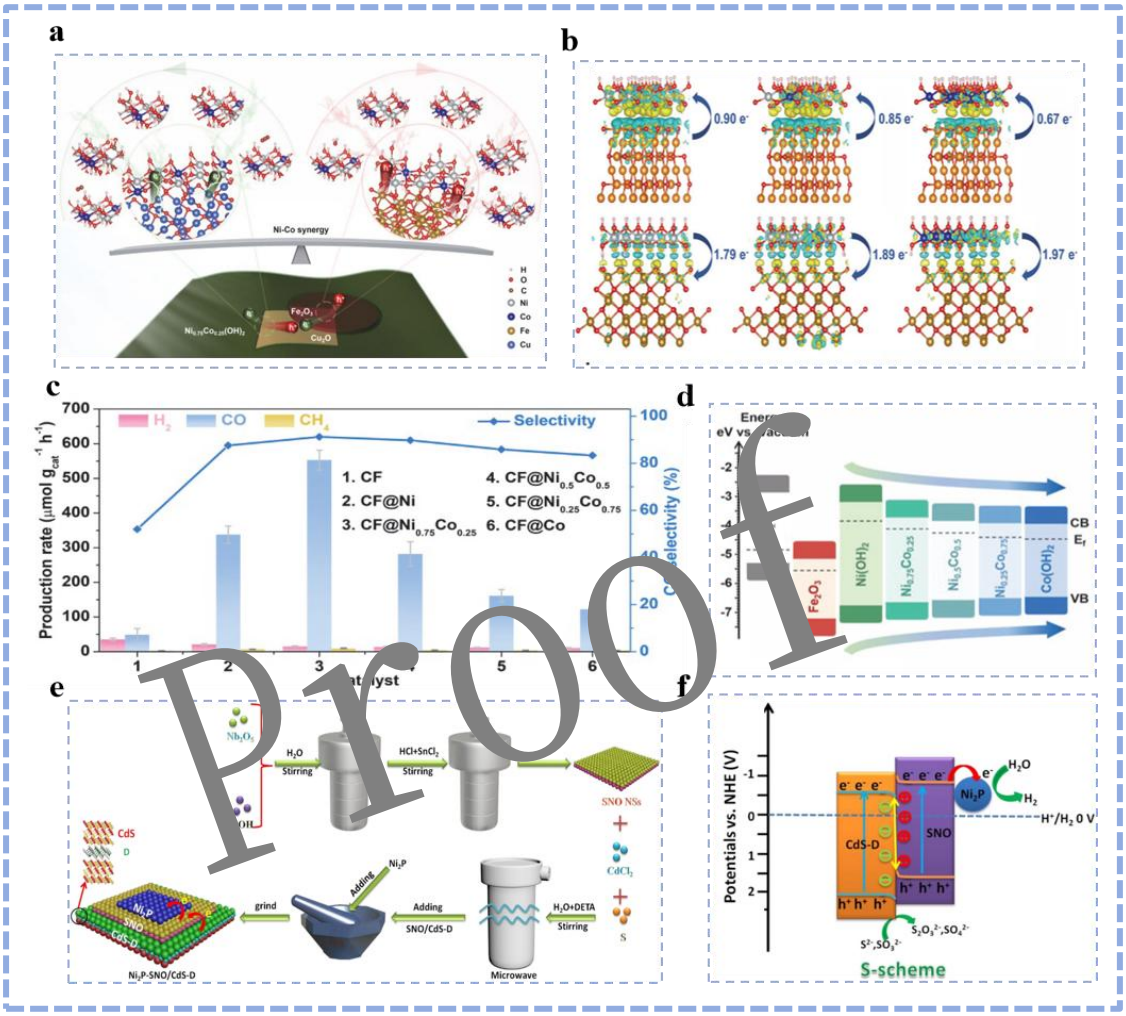

Fig 20. (a) Graphical abstract of the $Cu_2O/Fe_2O_3@Ni_xCo_{1-x}(OH)_2$ system. (b) DFT calculations on Ni-Co synergistic mechanisms. (c) Photocatalytic performance of CF@NiCo. (d) band structures (f) of Cu_2O, Fe_2O_3, and $Ni_xCo_{1-x}(OH)_2$.[56] (e) Schematic diagram of the synthesis of Ni_2P-SNO/CdS-D nanocomposite. (f) The proposed photocatalytic mechanism of Ni_2P-SNO/CdS-D nanocomposite under visible light ($\lambda > 420$ nm).[87]

For artificial photosynthesis, cocatalyst design should address both reduction and oxidation half-reactions. A representative example is the $Cu_2O/Fe_2O_3@Ni_xCo_{1-x}(OH)_2$ 2D/2D S-scheme system[56], in which Cu_2O and Fe_2O_3 nanosheets construct the S-scheme heterojunction, while in situ-grown Ni–Co bimetallic hydroxide acts as a bifunctional cocatalyst (Fig20.a). The $Ni_xCo_{1-x}(OH)_2$ cocatalyst promotes both CO_2 reduction and H_2O oxidation, facilitates interfacial charge transfer,

and suppresses side reactions and photocorrosion. In particular, appropriate Co incorporation modulates the band structure and d-band center, balances electron/hole extraction, and enhances CO_2 and H_2O adsorption/activation. Consequently, the optimized CF@$Ni_{0.75}Co_{0.25}$ delivered a CO production rate of 552.7 μmol/gcat/h, an O_2 production rate of 313.0 μmol/gcat/h, and a CO selectivity of 91.4% (Fig20.c). DFT calculations (Fig20.b) further revealed reduced reaction barriers for both CO_2-to-CO reduction and H_2O-to-O_2 oxidation, highlighting the importance of bifunctional cocatalyst engineering in overall artificial photosynthesis.

Overall, cocatalyst engineering provides an effective link between S-scheme charge separation and surface reaction kinetics. In 2D/2D S-scheme heterojunctions, suitable cocatalysts can extract and accumulate energetic carriers, create reaction-specific active sites, lower kinetic barriers, and direct interfacial reactions toward targeted pathways. Therefore, rational cocatalyst design should go beyond suppressing charge recombination and should instead coordinate carrier utilization with reaction-specific requirements, including reactive-species generation, H_2 evolution, CO_2 conversion, and coupled redox processes.

5.6 Single-Atom Engineering

Single-atom engineering provides an atomically precise approach for improving 2D/2D S-scheme heterojunctions.[150] Compared with conventional nanoparticle cocatalysts, atomically dispersed metal sites offer well-defined coordination structures, maximized metal utilization, and tunable local electronic environments. In S-scheme systems, such isolated sites can function as electron-trapping centers, interfacial charge-transfer nodes, and catalytic centers for surface reactions. Therefore, the significance of single-atom engineering lies not only in the incorporation of isolated metal atoms, but also in coupling these sites with the charge-migration and surface-reaction pathways of 2D/2D S-scheme heterojunctions. This coupling enables more efficient interfacial charge separation, site-directed carrier trapping, and reactant adsorption/activation.[151]

A representative example is the single-Ni-atom-anchored Ti-MOF/$BiVO_4$ 2D/2D S-scheme heterojunction.[150] In this system, atomically dispersed Ni (II) sites were immobilized within the coordination microenvironment of NTU-9 Ti-MOF, and the obtained Ni@MOF nanosheets were coupled with $BiVO_4$ nanosheets to construct an ultrathin 2D/2D S-scheme heterojunction (Fig21.a). The Ti-MOF component not only contributes to S-scheme charge separation but also provides a stable coordination environment and a CO_2-enriched local microenvironment for the isolated Ni sites, whereas $BiVO_4$ provides strongly oxidizing holes for water oxidation. XANES (Fig21.b) and EXAFS (Fig21.c) analyses confirmed that Ni was atomically dispersed in a dominant Ni–O_5

coordination configuration. In situ DRIFTS (Fig21.e) combined with DFT calculations (Fig21.f) indicated that the isolated Ni sites facilitated CO_2 adsorption and stabilized key Ni–COO* and Ni–COOH* intermediates, thereby lowering the kinetic barrier for selective CO formation. Consequently, the optimized Ni@6MOF/BVO exhibited a CO_2-to-CO photoconversion activity approximately 66-fold higher than that of $BiVO_4$ nanoparticles in pure water, along with a CO selectivity of 99.2%. This example suggests that coupling atomically dispersed active sites with tailored coordination microenvironments can effectively convert the charge-separation capability of 2D/2D S-scheme heterojunctions into enhanced CO_2 activation and selective CO production.

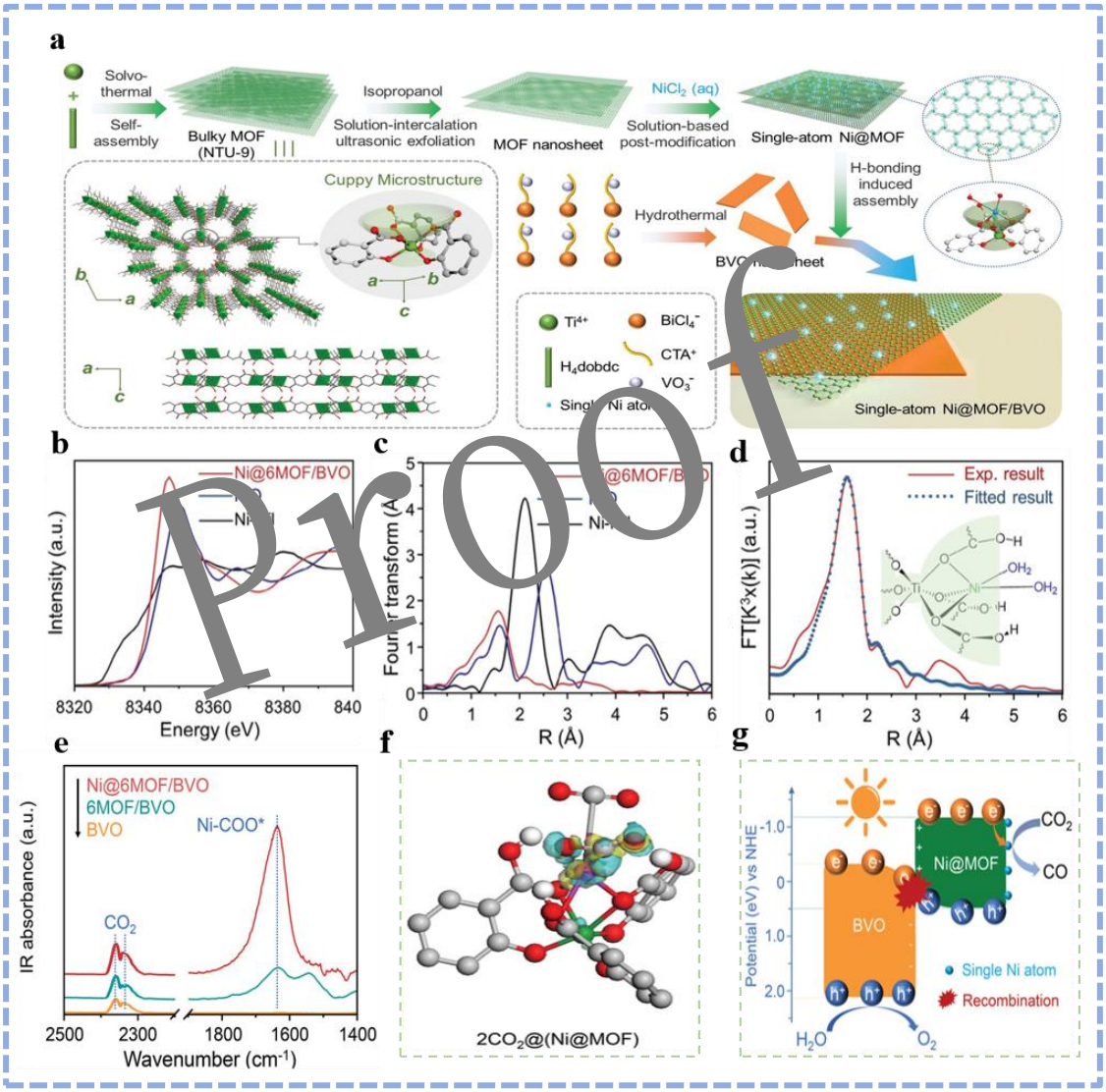

Fig 21. (a) Synthetic illustration of the single-atom Ni@MOF/BVO heterojunction photocatalyst. (b) Normalized XANES spectra of Ni@6MOF/BVO, NiO, and Ni-foil, respectively, at the Ni K-edge. (c) Fourier transformation of EXAFS spectra at the Ni K-edge. (d) The corresponding EXAFS fitting curves and simulated structure model of single-atom Ni site immobilized in the cuppy microstructure (light green) of MOF (inset). (e) DRIFTS for adsorption of gaseous CO_2/H_2O mixture on BVO, 6MOF/BVO, and Ni@6MOF/BVO in dark for 60 min. (f) Differential charge analysis of $2CO_2$@[Ni@MOF]. (g) Illustration of proposed photocatalytic

mechanism of Ni@6MOF/BVO based on S-scheme charge transfer for CO_2 conversion under the UV–vis light irradiation.[150]

Another representative example is the La-single-atom/dual-vacancy-engineered WS_{2-x}/La_1-$WO_{2.9}$ 2D/2D S-scheme heterojunction.[151] n this system, La single atoms and O/S dual vacancies were incorporated into an *in situ* formed $WS_{2-x}/WO_{2.9}$ 2D interface, integrating single-atom, defect, and S-scheme interface engineering. AC-HAADF-STEM and La L_3-edge EXAFS analyses confirmed atomically dispersed La species with La–O coordination, whereas EPR verified the presence of O/S vacancies. KPFM and in situ XPS results suggested that La single atoms enhanced the built-in electric field and acted as interfacial charge-transfer mediators. DFT calculations and in situ FTIR further indicated that this atomic-level regulation promoted N_2 adsorption/activation and favored an alternating hydrogenation pathway. Consequently, WS_{2-x}/La_1-$WO_{2.9}$ delivered an NH_3 generation rate of 124.9 μmol/g/h, highlighting the synergistic role of La single atoms, dual vacancies, and S-scheme charge transfer in photocatalytic N_2 fixation.

Collectively, single-atom engineering can be regarded as an atomically precise strategy for integrating interfacial charge-transfer regulation with surface reaction control in 2D/2D S-scheme heterojunctions. Atomically dispersed sites can function as electron-trapping centers and interfacial charge-transfer nodes, thereby facilitating the extraction and utilization of high-energy carriers retained through the S-scheme charge-transfer pathway. Future studies should further emphasize the coordinated optimization of single-atom anchoring sites, coordination structures, interfacial locations, and local reaction microenvironments. The integration of advanced in situ/operando characterizations with theoretical calculations will be essential for establishing reliable structure–charge transfer–reactivity relationships and for guiding the rational design of highly selective 2D/2D S-scheme photocatalysts.

5.7 Interfacial Strain Engineering

Interfacial strain engineering has emerged as an effective approach for modulating the band structure, built-in electric field, and surface reaction kinetics of 2D/2D S-scheme heterojunctions. In atomically thin materials, tensile or compressive strain can be introduced by lattice mismatch, van der Waals interlayer coupling, substrate interactions, or external mechanical perturbations, thereby altering local atomic configurations and interfacial electronic states.[152] Unlike doping, defect engineering, or cocatalyst modification, strain engineering allows continuous regulation of band gaps, band-edge positions, carrier transport properties, and adsorption energetics of key intermediates without substantially changing the chemical composition of the photocatalyst. Appropriate interfacial strain can therefore strengthen the built-in electric field, promote the

selective recombination of low-energy carriers, and reduce the kinetic barriers of surface reactions such as HER, OER, and CO_2 reduction.[153,154]

The Ga_2SSe/SnS_2[153] van der Waals heterojunction provides a representative theoretical model for strain-regulated 2D/2D S-scheme photocatalysts. As illustrated in Fig22.g, the built-in electric field at the interface drives an S-scheme charge-transfer pathway, enabling low-energy carriers to recombine while preserving electrons and holes with strong redox potentials. More importantly, this system reveals a strain-dependent balance between surface reaction kinetics and band-edge energetics. Tensile strain markedly improves HER kinetics, as reflected by the decrease in ΔG_H^* from 1.601 eV under −6% compressive strain to 0.405 eV under 6% tensile strain, approaching a more favorable hydrogen adsorption state (Fig22.h). However, tensile strain also shifts the CBM of Ga_2SSe downward and the VBM of SnS_2 upward, meaning that excessive strain may compromise the redox driving force required for overall water splitting (Fig22.i). This example highlights that interfacial strain engineering should be optimized within an appropriate window, rather than simply maximized, to balance light absorption, band-edge alignment, redox capability, and reaction barriers.

The strain-induced g-C_3N_4/ZnO heterojunction[155] further demonstrates that stress regulation can serve as an effective approach to inducing S-scheme heterojunction formation. As shown in Fig22.j, increasing the lattice parameter of the heterostructure continuously changes the work function and band alignment, leading to an S-scheme band configuration favorable for overall water splitting at a lattice parameter of 7.13 Å. In this configuration, strongly reductive electrons are retained on g-C_3N_4, whereas strongly oxidative holes remain on ZnO. The charge-density difference and planar-averaged charge-density profiles further reveal the formation of a built-in electric field from g-C_3N_4 to ZnO (Fig22.k), which promotes the recombination of low-energy electrons in ZnO with holes in g-C_3N_4 and establishes the S-scheme charge-transfer pathway. This example suggests that stress engineering can not only optimize existing S-scheme heterojunctions, but also induce S-scheme charge-transfer dynamics by regulating band alignment and interfacial electric fields.

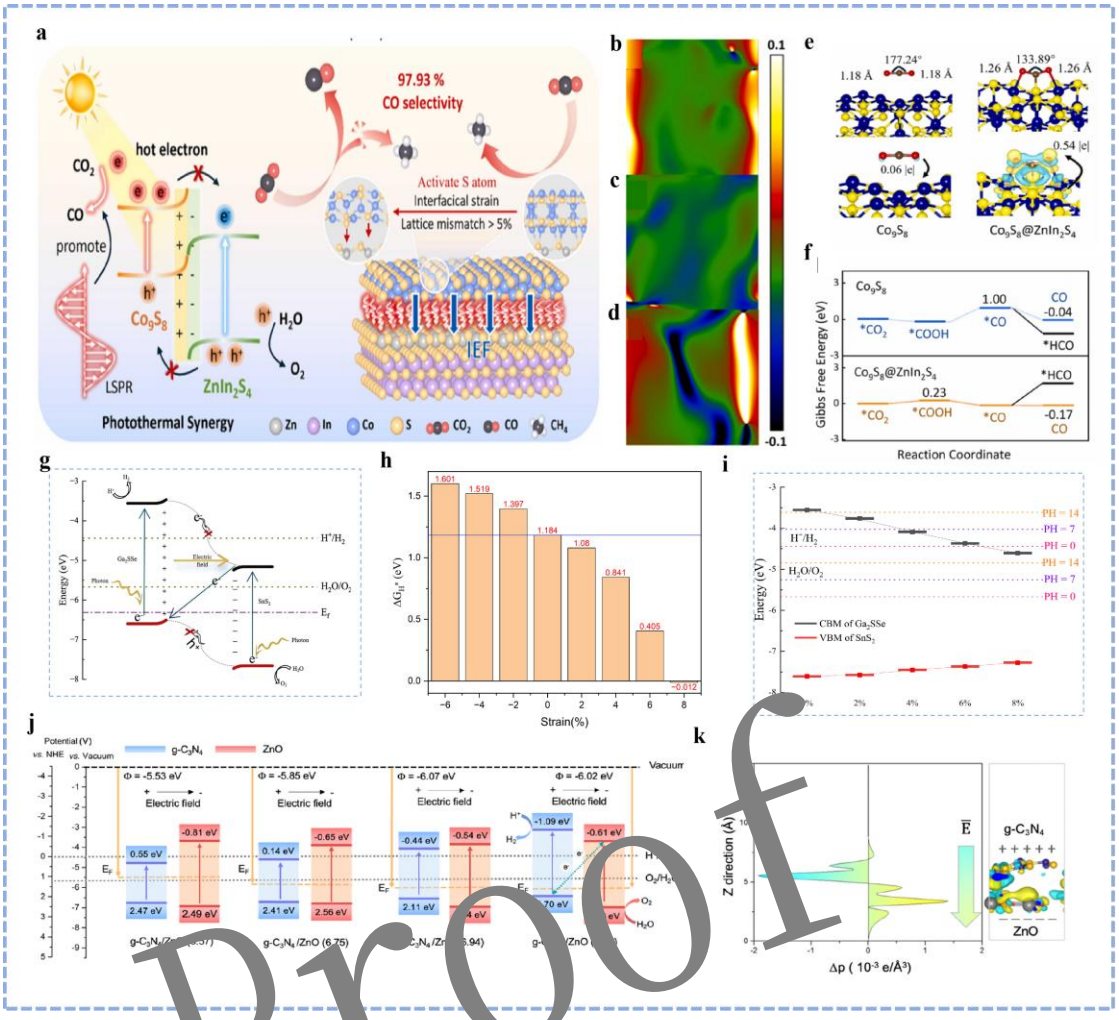

Fig 22. (a) Schematic of the mechanism for CO_2 photoreduction into CO over Co_9S_8@$ZnIn_2S_4$ (b-d) GPA (geometric phase analysis) patterns in εxx direction of $ZnIn_2S_4$, Co_9S_8, and Co_9S_8@$ZnIn_2S_4$. (e) Adsorption configurations and differential charge density plots of CO_2 on the surfaces of Co_9S_8 and Co_9S_8@$ZnIn_2S_4$, (f) Gibbs free energy diagram of the photocatalytic CO_2 reduction on pure Co_9S_8 and Co_9S_8@$ZnIn_2S_4$.[154] (g) Schematic illustration of band alignment and charge transfer mechanism in the Ga_2SSe/SnS_2 heterojunction. (h) ΔG_H* of HER free energy profiles under varying strains. (i) CBM and VBM positions of Ga_2SSe and SnS_2 under applied tensile strains.[153](j) Band alignments of g-C_3N_4/ZnO heterostructures with different lattice parameters. (k) Charge density difference and planar-averaged electron density difference Δρ(z) of the g-C_3N_4/ZnO heterostructure with a cell parameter of 7.13 Å. The yellow and cyan areas indicate electron accumulation and depletion, respectively.[155]

In addition to these 2D/2D theoretical models, the Co_9S_8@$ZnIn_2S_4$ system[154] provides experimental evidence for interfacial stress regulation. In this system, the lattice mismatch between Co_9S_8 and $ZnIn_2S_4$ induces localized interfacial strain, with GPA results showing that the strain is mainly concentrated at the heterointerface (Fig22.b–d). This interfacial stress not only regulates the charge-transfer direction and favors the formation of the S-scheme built-in electric field, but also reconstructs the surface reactive sites. Specifically, CO_2 adsorption configurations

and charge-density-difference analysis show that stress-induced surface reconstruction transforms the active motif of Co_9S_8 from Co–Co to Co–S–Co. As a result, CO_2 adsorption changes from a nearly linear configuration to a distinctly bent adsorption geometry, accompanied by an increase in electron transfer from 0.06 e to 0.54 e, indicating substantially enhanced CO_2 activation (Fig22.e). Free-energy calculations further show that Co_9S_8@$ZnIn_2S_4$ lowers the key barrier for CO_2 reduction and favors *CO desorption over further hydrogenation (Fig22.f), ultimately enabling highly selective photothermal reduction of low-concentration CO_2 (Fig22.a). This system demonstrates that interfacial stress can regulate not only charge dynamics but also active-site configurations and reaction selectivity.

Overall, interfacial strain engineering enables the coordinated optimization of S-scheme charge transfer and surface reactions through lattice distortion, band-structure modulation, built-in electric-field reconstruction, and reaction-barrier regulation. Future studies should focus on controllable methods for introducing and stabilizing interfacial strain, combined with GPA strain mapping, in situ/operando spectroscopy, and theoretical calculations to establish quantitative correlations among strain states, interfacial electric fields, charge-transfer pathways, and catalytic activity.

5.8 Facet engineering

Facet engineering has emerged as an effective strategy for atomic-level interface design in 2D/2D S-scheme heterojunctions. Different crystal facets generally possess distinct atomic arrangements, surface energies, work functions, surface potentials, and reactant adsorption behaviors, which can directly affect interfacial contact geometry, band bending, built-in electric-field strength, and interfacial charge-transfer resistance.[156] Compared with conventional heterojunction construction, facet engineering emphasizes the precise regulation of interfacial contact planes. By selectively exposing specific facets or constructing oriented facet-to-facet coupling, the interfacial electronic structure and S-scheme charge-transfer pathway can be rationally modulated.[157] This strategy therefore links controllable synthesis, interface-structure design, and charge-dynamics optimization, providing a rational route for developing high-performance 2D/2D S-scheme photocatalysts.[158,159]

The $ZnIn_2S_4$/BiOBr S-scheme heterojunction[158] provides a representative example of interfacial facet regulation. By growing $ZnIn_2S_4$ in situ on BiOBr nanosheets dominated by either the (010) or (001) facet, ZIS/BOB-(010) and ZIS/BOB-(001) heterojunctions were constructed, respectively (Fig23.a). Compared with ZIS/BOB-(010), ZIS/BOB-(001) exhibits a larger Fermi-level

difference, a stronger built-in electric field, and more pronounced band bending. These features accelerate the interfacial recombination of charge carriers with weak redox ability, while more effectively preserving electrons and holes with strong redox potentials on $ZnIn_2S_4$ and BiOBr, respectively, for photocatalytic H_2 evolution (Fig23.c). This result indicates that the selection of interfacial facets not only determines the structural contact mode of the heterojunction but also serves as a key parameter for tuning S-scheme charge migration and built-in electric-field strength.

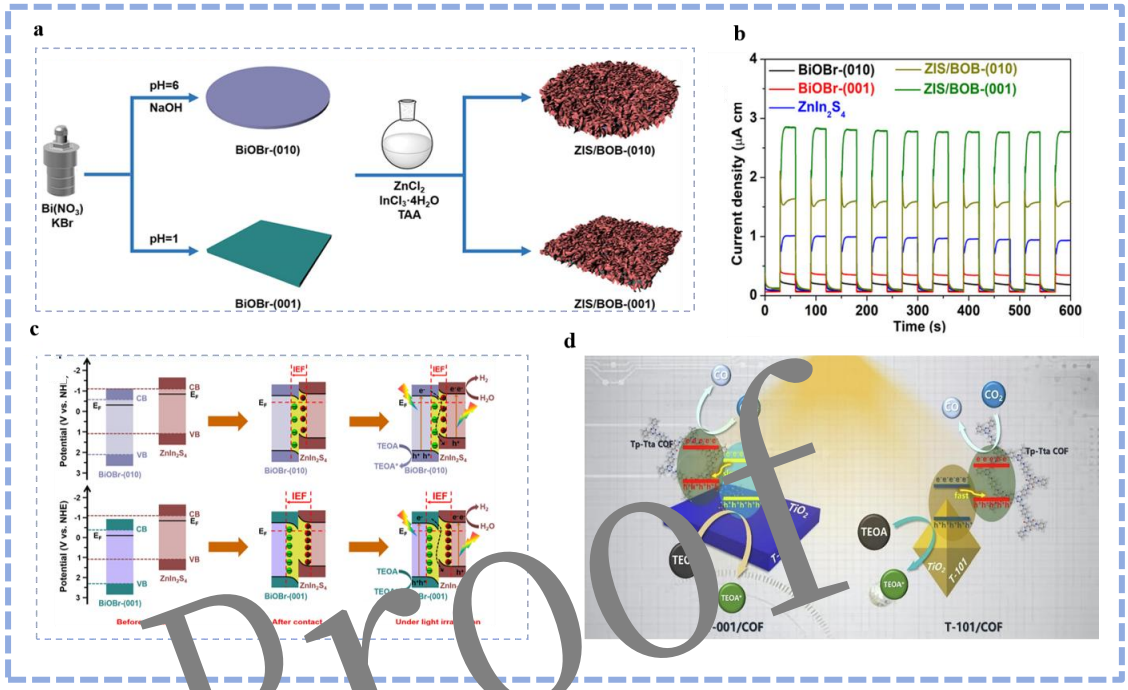

Fig 23. (a) Schematic Illustrating the Synthesis of ZIS/BOB Heterojunctions. (b) Charge kinetics analysis of ZIS/BOB and reference samples. (c) schematic illustrating the photocatalytic mechanisms in ZIS/BOB-(001) and ZIS/BOB-(010) heterojunctions: energy band diagrams, IEF-induced charge transfer/separation, and the formation of S-scheme heterojunctions under light irradiation for H_2 evolution.[158] (d) Schematic diagram of the relative band energy position and S-scheme charge transfer mechanism between Tp-Tta COF and TiO_2.[159]

The TiO_2/COF S-scheme heterostructure[159] further illustrates the role of facet effects in CO_2 photoreduction. By assembling two-dimensional Tp-Tta COF onto TiO_2 dominated by either (001) or (101) facets, T-001/COF and T-101/COF heterostructures were obtained. Compared with T-001/COF, T-101/COF exhibits more efficient interfacial charge separation and transfer. This improvement is mainly attributed to the electron-rich surface and more suitable conduction-band position of (101)-faceted TiO_2, which favor S-scheme recombination between electrons in the TiO_2 conduction band and holes in the COF valence band. As a result, electrons with strong reduction ability are retained on COF for CO_2 reduction. Consequently, T-101/COF achieves a higher CO evolution rate and selectivity, demonstrating that facet engineering can modulate not only interfacial charge dynamics but also reactant adsorption and product selectivity.

Overall, facet engineering enables the coordinated regulation of built-in electric fields, band bending, charge migration, and surface reactions in S-scheme heterojunctions by controlling exposed facets, interfacial contact orientation, and facet-dependent electronic structures. Future studies should focus on facet-controlled synthesis, oriented assembly, and atomic-level interface characterization, combined with in situ spectroscopy, potential mapping, and theoretical calculations to clarify how specific facet contacts influence Fermi-level equilibration, S-scheme charge-transfer pathways, and reaction kinetics. Such efforts will help advance 2D/2D S-scheme heterojunctions from empirical interface construction toward rational interface design.

6. Applications

Owing to their intimate face-to-face interfaces and S-scheme charge-transfer characteristics, 2D/2D S-scheme heterojunctions have been widely investigated for solar energy conversion and environmental remediation. The 2D/2D configuration is conducive to shortening carrier-migration distances and providing abundant interfacial charge-transfer pathways, while the S-scheme pathway may help maintain relatively strong redox capability under suitable band alignment and interfacial coupling. However, their photocatalytic performance is difficult to rationalize solely from the perspective of charge separation, because different reactions involve distinct thermodynamic requirements, kinetic limitations, intermediate-evolution pathways, and stability concerns. Accordingly, interface construction, interfacial bonding, elemental doping, defect engineering, cocatalyst regulation, and single-atom engineering are better examined in a reaction-specific context.

This section summarizes representative applications of 2D/2D S-scheme heterojunctions in H_2 evolution, CO_2 reduction, pollutant degradation, and H_2O_2 production, with emphasis on electron utilization, regulation of product selectivity, reactive oxygen species generation, and two-electron pathway control.

6.1 Photocatalytic hydrogen evolution

Hydrogen is widely recognized as a promising clean-energy carrier, and solar-driven photocatalytic water splitting offers a potentially sustainable route for H_2 production. Efficient photocatalytic H_2 evolution generally requires appropriate band-edge positions, adequate light-harvesting capability, efficient charge separation, and abundant active sites for the hydrogen evolution reaction (HER).[160,161] However, conventional single-component photocatalysts are often limited by the intrinsic trade-off between efficient charge separation and strong redox capability, making it difficult to simultaneously achieve broad light harvesting, rapid carrier transport, and

highly reductive electrons. In recent years, 2D/2D S-scheme heterojunctions have emerged as promising candidates for photocatalytic H_2 production because they integrate the structural merits of ultrathin nanosheets with the unique charge-transfer characteristics of S-scheme systems.[2]. In photocatalytic H_2 evolution, the overall efficiency is fundamentally governed by the generation, separation, transport, and consumption of photogenerated electrons. More importantly, electrons participating in proton reduction must retain sufficiently negative reduction potentials during interfacial transfer. Unlike conventional type-II heterojunctions, which commonly weaken redox ability owing to staggered band migration, S-scheme heterojunctions enable the spatial separation of charge carriers while preserving highly reductive electrons on the reduction photocatalyst under the driving force of band bending and internal electric fields. Meanwhile, the intimate face-to-face contact in 2D/2D architectures provides enlarged interfacial areas and shortened diffusion pathways, thereby facilitating directional charge transport and suppressing carrier recombination.[162,163] As a result, the improved H_2-evolution activity of 2D/2D S-scheme photocatalysts is generally associated with the synergistic optimization of redox capability, interfacial carrier dynamics, and surface HER kinetics.

Table 1. Photocatalytic hydrogen production performance of 2D/2D S-scheme heterojunctions

Photocatalyst	Dosage	Reaction solution	Light source	Hydrogen generation rate	Ref.
WO_3/g-C_3N_4	50 mg	80 mL 20 vol% lactic acid solution.	350 W Xe lamp.λ > 420 nm	982 μmol/g/h	[27]
SNO/CdS-D	30 mg	50 mL solution containing the Na_2S (2.10 g) and Na_2SO_3 (0.78 g)	300 W Xe lamp λ > 420 nm	11,992 μmol/g/h	[87]
Pg-C_3N_4/CdS-DETA	50 mg	100 mL 0.35 M Na_2S and 0.25 M Na_2SO_3 mixed aqueous solution (0.6 wt % Pt)	300 W Xe lamp λ > 400 nm	9738 μ mol/h/g	[86]

MoS_2/CoAl	50 mg	80mL solution of methanol （5 wt% MoS_2 ）	300 W Xe lamp	17.1 μmol/g/h	[164]
Ti_3C_2/$Zn_{0.7}Cd_{0.3}S$/Fe_2O_3	5 mg	80 mL of 0.25 M Na_2SO_3 and 0.35 M $Na_2S·9H_2O$ aqueous solution	300 W Xe lamp λ > 420 nm	27.24 mmol/g/h	[135]
$NiTe_2$ /g-C_3N_4	10 mg	100 mL of 20% TEOA (triethanolamine) solution. (1.0% wt.Pt)	300 W Xe lamp	12902.9 μmol/g/h	[165]
MX-CdS/WO_3	5 mg	80 mL of 10 wt% lactic acid solution.	300 W Xe lamp λ > 400 nm	27.5 mmol/g/h	[93]
Ti_3C_2/$ZnIn_2S_4$（ZIS）/CdS	5 mg	80 mL aqueous solution (with 15% triethanolamine). （1.0% wtTi_3C_2）	300 W Xe lamp > 420 nm	8.93 mmol/g/h	[166]
TpPa-1-COF/g- C_3N_4	40 mg	100.0 mL buffer solution with 100 mg sodium ascorbate（3wt % Pt）	300 W Xe lamp λ > 420 nm	1153μmol/g/h	[85]
$ZnIn_2S_4$/g-C_3N_4/Ti_3C_2	10 mg	8 mL of triethanolamine solution was added in 72 mL of the aqueous solution	300 W Xe lamp λ > 420 nm	2452.1μmol/g/h	[167]
CuS/Ni-MOFs-P	10 mg	30 mL of sacrificial reagent (V (triethanolamine): V (deionized water) = 15%) （20 mg of photosensitizer (EY) ）	5 W LED sunlight simulation channel	3122.76μmol/g/h	[82]

NiCo-LDH/g-C_3N_4	50 mg	100 mL of mixed aqueous solution （10 ml triethanolamine (TEOA) and 90 ml deionized water	300 W Xe lamp λ > 400 nm	755 μmol/g/h	[168]
CoAl-LDHs/$ZnIn_2S_4$ S	50 mg	90 mL of deionized water, and 10 mL of triethanolamine	300 W Xe lamp λ > 420 nm	1563.64 μmol/g/h	[100]
$WS_2/Zn_3In_2S_6$	10 mg	50ml aqueous solution containing 0.35 M $Na_2S·9H_2O/NaH_2PO_2$ (1:1 of molar ratio).	300 W Xe lamp.AM 1.5G filter	30.21 mmol/g/h	[169]
$In_2S_3/g-C_3N_4$	10 mg	50 ml of DI water with 10 vol % methanol	direct solar light	2528μmol/g/h	[169]
1T′-$MoS_2/ZnIn_2S_4$	10 mg	50 mL of solution (water: lactic acid = 4:1).	300 W Xe lamp.AM 1.5G filter	11.42mmol/g/h	[170]
H_2N–Cu–MOF / TpPa-1-COF	10 mg	100 mL of deionized water containing 100 mg （Pt）	300 W Xenon lamp λ ≥ 420 nm	15.3 mmol/g/h	[171]
$ZnIn_2S_4/Bi_4Ti_3O_{12}$	10 mg	50 mL of solution (Water:Triethanolamine = 4:1), (1 wt.% of Pt)	300 W Xe lamp.AM 1.5G filter	27.05 mmol/g/h	[172]
NH_2 - TiO_2 /ReS_2	50 mg	80 mL water and 20 mL ethanol.	300 W Xe lamp	451.3μmol/g/h	[88]

Bi_2MoO_6/ Zn-TCPP	10 mg	45 mL of aqueous solution with concentration of 2 M ascorbic acid (1.0 wt%Pt)	300 W Xenon lamp λ ≥ 420 nm	10900.94 umol/g/h	[89]
Py-COF / Py-HOF	2 mg	ascorbic acid (0.1 M, 80 ml) (5.0 wt%Pt)	350 W Xe lamp.λ > 420 nm	390.68 mmol/g/h	[117]
α-Fe_2O_3/BiOBr/ MoS_2	8 –10 mg	2 mL of deionized water and 16 mL of absolute ethanol and fill up to 80 mL with mineral water	300 W Xe lamp λ > 420 nm	57 mmol/g/h	[173]
Ni-TBAPy-MOF/TpPa-COF	2 mg	100 mL of 0.1 M ascorbic acid aqueous solution	350 W Xe lamp.λ > 420 nm	276 mmol/g/h	[174]
BP/Mn_xCd_{1-x}	10mg	4.2 g of sodium sulfide and 1.58 g of sodium sulfite were dissolved in 50 mL of aqueous solution	300 W xenon lamp.320< λ < 780 nm	55.8 mml/g/h	[175]
Zn_3In2S_6/ TiO_2	50 mg	100 mL of sacrificial agent (80 mL of deionized water and 20 mL of TEOA) 275 μL (H_2PtCl_6)	300 W xenon lamp.	6.74 mml/g/h	[176]

Hu et al.[171] reported a 2D/2D H_2N–Cu–MOF/TpPa-1-COF S-scheme heterojunction prepared by grinding and ultrasonication (Fig24.e). As shown in the figure, the 2D/2D MOF/COF composite exhibits markedly enhanced photocatalytic H_2-evolution activity compared with the individual H_2N–Cu–MOF and TpPa-1-COF components (Fig24.g). Notably, the optimized Pt-loaded composite

delivers a substantially higher H_2-production rate, demonstrating the synergistic effect of intimate 2D/2D interfacial contact and Pt-promoted HER kinetics. The face-to-face MOF/COF assembly, stabilized by hydrogen-bonding and π–π interactions, is beneficial for interfacial charge transfer, while Pt nanoparticles accelerate electron utilization at proton-reduction sites. These results indicate that the photocatalytic performance of organic 2D/2D S-scheme systems can be effectively enhanced by concurrently optimizing supramolecular interfacial assembly and surface reaction kinetics.

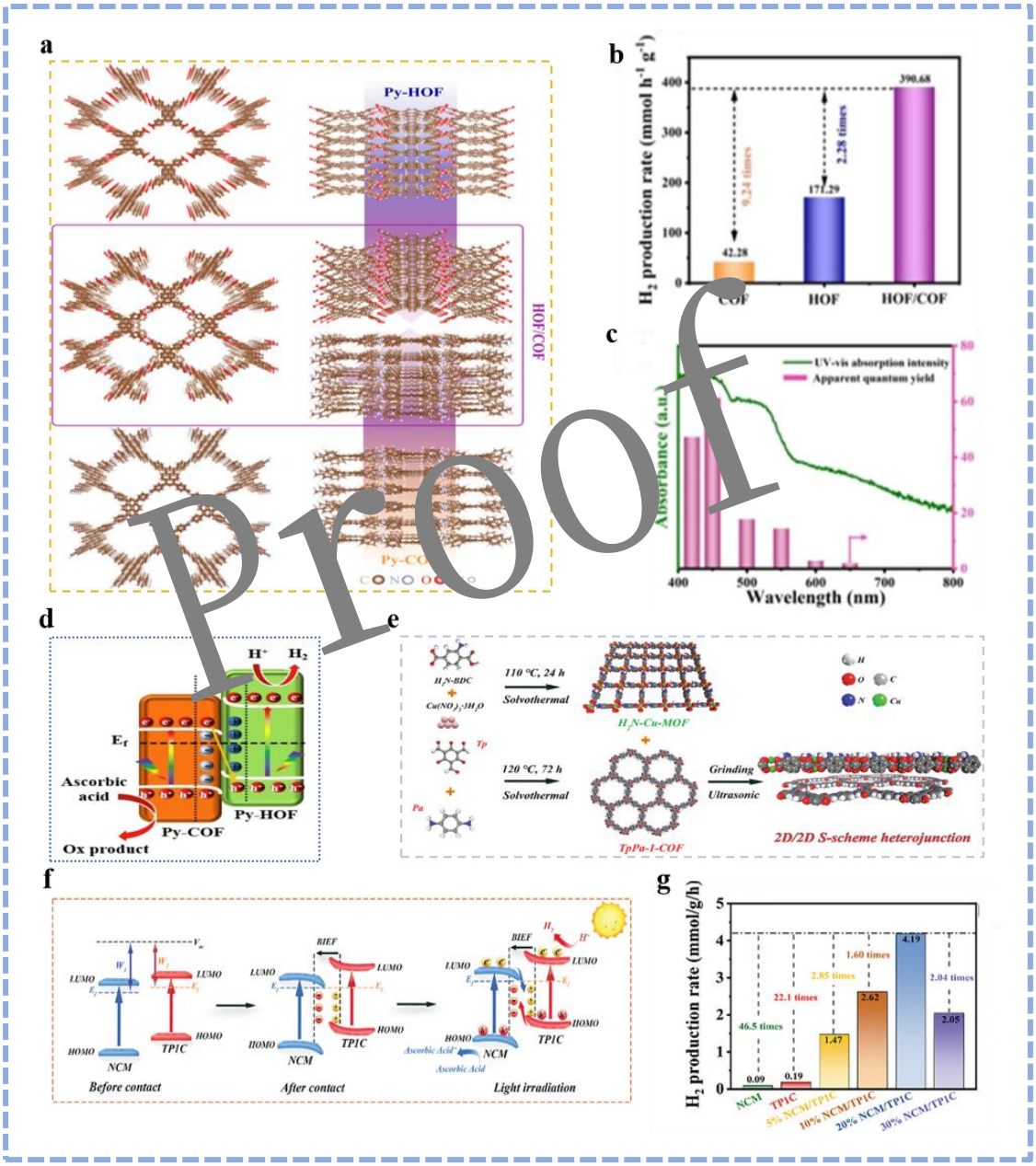

Fig 24. (a) Schematic illustration of synthesizing HOF/COF sample and structure of Py-HOF, Py-COF and Py-HOF/COF. (b) Average hydrogen evolution rate. (c)The apparent quantum yield of 10 mg HOF/COF. (d) Photocatalytic reaction mechanism of S-scheme heterojunction for HOF/COF.[117] (e) The illustration of the synthesis process of NCM/TP1C.(f) Schematic diagram

of photocatalytic mechanism research on NCM/TP1C hybrid material. (g) Photocatalytic hydrogen evolution activity of the synthesized products.[171]

Gao et al.[117] constructed a lattice- and dimension-matched Py-HOF/Py-COF 2D/2D S-scheme heterojunction (Fig24.a). The performance results shown in Fig24.b demonstrate that the HOF/COF hybrid exhibits a much higher H_2-production rate than pristine Py-HOF and Py-COF, highlighting the benefit of constructing a molecularly compatible organic-framework heterointerface. Compared with randomly stacked organic nanosheets, the lattice- and dimension-matched interface enables more extensive and continuous interfacial contact, thereby promoting charge separation and migration. The enhanced visible-light absorption and apparent quantum yield further verify the improved photocatalytic efficiency of the hybrid system. This study underscores the importance of interfacial compatibility in improving H_2-evolution performance in organic-framework-based S-scheme photocatalysts, although cocatalyst loading and reaction conditions should be considered when comparing activities among different systems.

Li et al. [177]further proposed an S-scheme homojunction by in situ growing pristine $ZnIn_2S_4$ on oxygen-doped $ZnIn_2S_4$ nanosheets. The reported activity comparison shows that the homojunction photocatalyst achieves substantially improved H_2-evolution performance compared with the corresponding single-component $ZnIn_2S_4$ samples. Oxygen doping modulates the electronic properties of $ZnIn_2S_4$, while the homogeneous interface facilitates charge transfer and suppresses charge recombination. This finding demonstrates that oxygen-doping-induced electronic modulation, coupled with homojunction engineering, provides an effective strategy for improving photocatalytic H_2 evolution.

Overall, the improved photocatalytic H_2-evolution performance of 2D/2D S-scheme heterojunctions is commonly linked to more effective utilization of photogenerated electrons. The S-scheme charge-transfer pathway is generally considered favorable for preserving electrons with relatively strong reduction capability, while the 2D/2D architecture may provide shortened migration distances and enlarged interfacial contact areas for charge transport. Nevertheless, efficient H_2 evolution is also closely related to the rapid extraction and consumption of electrons at suitable HER active sites. In this context, cocatalysts or conductive components, such as Pt, Ni_2P, MoS_2, and MXene, are often introduced to facilitate electron accumulation, proton adsorption, and surface reaction kinetics. Therefore, the future development of H_2-evolution-oriented 2D/2D S-scheme photocatalysts may benefit from the coordinated optimization of band alignment, interfacial charge transport, cocatalyst spatial distribution, and surface proton-reduction sites, instead of emphasizing apparent charge-separation efficiency alone.

6.2 Photocatalytic CO_2 reduction

With rapid industrialization and massive fossil fuel consumption, excessive CO_2 emissions are a primary driver of climate change and attendant environmental issues.[178] Consequently, CO_2 emission mitigation and valorization have attracted increasing attention in energy and environmental research. Solar-driven photocatalytic CO_2 reduction provides a green and sustainable route for converting CO_2 into value-added fuels and chemicals, including CO, CH_4, and CH_3OH.[178,179,180] However, the high thermodynamic stability and kinetic inertness of CO_2, combined with the involvement of multielectron/proton-transfer steps and diverse reaction intermediates, impose substantial challenges on CO_2 activation and product-selectivity control.[35] Photocatalytic CO_2 reduction involves a series of coupled elementary processes, including CO_2 adsorption, molecular activation, intermediate stabilization, proton-coupled electron transfer, and, in some cases, C–C coupling. Accordingly, photocatalyst design should move beyond charge-separation enhancement and place greater emphasis on active-site engineering, interfacial microenvironment modulation, and reaction-pathway regulation.[181]

Table 2 Photocatalytic CO_2 Reduction Performance of 2D/2D S-Scheme Heterojunctions

Photocatalyst	Dosage	Light source	Main Product and activity	Ref.
TiO_2 /C_3N_4 /Ti_3C_2	10 mg	350 W Xe lamp. λ > 420 nm	CO 4.39 μmol/g/h CH_4 1.20 μmol/g/h	[136]
Pt/BP-Bi_2WO_6	10 mg	350 W Xe lamp.	H_2 16.8μmol/g/h CO 20.5μmol/g/h	[182]
Bi_3NbO_7/g-C_3N_4	50 mg	Solar Simulator	CH_4 37.6 μmol/g/h	[183]
Zn-MOF/$BiVO_4$	20 mg	300 W Xe lamp. λ > 420 nm	CO 4.31μmol/g/h CH_4 0.62μmol/g/h	[184]
$BiVO_4$ /$CsPbBr_3$	10 mg	300 W Xe lamp.	CO 17μmol/g/h	[105]

Bi_2MoO_6 /BiOI	20 mg	300 W solar-simulated Xe arc lamp	CO 8.34 μmol/g/h CH_4 3.31 μmol/g/h	[185]
BP/BWO	5 mg	300 W Xe lamp.	BDA 413.3 μmol/g/h CO 12.4 μmol/g/h CH_3OH 8.6 μmol/g/h C_3H_4OH 61.3 μmol/g/h	[186]
$H_2WO_4/Cs_2AgBiBr_6$	5 mg	300 W Xe lamp. AM 1.5G filter	CH_4 22.6 μmol/g/h CO 14.58μmol/g/h	[145]
Bi_2MoO_6 /$Zn_3V_2O_8$	0.1g	300 W Xe lamp. λ > 420 nm	CO 7.67 μmol/g/h CH_4 0.46μmol/g/h	[187]
Cu[acs]/P-BDCNN	0.10 g	300 W Xe lamp. λ > 420 nm	C_2H_4 49.435μmol/g/h CH_4 32.1μmol/g/h CO 38.01 μmol/g/h	[188]
Bi_2O_2S/PCN	25mg	300 W Xe lamp.	CO 1.37 μmol/g/h	[189]
BiOI /HZnPCP	5 mg	300 W Xe lamp. 420 < λ < 780 nm	CH_4 577.1 μmol/g/cat/ h	[55]
WO_3/VS-$Zn_3In_2S_6$	20 mg	300 W Xe lamp with an infrared filter (380 nm to 780 nm)	CH_4 34.7 μmol/g/h CO 13.7 μmol/g/h	[67]
CNs/CCN	20 mg	300 W xenon lamp equipped with cutoff filters (λ > 420 nm, λ > 700 nm) t	CO 26.56 μmol/g/h CH_4 4.06 μmol/g/h	[190]
Cu_2O/Fe_2O_3@$Ni_{0.75}Co_{0.25}$	5 mg	300 W Xe lamp. 420 < λ < 780	CO 552.7 μmol/g/cat / h	[56]

		nm		
WO/InVO$_4$	10 mg	300 W Xe lamp. λ > 400 nm	CO 13.37 μmol/g	[191]
g-C$_3$N$_4$ /ZnIn$_2$S$_4$	5 mg	300 W Xe lamp. 420 < λ < 780 nm	CO 43.6 μmol/g/h	[90]
BiOI/Bi$_2$O$_2$CO$_3$	10 mg	300 W Xe lamp.	CO 8.11 μmol/g/h	[192]
In-ABDC （MOF）/WO$_3$	2 mg	300 W Xe lamp.with a 400 nm cutoff filter	CH$_3$OH 11.[illegible] μmol/g/h	[193]
In$_{2.77}$S$_4$/CuInS$_2$	30 mg	300 W xenon lamp with an AM1.5 filt[illegible]	C$_2$H$_4$ 47.2 [illegible]mol/g/h C[illegible] 0.9 μm[illegible]l/g/h	[194]
Bi$_2$MoO$_6$/ZnIn$_2$S 4	50 mg	300 W Xe a[illegible] lamp with a 420 nm filter.	CH$_4$ 95.2 μmol/g/h	[195]
CuSe/CuTCPP	10 mg	300 W Xe lamp.420 < λ < 2500nm	CO 198.4 μmol/g/h	[196]
g-C$_3$N$_4$/ZnIn$_2$S$_4$	5 mg	300 W Xeon lamp 320 nm < λ < 780 nm	CO 43.6 μmol/g/h	[197]

2D/2D S-scheme heterojunctions construct efficient interfacial charge-transfer channels for photocatalytic CO_2 reduction and enable active-site-mediated modulation of key intermediate evolution, thus regulating product selectivity. In the BP/Bi_2WO_6 system,[186] the intimate coupling between 2D BP and Bi_2WO_6 nanosheets forms an S-scheme heterojunction (Fig25.a), in which the interfacial Bi–O–P channel facilitates photogenerated charge separation and promotes electron accumulation at the BP reduction sites. Coupling CO_2 reduction with benzylamine oxidation lowers

the kinetic barrier of the oxidative half-reaction and improves the local CO_2/proton supply, thus promoting continuous proton-coupled electron transfer and C–C coupling. Product distribution (Fig25.c) and energy-barrier analyses (Fig25.d,e) indicate that 6%BP/BWO favors further hydrogenation of *CO and subsequent C–C coupling, thereby shifting the CO_2 reduction pathway from C_1 products toward C_2H_5OH formation.

In contrast, the Zn-MOF/$BiVO_4$ system[184] exemplifies the role of MOF metal nodes in regulating CO_2 adsorption/activation and the C_1 product pathway. The porphyrin-based Zn-MOF and $BiVO_4$ nanosheets form an intimate 2D/2D S-scheme heterojunction through hydroxyl-induced assembly (Fig25.f), where the porous framework and dispersed $Zn_2(COO)_4$ metal nodes of Zn-MOF facilitate CO_2 adsorption and activation. In situ DRIFTS (Fig25.i) results reveal the formation of key intermediates, including monodentate/bidentate carbonate species, HCO_3^-, COO^-, and *COOH, on the 20Zn-MOF/BVON surface, suggesting that CO_2 conversion in this system mainly proceeds through CO_2 adsorption, *COOH formation, *CO generation, and CO desorption. These results indicate that product selectivity in 2D/2D S-scheme heterojunctions is not governed solely by charge separation but is collectively determined by interfacial charge transfer, active-site structure, intermediate stabilization, and the synergistic regulation of the oxidative half-reaction.

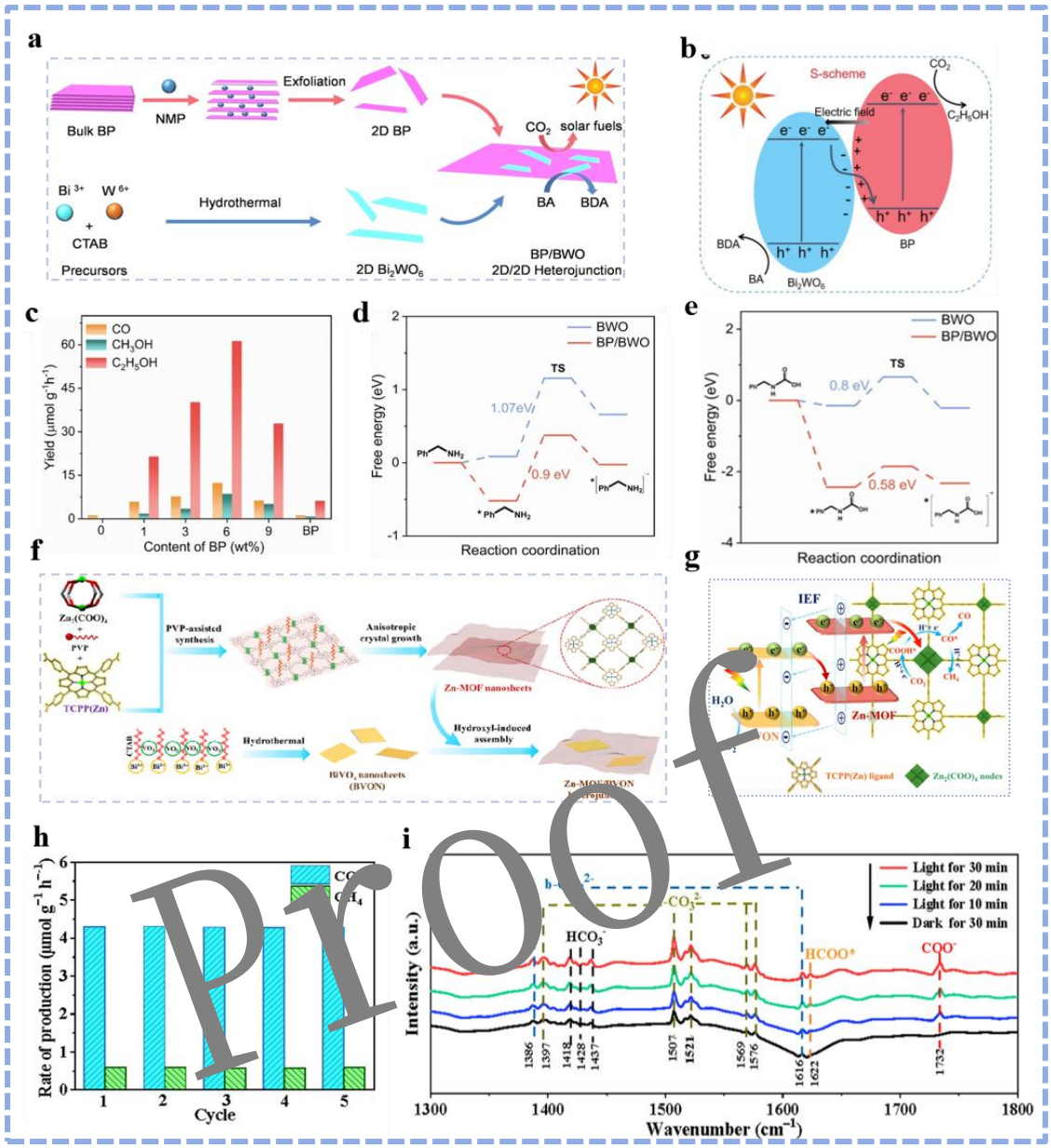

Fig 25. (a) Illustration of the fabrication of BP/BWO heterojunction. (b) Proposed mechanism for the photocatalytic CO_2 reduction coupled with BA oxidation on BP/BWO. (c) The yield of CO_2 reduction. Free energy diagrams for the adsorption and activation of (d) BA and (e) BCA on BWO and BP/BWO surfaces.[186] (e) Photocatalytic activities for CO_2 conversion of BVON, g-C3N4/BVON and 20Zn-MOF/BVON under visible-light irradiation. (f) Schematic diagram of the synthetic process for 2D/2D Zn-MOF/BVON heterojunctions. (g) Schematic of photogenerated charges transfer in Zn-MOF/BVON heterojunctions during CO_2 photoreduction process. (h) CO_2 conversion of BVON and xZn-MOF/BVON heterojunctions under visible-light irradiation. (i) In-situ DRIFT spectra of 20Zn-MOF/BVON heterojunction with different light irradiation intervals. [184]

In summary, the design of 2D/2D S-scheme photocatalysts for CO_2 reduction should evolve from charge-separation optimization toward the integrated regulation of charge transfer, intermediate evolution, and local reaction environments. While rational band alignment and

interfacial engineering are crucial for retaining electrons with strong reduction ability, product selectivity is largely dictated by CO_2 adsorption/activation and the stabilization or conversion of key intermediates. For C_1 products, controlling *COOH formation and *CO desorption is essential, whereas the formation of C_2 and higher-carbon products requires the enrichment of carbon-containing intermediates and adjacent active sites that favor C–C coupling. Representative Zn-MOF/$BiVO_4$ and BP/Bi_2WO_6 systems demonstrate that MOF metal nodes, interfacial bonds, and electron-rich low-dimensional sites can steer the *COOH/*CO pathway, *CO hydrogenation, and C–C coupling. Future studies should integrate in situ spectroscopy, isotope-labeling experiments, and theoretical calculations to resolve the dynamic evolution of key intermediates and establish more reliable structure–activity–selectivity relationships for CO_2 photoconversion.

6.3 Pollutant degradation

Rapid economic development and the continuous discharge of refractory organic pollutants have created an increasing demand for sustainable water-remediation technologies. Semiconductor photocatalysis provides a green strategy for pollutant degradation by harvesting solar energy to generate electron–hole pairs. During photocatalytic degradation, photogenerated holes can directly oxidize adsorbed pollutants or convert surface-adsorbed H_2O/OH^- into •OH, whereas photogenerated electrons reduce dissolved O_2 to $•O_2^-$, thereby driving the oxidative decomposition and mineralization of organic contaminants[198,199]. However, rapid charge recombination often suppresses ROS generation and limits photocatalytic efficiency.2D/2D S-scheme heterojunctions are particularly attractive for ROS-mediated degradation because their intimate interfacial contact and internal electric field promote directional charge separation while preserving carriers with strong redox potentials[83,200,201]. Accordingly, their degradation performance is governed not only by charge-separation efficiency but also by ROS-generation and hole-oxidation pathways, active-site accessibility, and structural stability in complex aqueous environments.[202]

Table 3. Photocatalytic degradation performance of 2D/2D S-scheme photocatalysts

Photocatalyst	Dosage	Light source	pollutions initial concentration	degradation rate k(min^{-1})	Ref.

WO_3/g-C_3N_4	50 mg	300 W Xe lamp. λ > 420 nm	TC 20 mg/L	0.0378	[203]
Bi_2MoO_6 /g-C_3N_4	5 mg	300 W Xe lamp. λ > 420 nm	RhB 5 mg /L	0.0808	[147]
α-Fe_2O_3 /Bi_2WO_6	20 mg	300 W Xe lamp. λ > 400 nm	MB 5 mg/L	0.1895	[204]
BiOBr/g-C_3N_4	30 mg	300 W Xe lamp. λ > 400 nm	RhB 10 mg/L	0.01274	[96]
N-ZnO/g-C_3N_4	20mg	300 W Xe lamp. λ > 420 nm	NOR 10MG/L	0.034	[205]
g-C_3N_4 /BiOBr	20 mg	300 W Xe lamp. λ > 400 nm	ADN 20 mg/L	0.1528	[206]
Bi_2WO_6/g-C_3N_5	0 mg	300 W Xe mp.	TC 10 mg/L	0.098	[207]
g-C_3N_5 /$Bi_4O_5Br_2$	50 mg	500 W Xe lamp.	ciprofloxacin (CP) bisphenol-A (BP) 20 mg/L	K_{CP}=0.051 k_{BP}=0.048	[208]
$ZnIn_2S_4$ /$Bi_4Ti_3O_{12}$	10 mg	300 W Xe lamp. λ > 420 nm	TC 20ppm	0.02234	[209]
BiOCl/MoS_2	10 mg	300 W Xe lamp. λ > 420 nm	TC 10 mg/L	0.104	[138]
HGO/CLS	2.5mg	300 W Xe lamp. λ > 420 nm	RhB 100 mg/L	0.0091	[210]

$MgO/g\text{-}C_3N_4$	100 mg	300 W Xe lamp. λ > 420 nm	RhB 100 mg/L	0.02633	[140]
Ni-MOF/BiOCl	50 mg	32 W UV lamp (λ = 254 nm)	TC 10 mg/L	0.00274	[211]
$BiVO_4$ /Cu-TCPP	20 mg	300 W Xe lamp. λ > 420 nm	CIP 10 mg/L	0.2426	[212]
In_2O_3 /$FeIn_2S_4$	20 mg	300 W Xe lamp. λ > 420 nm	TC, 20 mg/L	0.0582	[213]
Co-$Bi_2O_2CO_3$/BiOI	25 mg	350 W Xe lamp. λ > 420 nm	EDCs 10 mg/L	0.0574	[214]
PCN/BOCI	50 mg	300 W Xe lamp. λ > 420 nm	TC 10 mg/L	0.0522	[139]
K-C_3N_4 /BiOBr	20 mg	300 W Xe lamp.	TC 20 mg/L	0.083	[215]
BiOCl /Bi_2MoO_6	10 mg	300 W Xe lamp. λ > 420 nm	TC 10mg/L	0.0442	[176]
FeOOH /BiOCl	10 mg	3 W LED lamp λ = 365 nm	TC 10mg/L	0.024	[216]

Several representative systems demonstrate how 2D/2D S-scheme architectures regulate ROS generation during photocatalytic pollutant degradation. Huang et al.[202] constructed a $Bi_2MoO_6/BiOCl_{0.7}I_{0.3}$ 2D/2D S-scheme van der Waals heterojunction for tetracycline hydrochloride degradation. The optimized BMO-BOCI composite promoted interfacial charge separation and enhanced the generation of both $\bullet O_2^-$ and •OH, indicating that 2D/2D S-scheme coupling can preserve carriers with sufficient redox potentials for O_2 reduction and H_2O/OH^- oxidation.

The CNQDs/TCN/$ZnIn_2S_4$ system[217] illustrates how multilevel interfacial engineering can broaden ROS-generation pathways. By integrating CNQDs-induced Schottky contacts with a TCN/$ZnIn_2S_4$ S-scheme heterojunction (Fig26.a), additional electron-migration channels are established beyond the binary 2D/2D interface. Radical-trapping results (Fig26.c,d) show that •OH, $•O_2^-$, and h^+ jointly contribute to n-tetradecane degradation. In the binary TCN/$ZnIn_2S_4$ system, •OH serves as the dominant oxidative species, whereas CNQDs incorporation further promotes $•O_2^-$ formation by facilitating electron extraction and O_2 reduction. These results suggest that Schottky/S-scheme coupling enables both hole-driven •OH formation and electron-mediated O_2 activation, thereby supporting efficient petroleum hydrocarbon degradation in complex aqueous environments.

The PCN/BOCI system[139] demonstrates that heteroatom doping and 2D/2D van der Waals coupling can further tune the dominant ROS pathway. In the P-doped g-C_3N_4/$BiOCl_{0.75}I_{0.25}$ heterojunction, P doping modulates the electronic structure of g-C_3N_4 (Fig26.f), while the intimate 2D/2D interface facilitates directional S-scheme charge transfer. Quenching (Fig23.i) and EPR results (Fig26.g,h) indicate that h^+ and $•O_2^-$ are the primary active species for tetracycline degradation, with a comparatively minor contribution from •OH. Accordingly, PCN/BOCI degradation mainly proceeds through a coupled h^+/$•O_2^-$ oxidation pathway, in which holes directly oxidize adsorbed pollutants and electrons reduce dissolved O_2 to $•O_2^-$.

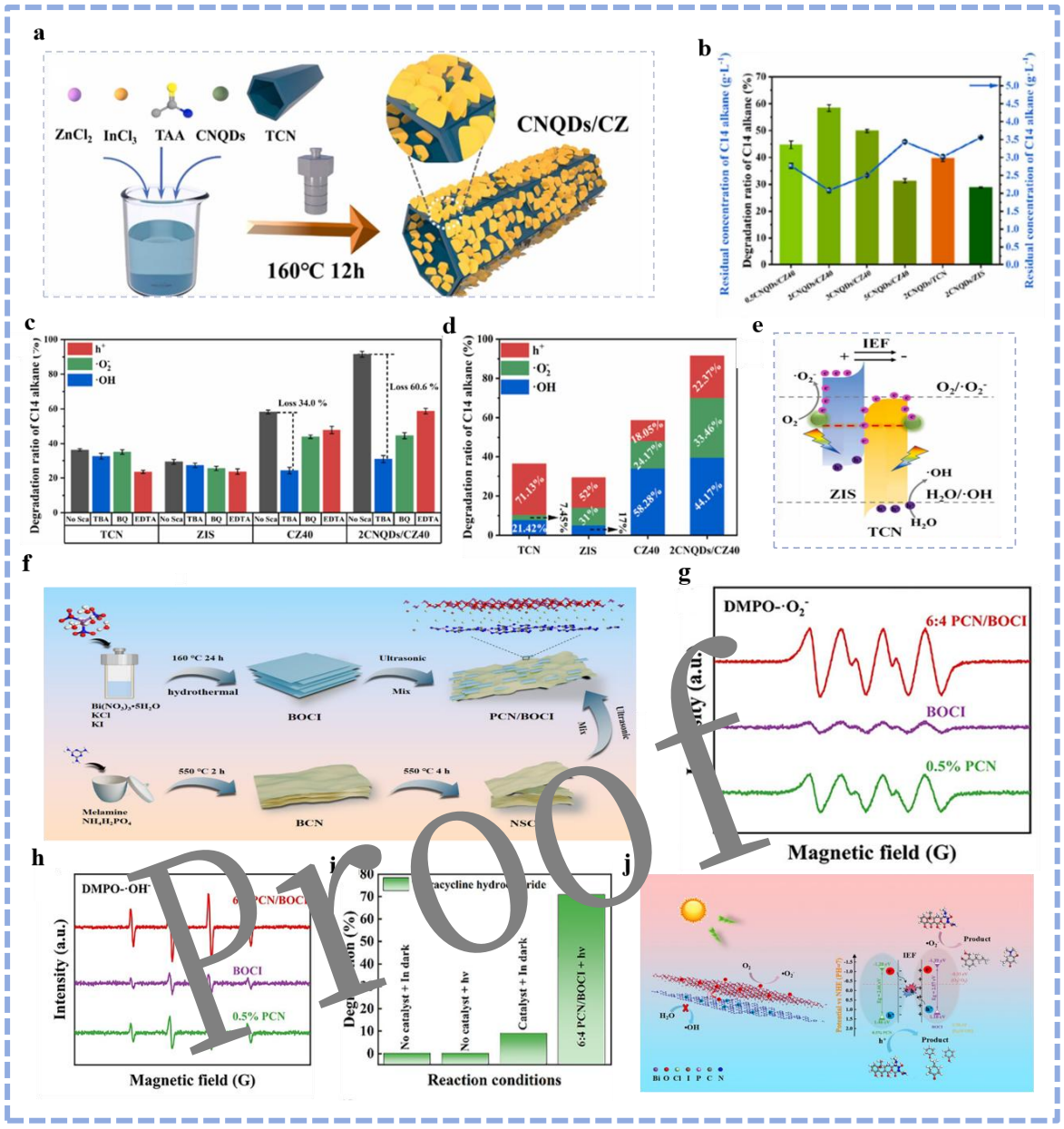

Fig 26. (a) Schematic illustration of preparation processes of 2CNQDs/CZ_{40}. (b) Photocatalytic activity for the removal of C_{14} and its residual concentration for 2CNQDs/TCN, 2CNQDs/ZIS and CNQDs/CZ_{40} series with 5 g/L C_{14}. (c) Photocatalytic degradation of C_{14} with different scavengers over samples. (d) Contribution of active radicals to the degradation of C_{14}, assuming that only •OH, •O_2- and h+ in the system, (e) Schematic illustration of TCN and ZIS band structure after contact, and S-scheme charge-transfer pathway under irradiation.[217] (f) Schematic illustration of the preparation process of PCN, BOCI and PCN/BOCI. ESR spectra of (g) DMPO-•O_2− and (h) DMPO-•OH. (i) Photocatalytic degradation under different reaction conditions. (j) Photocatalytic reaction mechanism for PCN-BOCI heterojunction under the illumination.[139]

Overall, ROS generation provides a key mechanistic bridge between S-scheme charge transfer and photocatalytic pollutant degradation. For 2D/2D S-scheme photocatalysts designed for environmental remediation, efficient charge separation alone is insufficient; the spatial

distribution and redox capability of the retained carriers must be precisely regulated to promote O_2 reduction, H_2O/OH^- oxidation, and direct hole oxidation. Interfacial coupling, heteroatom doping, defect engineering, cocatalyst loading, quantum-dot modification, and van der Waals interface construction can all modulate the relative contributions of h^+, $\bullet O_2^-$, and •OH. Future design should therefore integrate directional charge migration with controllable ROS generation, while ensuring sufficient active-site exposure and structural stability in complex aqueous environments. Establishing clear structure–charge dynamics–ROS generation–degradation relationships will be essential for developing efficient and durable photocatalysts for environmental remediation.

6.4 Photocatalytic H_2O_2 Production

Hydrogen peroxide (H_2O_2) is widely used in environmental remediation, chemical synthesis, and antibacterial treatment, making its green and efficient production highly important. The traditional anthraquinone process suffers from high energy consumption, a complicated procedure, and pollution issues, while direct synthesis is also limited by safety concerns and low selectivity.[36] Photocatalytic H_2O_2 production has therefore attracted increasing attention as a mild and sustainable alternative. In most semiconductor photocatalytic systems, H_2O_2 is mainly generated through the two-electron oxygen reduction reaction ($2e^-$ ORR), whereas the two-electron water oxidation pathway is limited by sluggish kinetics and competing oxygen evolution.[218,219] Efficient H_2O_2 photosynthesis thus requires not only effective charge separation, but also selective O_2 activation, stabilization of oxygenated intermediates, suppression of the competing four-electron ORR, and inhibition of H_2O_2 decomposition. 2D/2D S-scheme heterojunctions provide a promising platform for this reaction because their extended interfacial contact, shortened charge-transfer distance, and built-in electric field facilitate directional carrier migration while preserving strong redox potentials.[220] When coupled with defect engineering, heteroatom doping, or polar-interface regulation, these systems can further modulate local electronic structures and surface reaction pathways, thereby enhancing ORR selectivity and steering ROS generation toward H_2O_2. Therefore, the design of 2D/2D S-scheme photocatalysts for H_2O_2 production should move beyond charge-separation enhancement alone and emphasize the integrated regulation of interfacial charge transfer, O_2 activation, reaction selectivity, and peroxide stability.

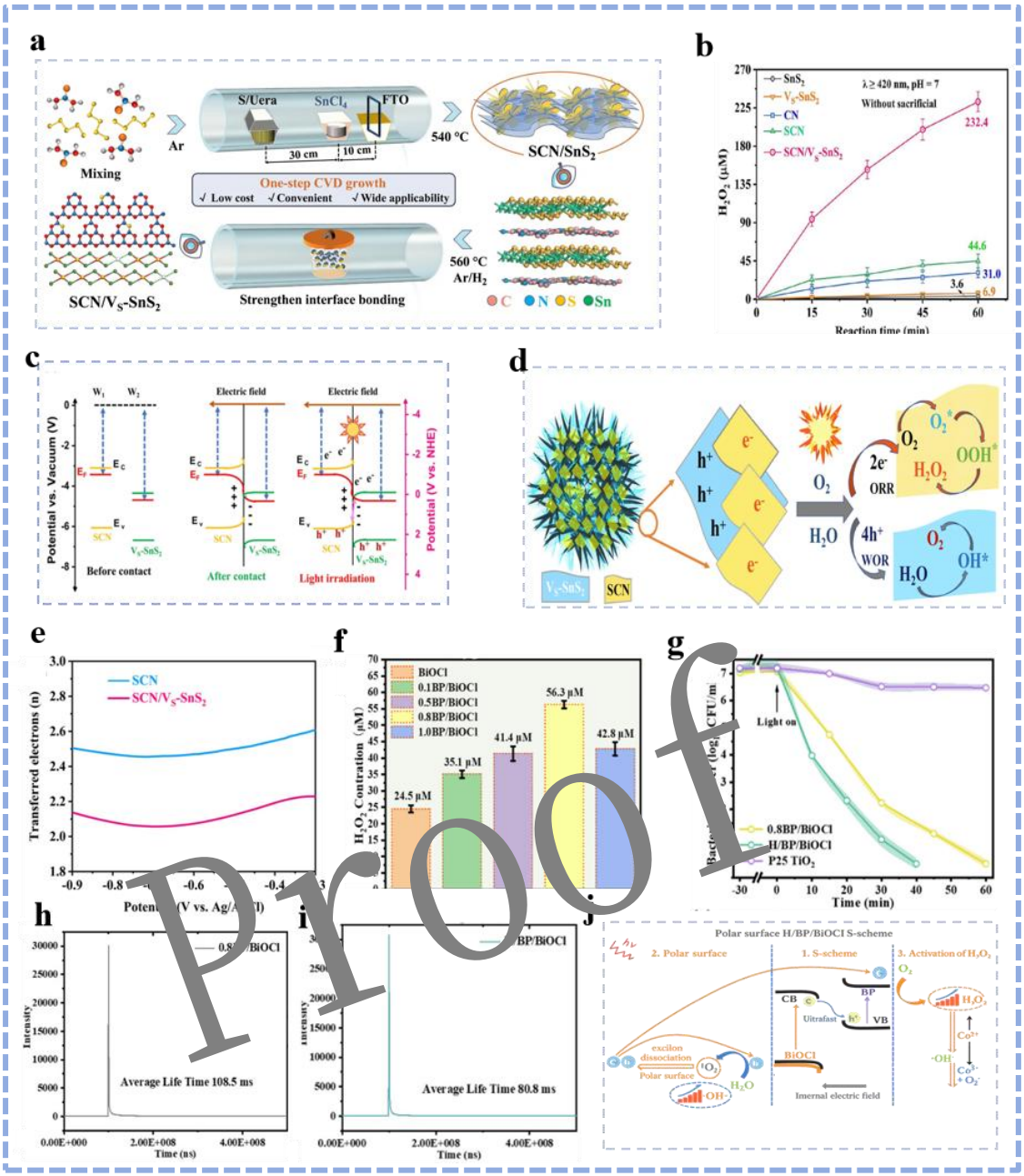

Fig 27. (a) Schematic illustration of SCN/V_S-SnS_2 heterojunction synthesis by one-step CVD growth. (b)Time profiles of H_2O_2 yield for prepared samples in pure water. (c) The schematic diagram for the enhanced photogenerated carrier transfer of SCN/V_S-SnS_2 heterojunction with internal electric field. (d) Proposed reaction mechanism for the H_2O_2 generation over S-scheme SCN/V_S-SnS_2 catalyst.[221] (e) The average number of transferred electrons over SCN_2 and SCN/VS-SnS_2 catalyst. (f) Accumulated concentrations of H_2O_2 in BiOCl and BP/BiOCl systems. (g) Photocatalytic disinfection performances of the samples under simulated-sunlight irradiation. (h-i) TRPH measured at 77 K (j) Schematic illustration of the photocatalytic bacterial inactivation mechanism.[64]

Shi et al.[221] developed a homogeneously distributed SCN/VS-SnS_2 2D/2D S-scheme heterojunction through one-step CVD growth (Fig27.a). The schematic illustrations indicate that the in situ coupling of S-doped carbon nitride with S-vacancy-containing SnS_2 generates an intimate

2D/2D interface, which shortens the interfacial charge-transfer distance and reinforces the built-in electric field. Such an interfacial configuration favors directional S-scheme charge migration, retaining highly reducing electrons on SCN for O_2 reduction and strongly oxidizing holes on VS-SnS_2 for hole-mediated water oxidation (Fig27.c, d). Consequently, SCN/VS-SnS_2 exhibits substantially enhanced H_2O_2 production in pure water compared with the individual components (Fig27.b). The average electron-transfer number close to two further suggests a preferential $2e^-$ ORR pathway, rather than the competing four-electron ORR (Fig23.e). These results demonstrate that efficient H_2O_2 photosynthesis in this system arises from the cooperative optimization of S-scheme charge transfer, S-doping-induced O_2 activation, and S-vacancy-assisted water oxidation.

Zhang et al. [64] further emphasized the role of polar-surface regulation in a BP/BiOCl-based 2D/2D S-scheme heterojunction. Compared with pristine BiOCl, BP/BiOCl shows enhanced H_2O_2 accumulation (Fig27.f), indicating that 2D/2D S-scheme coupling facilitates O_2-reduction-dominated H_2O_2 formation. Upon polar-surface modification, the shortened triplet-exciton lifetime of H/BP/BiOCl evidences accelerated exciton dissociation (Fig27.h,i), which is associated with a shift in ROS evolution from short-lived $^1O_2$ toward H_2O_2 generation. The improved bacterial inactivation efficiency under simulated sunlight further indicates that H_2O_2-mediated ROS chemistry contributes to photocatalytic water disinfection (Fig27.g). Therefore, polar-interface engineering expands the role of 2D/2D S-scheme heterojunctions from charge-separation enhancement to pathway-selective ROS regulation for H_2O_2 production and antibacterial applications.

Overall, photocatalytic H_2O_2 production over 2D/2D S-scheme heterojunctions should be viewed as a pathway-selective redox process rather than merely a charge-separation enhancement strategy. The intimate 2D/2D interface, built-in electric field, and S-scheme charge-transfer pathway can maintain the high redox potentials of photogenerated carriers, while defect engineering, heteroatom doping, and polar-interface regulation further modulate O_2 activation, oxygenated-intermediate stabilization, exciton dissociation, and ROS generation pathways. These effects collectively favor the $2e^-$ ORR pathway, suppress competing side reactions, and inhibit H_2O_2 decomposition. Therefore, future development of 2D/2D S-scheme photocatalysts should emphasize the integrated regulation of interfacial charge transfer, surface reaction selectivity, and H_2O_2 formation, preservation, and downstream activation, particularly for water disinfection and environmental remediation applications.

7. Conclusions and Outlook

2D/2D S-scheme heterojunctions have emerged as promising photocatalytic platforms for solar energy conversion and environmental remediation. Their face-to-face architectures afford large interfacial contact areas, shortened carrier migration distances, abundant exposed active sites, and favorable conditions for the formation of built-in electric fields. Driven by band bending and interfacial electric fields, low-energy electrons and holes selectively recombine at the heterointerface, while electrons with high reduction potentials and holes with high oxidation potentials are well retained for subsequent surface redox reactions. This unique charge-transfer mode enables efficient carrier separation while preserving robust redox capabilities, which is essential for photocatalytic H_2 evolution, CO_2 reduction, pollutant degradation, and H_2O_2 production.

Recent advances have deepened the fundamental understanding of interface construction, charge-transfer mechanisms, and reaction-specific optimization of 2D/2D S-scheme systems. Interface engineering has evolved from simple physical assembly to more controllable strategies, including in situ growth, interfacial bonding, molecular bridging, defect regulation, and surface chemical modification. Meanwhile, characterization techniques such as TEM/HRTEM, AFM, XPS, KPFM, EPR, in situ XPS, transient spectroscopy, together with DFT theoretical calculations, have provided solid and reliable evidence for verifying the S-scheme charge migration behavior. Furthermore, modification strategies involving heteroatom doping, defect engineering, cocatalyst loading, single-atom regulation, and multidimensional interface construction have significantly promoted interfacial charge transfer, improved active-site utilization, and optimized surface reaction kinetics.

Despite these remarkable achievements, several critical challenges still remain. The precise modulation of stacking orientation, interlayer spacing, interfacial bonding configuration, defect distribution, and active-site location at 2D/2D heterointerfaces remains difficult to realize. In addition, the identification of S-scheme charge transfer heavily relies on indirect experimental evidence, making it difficult to unambiguously distinguish S-scheme pathways from Type-II transfer, Z-scheme transfer, defect-mediated migration, and cocatalyst-assisted charge extraction. Moreover, quantitative correlations among work-function difference, built-in electric-field strength, interfacial coupling intensity, carrier dynamics, and photocatalytic activity have not been fully established. The practical applications of 2D/2D S-scheme photocatalysts are also restricted by inherent photocorrosion, difficult catalyst recovery, unsatisfactory long-term stability, dependence on sacrificial agents or noble metals, and the lack of unified and standardized performance evaluation protocols.

Future research should be directed toward predictive, mechanism-guided, and application-oriented photocatalyst design. Machine learning and high-throughput computational screening can accelerate the rational selection of optimal 2D/2D material combinations by theoretically predicting band alignment, work-function difference, interfacial stability, charge-transfer behavior, and adsorption energies of key reaction intermediates. Such data-driven strategies can effectively expand the material library beyond conventional g-C_3N_4 and Bi-based systems to emerging candidates, including MXenes, MOFs, COFs, HOFs, black phosphorus, layered double hydroxides, and halide perovskites.

From a mechanistic perspective, advanced in situ and operando characterization techniques should be extensively adopted to dynamically track interfacial charge migration, active-site evolution, surface reconstruction, and intermediate transformation under realistic reaction conditions. The integration of operando spectroscopy, time-resolved kinetic analysis, isotope-labeling experiments, and theoretical simulations is crucial for distinguishing genuine S-scheme charge transfer from other competing charge-transfer pathways and establishing a comprehensive structure–charge dynamics–intermediate–activity relationship.

For practical deployment, conventional powder photocatalysts require structural integration and device optimization, such as immobilized films, membranes, functional electrodes, monolithic carriers, and continuous-flow reactors. Such structural configurations can effectively address catalyst recycling issues, enhance mass transfer efficiency, improve operational stability, and enable reliable long-term performance evaluation under application-relevant conditions. The integration of data-driven material screening, operando mechanistic analysis, and reactor-level engineering will further promote the development of 2D/2D S-scheme heterojunctions from fundamental laboratory research to practical technologies for sustainable energy conversion and environmental purification.

References

[1] Bin Qi, Rongchen Shen, Ziyang Ke, Song Wang, Youji Li, Peng Zhang, Difa Xu, Xin Li. 2D sp_2 carbon-conjugated covalent organic frameworks: photocatalytic platforms for solar energy conversion. Rare Metals,2025. https://doi.org/10.1007/s12598-025-03604-4.

[2] Wang Wang, Bei Cheng, Guoqiang Luo, Jiaguo Yu, Shaowen Cao. S-scheme heterojunction photocatalysts based on 2D materials. Materials Today,2024 81, 137-158. https://doi.org/10.1016/j.mattod.2024.10.006.

[3] Qing Guo, Chuanyao Zhou, Zhibo Ma, Xueming Yang. Fundamentals of TiO_2 Photocatalysis: Concepts, Mechanisms, and Challenges. Advanced Materials,2019 31 (50). https://doi.org/10.1002/adma.201901997.

[4] Yihong Shao, Rongchen Shen, Song Wang, Shijie Li, Peng Zhang, Xin Li. Composition engineering in covalent organic frameworks for tailored photocatalysis. Acta Physico-Chimica Sinica,2025 41 (12), 100176. https://doi.org/10.1016/j.actphy.2025.100176.

[5] Ruijie Yang, Xingying Fan, Yuhong Zhang, Long Mei, Ronghshu Zhu, Jiaqian Qin, Jinguang Hu, Zhangxing Chen, Yunhai Ng, Damien Voiry, Shuang Li, Qingye Lu, Qian Wang, Jimmyc Yu, Zhiyuan Zeng. 2D Transition Metal Dichalcogenides for Photocatalysis. Angewandte Chemie International Edition,2023 62 (13). https://doi.org/10.1002/anie.202218016.

[6] Xin Guo, Bo Wen, Dong Tang, Jiayue Liu, Youji Li, Zhiliang Jin. Synergism between Surface Engineering and S-Scheme Heterojunctions for Efficient Photocatalytic H_2 Evolution. Chemistry of Materials,2025. https://doi.org/10.1021/acs.chemmater.5c00647.

[7] Xinwan Zhao, Xiaoyue Zhang, Minjun Lei, Xiaoli Ma, Youji Li, Zhiliang Jin. Synergistic effect of morphology regulation of $LaNiO_3$ S-scheme heterojunction for enhanced photocatalytic hydrogen production. Journal of Materials Science &Amp; Technology,2025. https://doi.org/10.1016/j.jmst.2025.05.024.

[8] Xinghou He, Tianhan Kai, Ping Ding. Heterojunction photocatalysts for degradation of the tetracycline antibiotic: a review. Environmental Chemistry Letters,2021 19 (6), 4563-4601. https://doi.org/10.1007/s10311-021-01295-8.

[9] Xiaosong Zhou, Zixuan Liang, Zhoupeng Wu, Xunfu Zhou, Xiaomei Ning, Liang Zhan, Jin Luo. Reasonably constructing $BiVO_4$/CoNiFe-LDH S-scheme heterojunction with fast interface charge transfer for efficient photodegradation of tetracycline. Advanced Powder Technology,2025

36 (5), 104858. https://doi.org/10.1016/j.apt.2025.104858.

[10] Muhammadasim Khan, Sadaf Mutahir, Imrana Shaheen, Yuan Qunhui, Mohamed Bououdina, Muhammad Humayun. Recent advances over the doped g-C_3N_4 in photocatalysis: A review. Coordination Chemistry Reviews,2025 522, 216227. https://doi.org/10.1016/j.ccr.2024.216227.

[11] Bikash Mishra, Akhtar Alam, Avanti Chakraborty, Bidhan Kumbhakar, Samrat Ghosh, Pradip Pachfule, Arne Thomas. Covalent Organic Frameworks for Photocatalysis. Advanced Materials,2024. https://doi.org/10.1002/adma.202413118.

[12] Chuanbiao Bie, Bei Cheng, Jiajie Fan, Wingkei Ho, Jiaguo Yu. Enhanced solar-to-chemical energy conversion of graphitic carbon nitride by two-dimensional cocatalysts. EnergyChem,2021 3 (2), 100051. https://doi.org/10.1016/j.enchem.2021.100051.

[13] Chuanbiao Bie, Linxi Wang, Jiaguo Yu. Challenges for photocatalytic overall water splitting. Chem,2022 8 (6), 1567-1574. https://doi.org/10.1016/j.chempr.2022.04.013.

[14] Haowei Huang, Davy Verhaeghe, Bo Weng, Biplab Ghosh, Hongwen Zhang, Johan Hofkens, Juliana Steele, Maartenbj Roeffaers. Metal Halide Perovskite Based Heterojunction Photocatalysts. Angewandte Chemie International Edition 2022 61 (24). https://doi.org/10.1002/anie.202203261.

[15] Wei Zhao, Yue Feng, Haibo Huang, Pengcheng Zhou, Jing Li, Lili Zhang, Benlin Dai, Jiming Xu, Fengxia Zhu, Ni Sheng, Dennisyc Leung. A novel Z-scheme Ag_3VO_4/$BiVO_4$ heterojunction photocatalyst: Study on the excellent photocatalytic performance and photocatalytic mechanism. Applied Catalysis B: Environmental,2019 245, 448-458. https://doi.org/10.1016/j.apcatb.2019.01.001.

[16] Haitao Ren, Zongcheng Miao, Yuzhen Zhao, Shahnaz Ghasemi, Xiangbo Feng, Enzhou Liu, Mohsen Padervand. Advances and challenges in multiple S-scheme heterojunction photocatalysts. Journal of Alloys and Compounds,2025 1028, 180646. https://doi.org/10.1016/j.jallcom.2025.180646.

[17] Xinhe Wu, Guoqiang Chen, Juan Wang, Jinmao Li, Guohong Wang. Review on S-Scheme Heterojunctions for Photocatalytic Hydrogen Evolution. Acta Physico Chimica Sinica,2023, 2212016. https://doi.org/10.3866/pku.whxb202212016.

[18] Yang Li, Xin Li, Huaiwu Zhang, Jiajie Fan, Quanjun Xiang. Design and application of active sites in g-C_3N_4-based photocatalysts. Journal of Materials Science & Technology,2020 56, 69-88. https://doi.org/10.1016/j.jmst.2020.03.033.

[19] Qianxia Liu, Zhuan Wang, Hailong Chen, Haoyi Wang, Hui Song, Jinhua Ye, Yuxiang Weng.

Rules for Selecting Metal Cocatalyst Based on Charge Transfer and Separation Efficiency between ZnO Nanoparticles and Noble Metal Cocatalyst Ag/ Au/ Pt. ChemCatChem,2020 12 (15), 3838-3842. https://doi.org/10.1002/cctc.202000280.

[20] Dan Wang, Fang-xin Yin, Bei Cheng, Yang Xia, Jia-guo Yu, Wing-kei Ho. Enhanced photocatalytic activity and mechanism of CeO_2 hollow spheres for tetracycline degradation. Rare Metals,2021 40 (9), 2369-2380. https://doi.org/10.1007/s12598-021-01731-2.

[21] Pooja Dhiman, Garima Rana, Amit Kumar, Gaurav Sharma, Dai-vietn Vo, Mu. Naushad. ZnO-based heterostructures as photocatalysts for hydrogen generation and depollution: a review. Environmental Chemistry Letters,2022 20 (2), 1047-1081. https://doi.org/10.1007/s10311-021-01361-1.

[22] Yuan Teng, Jing Zhao, Ziming Ye, Chaowen Tan, Lingling Ning, Yiyang Zhou, Zhilian Wu, Daibin Kuang, Youji Li. Covalent Organic Framework Encapsulating Layered Oxide Perovskite for Efficient Photosynthesis of H_2O_2. Advanced Energy Materials,2024. https://doi.org/10.1002/aenm.202404029.

[23] Bin Han, Peng Zhu, Yao Liu, Qingqing Qiu, Jinhui Li, Tongxiang Liang, Tengfeng Xie. Enhanced photocatalytic degradation activity via a stable perovskite-type $LaFeO_3/In_2S_3$ Z-scheme heterostructured photocatalyst: Unobstructed photoexcited charge behavior of Z-scheme photocatalytic system exploration. Journal of Alloys and Compounds,2022 901, 163628. https://doi.org/10.1016/j.jallcom.2022.163628.

[24] Qi Xiao, Ting Yu, Qianhe Zhou, Liangyu Li, Chuntao Chang, Dawei Gao, Danyang Li, Feifei You. Nanostructured ZnO/ZnS with Type-II Hetero-junction for Efficient CO_2 Photoreduction. Chemical Research in Chinese Universities,2024 40 (3), 484-489. https://doi.org/10.1007/s40242-024-4022-8.

[25] Ye Yuan, Rui-tang Guo, Long-fei Hong, Xiang-yin Ji, Zhi-dong Lin, Zheng-sheng Li, Wei-guo Pan. A review of metal oxide-based Z-scheme heterojunction photocatalysts: actualities and developments. Materials Today Energy,2021 21, 100829. https://doi.org/10.1016/j.mtener.2021.100829.

[26] Aijiao Zhou, Lei Liao, Xumeng Wu, Kai Yang, Chenxiu Li, Wanpeng Chen, Pengchao Xie. Fabrication of a Z-scheme nanocomposite photocatalyst for enhanced photocatalytic degradation of ibuprofen under visible light irradiation. Separation and Purification Technology,2020 250, 117241. https://doi.org/10.1016/j.seppur.2020.117241.

[27] Junwei Fu, Quanlong Xu, Jingxiang Low, Chuanjia Jiang, Jiaguo Yu. Ultrathin 2D/2D $WO_3/g\text{-}C_3N_4$ step-scheme H_2-production photocatalyst. Applied Catalysis B: Environmental,2019

243, 556-565. https://doi.org/10.1016/j.apcatb.2018.11.011.

[28] Xinxin Liang, Yongqian Cui, Qingyun Tian, Tingting Jia, Qibing Dong, Ximing Li, Ting Gao, Chao Ma, Chuanyi Wang. Photoreforming polylactic acid plastics into pyruvate over CdS/$Bi_4Ti_3O_{12}$ S-scheme heterojunction: Successive removal of hydrogen from α-C. Chinese Chemical Letters,2026 37 (2), 111097. https://doi.org/10.1016/j.cclet.2025.111097.

[29] Xingyan Liu, Kaili Wu, Yacen Tang, Ning Qi, Yumeng Zhang, Youzhou He, Min Fu, Yanhui Ao. Ti_3C_2 MXene-derived TiO_2@C attached on Bi_2WO_6 with oxygen vacancies to fabricate S-scheme heterojunction for photocatalytic antibiotics degradation and NO removal. Chinese Chemical Letters,2025 36 (11), 110882. https://doi.org/10.1016/j.cclet.2025.110882.

[30] Hongrui Zhang, Miaoying Cui, Yongjie Lv, Yongfang Rao, Yu Huang. A short review on research progress of $ZnIn_2S_4$-based S-scheme heterojunction: Improvement strategies. Chinese Chemical Letters,2025 36 (4), 110108. https://doi.org/10.1016/j.cclet.2024.110108.

[31] Yan Cao, Lin Ye, Yangchen Yuan, Ruitao Yang, Hui Hong, Jingwen Chen, Jinyi Lu, Entian Cui, Jizhou Jiang. Ni–N bonds boost S-scheme charge transfer in NiSe/Cv-C_3N_5 for efficient water splitting. Chinese Journal of Catalysis,2025 78, 229-241. https://doi.org/10.1016/s1872-2067(25)64832-7.

[32] Xingang Fei, Haiyan Tan, Bei Cheng, Bicheng Zhu, Liuyang Zhang. 2D/2D Black Phosphorus/g-C_3N_4 S-Scheme Heterojunction Photocatalysts for CO_2 Reduction Investigated using DFT Calculations. Acta Phys. -Chim,2020, 2010027. https://doi.org/10.3866/PKU.WHXB202010027.

[33] Wenliang Wang, Haochun Zhang, Yigang Chen, Haifeng Shi. Efficient Degradation of Tetracycline via Coupling of Photocatalysis and Photo-Fenton Processes over a 2D/2D α-Fe_2O_3/g-C_3N_4 S-Scheme Heterojunction Catalyst. Acta Phys. -Chim,2022, 2201008. https://doi.org/10.3866/PKU.WHXB202201008.

[34] Bicheng Zhu, Bei Cheng, Jiajie Fan, Wingkei Ho, Jiaguo Yu. g-C_3N_4-Based 2D/2D Composite Heterojunction Photocatalyst. Small Structures,2021 2 (12). https://doi.org/10.1002/sstr.202100086.

[35] Jiani Lu, Shaonan Gu, Hongda Li, Yinan Wang, Meng Guo, Guowei Zhou. Review on multi-dimensional assembled S-scheme heterojunction photocatalysts. Journal of Materials Science & Technology,2023 160, 214-239. https://doi.org/10.1016/j.jmst.2023.03.027.

[36] Yuhao Yan, Lei Hao, Zhiqiang Ren, Rongchen Shen, Guijie Liang, Peng Zhang, Yuan Teng, Difa Xu, Xin Li. Design and modification strategies of covalent organic frameworks for photocatalytic hydrogen/hydrogen peroxide production. Journal of Materials Science &Amp; Technology,2025. https://doi.org/10.1016/j.jmst.2025.06.015.

[37] Xinhe Wu, Guoqiang Chen, Juan Wang, Jinmao Li, Guohong Wang. Review on S-Scheme Heterojunctions for Photocatalytic Hydrogen Evolution. Acta Physico Chimica Sinica,2023, 2212016. https://doi.org/10.3866/pku.whxb202212016.

[38] C Karthikeyan, Prabhakarn Arunachalam, K Ramachandran, Abdullahm Al-Mayouf, S Karuppuchamy. Recent advances in semiconductor metal oxides with enhanced methods for solar photocatalytic applications. Journal of Alloys and Compounds,2020 828, 154281. https://doi.org/10.1016/j.jallcom.2020.154281.

[39] Alisha Shabbir, Sabahat Sardar, Asad Mumtaz. Mechanistic investigations of emerging type-II, Z-scheme and S-scheme heterojunctions for photocatalytic applications – A review. Journal of Alloys and Compounds,2024 1003, 175683. https://doi.org/10.1016/j.jallcom.2024.175683.

[40] Fulai Liu, Rui Shi, Zhuan Wang, Yuxiang Weng, Chiming Che, Yong Chen. Direct Z-Scheme Hetero-phase Junction of Black/Red Phosphorus for Photocatalytic Water Splitting. Angewandte Chemie International Edition,2019 58 (34), 11791-11795. https://doi.org/10.1002/anie.201906416.

[41] Hiroaki Tada, Tomohiro Mitsui, Tomokazu Kiyonaga, Tomoki Akita, Koji Tanaka. All-solid-state Z-scheme in CdS–Au–TiO_2 three-component nanojunction system. Nature Materials,2006 5 (10), 782-786. https://doi.org/10.1038/nmat1734.

[42] Xiaosong Zhou, Jiabao Yang, Limin Xu, Siyu Wu, Minyi Xie, Qiongdan Liang, Jin Luo, Xuliang Fan, Xunfu Zhou, Xiaomin Zhou. Weakness-complementing Z-scheme black phosphorus/TiO_2 heterojunction with efficient charge separation and photocatalytic overall water splitting activity. Journal of Colloid and Interface Science,2025 689, 137240. https://doi.org/10.1016/j.jcis.2025.03.029.

[43] Huihuang Mao, Tao Wen, Caifeng Huang, Lisong Feng, Fugang Qi, Yun Zhou. Covalent triazine frameworks synergized with $ZnIn_2S_4$ to construct S-scheme heterojunction for achieving effective photocatalytic hydrogen evolution. Separation and Purification Technology,2026, 137381. https://doi.org/10.1016/j.seppur.2026.137381.

[44] Mingyang Xu, Zhenzhen Li, Rongchen Shen, Xin Zhang, Zhihong Zhang, Peng Zhang, Xin Li. Constructing S-scheme heterojunction between porphyrinyl covalent organic frameworks and Nb_2C MXene for photocatalytic H_2O_2 production. Chinese Journal of Catalysis,2025 70, 431-443. https://doi.org/10.1016/s1872-2067(24)60247-0.

[45] Liuyang Zhang, Jianjun Zhang, Huogen Yu, Jiaguo Yu. Emerging S-Scheme Photocatalyst. Advanced Materials,2022 34 (11), 2107668. https://doi.org/10.1002/adma.202107668.

[46] Fangyi Li, Guihua Zhu, Jizhou Jiang, Lang Yang, Fengxia Deng, Arramel, Xin Li. A review

of updated S-scheme heterojunction photocatalysts. Journal of Materials Science & Technology,2024 177, 142-180. https://doi.org/10.1016/j.jmst.2023.08.038.

[47] Zhen Zhang, Johnt Yates. Band Bending in Semiconductors: Chemical and Physical Consequences at Surfaces and Interfaces. Chemical Reviews,2012 112 (10), 5520-5551. https://doi.org/10.1021/cr3000626.

[48] Bicheng Zhu, Jian Sun, Yanyan Zhao, Liuyang Zhang, Jiaguo Yu. Construction of 2D S-Scheme Heterojunction Photocatalyst. Advanced Materials,2024 36 (8), 2310600. https://doi.org/10.1002/adma.202310600.

[49] Chenhui Wang, Yuanyuan Zhao, Chao Cheng, Qian Li, Changfa Guo, Yong Hu. S-scheme heterojunction photocatalysts: Mechanism, challenges and opportunities. Coordination Chemistry Reviews,2024 521, 216177. https://doi.org/10.1016/j.ccr.2024.216177.

[50] Yuanpeng Dong, Peizhu Ji, Xinyue Xu, Rong Li, Yin Wang, Kevinpeter Homewood, Xiaohong Xia, Yun Gao, Xuxing Chen. Rational Design and Construction of aCdS QDs /$InVO_4$ Atomic-Layer (110)/(110) Facet S-Scheme Heterojunction for Highly Efficient Photocatalytic Degradation of C_2H_4. Energy & Environmental Materials,2024 7 (3), e12643. https://doi.org/10.1002/eem2.12643.

[51] Boning Feng, Bin Qi, Song Wang, Peng Zhang, Rongchen Shen, Huiji Li, Xin Li. Elucidating the Charge-Separation and Oxidation Dynamics in Fluorenone-COF/CdS S-Scheme Heterojunction for Photocatalytic Benzaldehyde and Hydrogen Production. Energy & Environmental Materials,2025. https://doi.org/10.1002/eem2.70153.

[52] Tengyuan Gao, Xiufan Liu, Qingshan Feng, Xinhe Wu, Juan Wang, Guohong Wang. Microwave assisted rapid synthesis of TiO_2 NFs@COF S-scheme heterojunction photocatalyst for highly efficient photocatalytic hydrogen evolution. Journal of Colloid and Interface Science,2025 698, 138075. https://doi.org/10.1016/j.jcis.2025.138075.

[53] Minglei Jia, Wei Zhu, Zhaoyang Han, Bing Wang. The polarization effect promotes 2D GeSe/XS_2 (X=Sn, Zr, Hf) van der Waals heterostructure formed S-scheme photocatalyst. International Journal of Hydrogen Energy,2024 95, 165-172. https://doi.org/10.1016/j.ijhydene.2024.11.218.

[54] Huarui Han, Songbai Zhang, Shushan Song, Weijie Zhang, Dandan Liu, Ziheng Song, Qianyu Wang, Changchang Ma, Sheng Feng, Xuemei Duan. Construction of Bi_2O_3−x/NiAl-LDH S-scheme heterojunction for boosting photothermal-assisted photocatalytic CO_2 reduction. Applied Surface Science,2024 662, 160122. https://doi.org/10.1016/j.apsusc.2024.160122.

[55] Yan Zhang, Fengying Cao, Shuyi Zhao, Jinkai Zhang, Shuxian Zhong, Hui Mao, Leihong Zhao, Song Bai. Efficient Charge and Proton Balance Enabled by a 2D/2D S-Scheme Heterojunction

with a Nanochamber Design for Better Synergy of Photocatalytic CO_2 Methanation and Benzylamine Oxidation. Advanced Functional Materials,2025 35 (3), 2413830. https://doi.org/10.1002/adfm.202413830.

[56] Lingxuan Hu, Yan Zhang, Qian Lin, Fengying Cao, Weihao Mo, Shuxian Zhong, Hongjun Lin, Liyan Xie, Leihong Zhao, Song Bai. Unraveling the Ni-Co synergy in bifunctional hydroxide cocatalysts for better cooperation of CO_2 reduction and H_2O oxidation in 2D S-scheme photosynthetic systems. Chinese Journal of Catalysis,2025 68, 311-325. https://doi.org/10.1016/S1872-2067(24)60174-9.

[57] Shengyong Jian, Qingquan Xiao, Jin Huang, Jianfeng Ye, Liqin Zhang, Linjun Xu, Quan Xie. A Highly Efficient Bi_2O_2Se/Bi_2WO_6 S-Scheme Heterojunction Photocatalyst for Solar Water Splitting: A First-Principles Study. Langmuir,2025. https://doi.org/10.1021/acs.langmuir.5c02996.

[58] Tong Zhou, Xue Liu, Liang Zhao, Mingtao Qiao, Wanying Lei. Efficient Photocatalytic H_2O_2 Production and Cr(VI) Reduction over a Hierarchical Ti_3C_2/In_4SnS_8 Schottky Junction. Acta Physico-Chimica Sinica,2024 40 (10), 2309020. https://doi.org/10.3866/PKU.WHXB202309020.

[59] Shuaiqi Gong, Xue Teng, Yanli Niu, Xuan Liu, Mingze Xu, Chen Xu, Lvlv Ji, Zuofeng Chen. Construction of S-scheme 0D/2D heterostructures for enhanced visible-light-driven CO_2 reduction. Applied Catalysis B: Environmental,2021 299, 120521. https://doi.org/10.1016/j.apcatb.2021.120521.

[60] Pengfei Xia, Shaowen Cao, Bicheng Zhu, Mingjin Liu, Miusi Shi, Jiaguo Yu, Yufeng Zhang. Designing a 0D/2D S-Scheme Heterojunction over Polymeric Carbon Nitride for Visible-Light Photocatalytic Inactivation of Bacteria. Angewandte Chemie International Edition,2020 59 (13), 5218-5225. https://doi.org/10.1002/anie.201916012.

[61] Yue Huang, Feifei Mei, Jinfeng Zhang, Kai Dai, Graham Dawson. Construction of 1D/2D $W_{18}O_{49}$/Porous g-C_3N_4 S-Scheme Heterojunction with Enhanced Photocatalytic H_2 Evolution. Acta Phys. -Chim,2021, 2108028. https://doi.org/10.3866/PKU.WHXB202108028.

[62] Keren Shi, Ziyan Wang, Qiaowei Xiao, Xiaoyu Li, Wende Yi, Changyi Yang, Huiqin Yao. Multilayer hollow tubular 1D/2D Co_9S_8/Bi_2MoO_6 S-scheme heterojunctions: Enhanced dual-functional photocatalysis for H_2 production and organic pollutant degradation. Journal of Environmental Management,2026 398, 128428. https://doi.org/10.1016/j.jenvman.2025.128428.

[63] Qi Chen, Cheng Liu, Rui Liu, Yidong Hou, Jinhong Bi, Jimmyc Yu, Ling Wu. Ultrathin 2D/2D MoS_2/Bi_2WO_6 S-scheme heterojunction for boosting photocatalytic degradation of ciprofloxacin. Separation and Purification Technology,2025 355, 129768. https://doi.org/10.1016/j.seppur.2024.129768.

[64] Kangning Zhang, Hao Yang, Chuanhao Liu, Xixiu Zhou, Dongyang He, Jiao Qu. Polar-Surface-Directed H_2O_2 Generation and Activation via a 2D/2D S-Scheme Heterojunction. Small,2026 22 (5), e12415. https://doi.org/10.1002/smll.202512415.

[65] Qiang Li, Lijie Wang, Jupu Song, Yajing Huang, Guoyu Xie, Yi Liu, Hong Li. Novel 2D/2D S-scheme Ni doped SnS_2/BiOBr heterostructures with enhanced photocatalytic activity. Arabian Journal of Chemistry,2023 16 (9), 105081. https://doi.org/10.1016/j.arabjc.2023.105081.

[66] Abdullah Bafaqeer, Anizchennampilly Ummer, Anasa Ahmed, Rayeds Alshareef. Construction of 2D/2D S-scheme Pg-C_3N_4/Fe_2TiO_5 nanosheets with enhanced photogenerated charge separation for highly selective photoconversion of CO_2 into fuels. Journal of Alloys and Compounds,2025 1020, 179287. https://doi.org/10.1016/j.jallcom.2025.179287.

[67] Xiaoyan Zhang, Wenkang Ni, Xuanyu Yue, Zhijie Wang, Zizhong Zhang, Ke Wang, Wenxin Dai, Xianzhi Fu. Synergistic effect between sulfur vacancies and S-scheme heterojunctions in WO_3/VS-Zn_3In2S_6 for enhanced photocatalytic CO_2 reduction in H_2O vapor. Journal of Colloid and Interface Science,2025 678, 233-245. https://doi.org/10.1016/j.jcis.2024.09.023.

[68] Hongzhao Deng, Xingang Fei, Yi Yang, Jiajie Fan, Jiaguo Yu, Bei Cheng, Liuyang Zhang. S-scheme heterojunction based on p-type $ZnMn_2O_4$ and n-type ZnO with improved photocatalytic CO_2 reduction activity. Chemical Engineering Journal,2021 409, 127377. https://doi.org/10.1016/j.cej.2020.127377.

[69] Seyedmajid Ghoreishian, Nugalursharmugam Ranjith, Bumjun Park, Seung-kyu Hwang, Rezvan Hosseini, Reza Behjatmanesh-Ardakani, Seiedmahdi Pourmortazavi, Hyunuk Lee, Byoungchul Son, Somayeh Mirsadeghi, Young-kyu Han, Yunsuk Huh. Full-spectrum-responsive Bi_2S_3@CdS S-scheme heterostructure with intimated ultrathin RGO toward photocatalytic Cr(VI) reduction and H_2O_2 production: Experimental and DFT studies. Chemical Engineering Journal,2021 419, 129530. https://doi.org/10.1016/j.cej.2021.129530.

[70] Baolong Zhang, Bin Sun, Fangxuan Liu, Tingting Gao, Guowei Zhou. TiO_2-based S-scheme photocatalysts for solar energy conversion and environmental remediation. Science China Materials,2024 67 (2), 424-443. https://doi.org/10.1007/s40843-023-2754-8.

[71] Xinhe Wu, Lihong Tan, Guoqiang Chen, Jiayue Kang, Guohong Wang. g-C_3N_4-based S-scheme heterojunction photocatalysts. Science China Materials,2024 67 (2), 444-472. https://doi.org/10.1007/s40843-023-2755-2.

[72] Leonardoe Navarrete-Cevallos, Ronald Vargas, Patricioj Espinoza-Montero. Fundamentals and environmental applications of bismuth vanadate through photoelectrocatalysis. Npj Clean Water,2025 8 (1). https://doi.org/10.1038/s41545-025-00511-0.

[73] Zhiliang Jin, Tian Wang, Entian Cui, Xiuli Yang. Constructing a tandem heterojunction: S-scheme heterojunction and Ohmic junction based on graphdiyne, synergistically optimizing photocatalytic hydrogen evolution. Chemical Engineering Journal,2023 477, 147210. https://doi.org/10.1016/j.cej.2023.147210.

[74] Tian Luo, Leisan Gilmanova, Stefan Kaskel. Advances of MOFs and COFs for photocatalytic CO_2 reduction, H_2 evolution and organic redox transformations. Coordination Chemistry Reviews,2023 490, 215210. https://doi.org/10.1016/j.ccr.2023.215210.

[75] Pooja Shandilya, Shabnam Sambyal, Rohit Sharma, Parteek Mandyal, Baizeng Fang. Properties, optimized morphologies, and advanced strategies for photocatalytic applications of WO_3 based photocatalysts. Journal of Hazardous Materials,2022 428, 128218. https://doi.org/10.1016/j.jhazmat.2022.128218.

[76] Feiyan Xu, Kai Meng, Bei Cheng, Shengyao Wang, Jingsan Xu, Jiaguo Yu. Unique S-scheme heterojunctions in self-assembled TiO_2/$CsPbBr_3$ hybrids for CO_2 photoreduction. Nature Communications,2020 11 (1). https://doi.org/10.1038/s41467-020-18350-7.

[77] Chadawan Khamdang, Sirisak Singsen, Apinya Ngoipala, Itthipon Fongkaew, Anchalee Junkaew, Suwit Suthirakun. Computational Design of a Strain-Induced 2D/2D g-C_3N_4/ZnO S-Scheme Heterostructured Photocatalyst for Water Splitting. ACS Applied Energy Materials,2022 5 (11), 13997-14007. https://doi.org/10.1021/acsaem.2c02600.

[78] Ziming Wang, Yaoyang Xue, Quanjun Xiang. MOFs-based S-scheme heterojunction photocatalysts. Coordination Chemistry Reviews,2024 504, 215674. https://doi.org/10.1016/j.ccr.2024.215674.

[79] Xinhe Wu, Mahmoud Sayed, Guohong Wang, Weilai Yu, Bicheng Zhu. COF-Based S-Scheme Heterojunction Photocatalyst. Advanced Materials,2026 38 (2), e11322. https://doi.org/10.1002/adma.202511322.

[80] Yajing Ren, Yunfeng Li, Guixu Pan, Ning Wang, Yan Xing, Zhenyi Zhang. Recent progress in CdS-based S-scheme photocatalysts. Journal of Materials Science & Technology,2024 171, 162-184. https://doi.org/10.1016/j.jmst.2023.06.052.

[81] Lijun Chen, Guanwen Su, Chenguang Wang, Leping Dang, Hongyuan Wei. S-scheme heterojunction BP/WO_3 with tight interface firstly prepared in magnetic stirring reactor for enhanced photocatalytic degradation of hazardous contaminants under visible light. Separation and Purification Technology,2022 292, 120986. https://doi.org/10.1016/j.seppur.2022.120986.

[82] Youlin Wu, Haiyan Zhang, Youji Li, Zhiliang Jin. Partial phosphating of Ni-MOFs and Cu_2S snowflakes form 2D/2D structure for efficiently improved photocatalytic hydrogen evolution.

International Journal of Hydrogen Energy,2022 47 (86), 36530-36542. https://doi.org/10.1016/j.ijhydene.2022.08.205.

[83] Kejun Bi, Meng Wang, Haoyu Li. Synthesis of S scheme 2D/2D g-C_3N_5/g-C_3N_4 heterojunction for photocatalytic degradation tetracycline. Surfaces and Interfaces,2024 50, 104487. https://doi.org/10.1016/j.surfin.2024.104487.

[84] Wenliang Liu, Yuqi Wang, Kai Qi, Yan Wang, Fushan Wen, Jiqian Wang. Superb photocatalytic activity of 2D/2D Cl doped g-C_3N_4 nanodisc/Bi_2WO_6 nanosheet heterojunction: Exploration of photoinduced carrier migration in S-scheme heterojunction. Journal of Alloys and Compounds,2023 933, 167789. https://doi.org/10.1016/j.jallcom.2022.167789.

[85] Pengyu Dong, Aicaijun Zhang, Ting Cheng, Jinkang Pan, Jun Song, Lei Zhang, Rongfeng Guan, Xinguo Xi, Jinlong Zhang. 2D/2D S-scheme heterojunction with a covalent organic framework and g-C_3N_4 nanosheets for highly efficient photocatalytic H_2 evolution. Chinese Journal of Catalysis,2022 43 (10), 2592-2605. https://doi.org/10.1016/s1872-2067(22)64094-4.

[86] Xing Chen, Taiping Hu, Jinfeng Zhang, Changchun Yang, Kai Dai, Chengsi Pan. Diethylenetriamine synergistic boosting photocatalytic performance with porous g-C_3N_4/CdS-diethylenetriamine 2D/2D S-scheme heterojunction. Journal of Alloys and Compounds,2021 863, 158068. https://doi.org/10.1016/j.jallcom.2020.158068.

[87] Taiping Hu, Kai Dai, Jinfeng Zhang, Shifu Chen. Noble-metal-free Ni_2P modified step-scheme $SnNb_2O_6$/Cd-diethylenetriamine for photocatalytic hydrogen production under broadband light irradiation. Applied Catalysis B: Environmental,2020 269, 118844. https://doi.org/10.1016/j.apcatb.2020.118844.

[88] Huihui Weng, Houjiang Liu, Guijun Yang, Jiawei Ding, Chuangchuang Gong, Yuanyuan Fu, Jin Cui, Liying Ma, Chunnian He, Naiqin Zhao, Fang He. Construction of 2D/2D NH_2-TiO_2/ReS_2 molecular-connected heterojunction to achieve selective carrier transport for photocatalytic hydrogen production. Chemical Engineering Journal,2024, 151687. https://doi.org/10.1016/j.cej.2024.151687.

[89] Haibo Zhou, Kaili Wu, Xunwen Luo, Qinghong Cai, Jia Zeng, Youzhou He, Xingyan Liu, Siqi Li, Siping Wei. Construction of 2D/2D S-scheme Bi_2MoO_6/Zn-TCPP heterojunction via in-situ self-assembly growth strategy to enhance interface effect for efficient photocatalytic hydrogen production. Journal of Colloid and Interface Science,2025 677, 827-841. https://doi.org/10.1016/j.jcis.2024.08.122.

[90] Lei Li, Xinyan Dai, Kangjie Gao, Hangjing Yu, Fang Chen, Wentao Wang, Jiqiang Ning, Yong Hu. Customized interfacial electronic interactions in protonated g-C_3N_4/$ZnIn_2S_4$ S-scheme 2D/2D

edge-to-face heterostructures for boosted C_O2 photoconversion. Chemical Engineering Journal,2025 514, 163193. https://doi.org/10.1016/j.cej.2025.163193.

[91] Tengfei Cao, Quanlong Xu, Jun Zhang, Shenggao Wang, Tingmin Di, Quanrong Deng. S-scheme g-C_3N_4/BiOBr heterojunction for efficient photocatalytic H_2O_2 production. Chinese Journal of Catalysis,2025 72, 118-129. https://doi.org/10.1016/s1872-2067(24)60277-9.

[92] Doudou Ren, Weinan Zhang, Yingna Ding, Rongchen Shen, Zhimin Jiang, Xinyong Lu, Xin Li. In Situ Fabrication of Robust Cocatalyst-Free CdS/g-C_3N_4 2D–2D Step-Scheme Heterojunctions for Highly Active H_2 Evolution. Solar RRL,2019 4 (8). https://doi.org/10.1002/solr.201900423.

[93] Junxian Bai, Rongchen Shen, Zhimin Jiang, Peng Zhang, Youji Li, Xin Li. Integration of 2D layered CdS/WO_3 S-scheme heterojunctions and metallic Ti_3C_2 MXene-based Ohmic junctions for effective photocatalytic H_2 generation. Chinese Journal of Catalysis,2022 43 (2), 359-369. https://doi.org/10.1016/s1872-2067(21)63883-4.

[94] Keke Li, Yating Zhang, Jia Jia, Lisi Zheng, Boni Li, Xue Li, Tian Zhang, Xiangyu Feng, Guoyang Liu. 2D/2D Carbon Nitride/Zn-Doped Bismuth Vanadium Oxide S-Scheme Heterojunction for Enhancing Photocatalytic CO_2 Reduction into Methanol. Industrial &Amp; Engineering Chemistry Research,2023 62 (13), 5552-5562. https://doi.org/10.1021/acs.iecr.2c03536.

[95] Quanlong Xu, S Wageh, Ahmed A Al-Ghamdi, Xin Li. Design principle of S-scheme heterojunction photocatalyst. Journal of Materials Science & Technology,2022 124, 171-173. https://doi.org/10.1016/j.jmst.2022.02.016.

[96] Bin Zhang, Xiaoyun Hu, Shizhou Liu, Jun Fan. Novel S-scheme 2D/2D BiOBr/g-C_3N_4 heterojunctions with enhanced photocatalytic activity. Chinese Journal of Catalysis,2021 42 (9), 1519-1529. https://doi.org/10.1016/s1872-2067(20)63765-2.

[97] Colin Ophus. Four-Dimensional Scanning Transmission Electron Microscopy (4D-STEM): From Scanning Nanodiffraction to Ptychography and Beyond. Microscopy and Microanalysis,2019 25 (3), 563-582. https://doi.org/10.1017/s1431927619000497.

[98] Rf Egerton. Radiation damage to organic and inorganic specimens in the TEM. Micron,2019 119, 72-87. https://doi.org/10.1016/j.micron.2019.01.005.

[99] Shinygolda A, Ajithp Varghese, Navid Rabiee, Bernaurdshaw Neppolian, Sandeepkumar Lakhera. Synergistic hydrogen generation through a 2D-2D $NiCuInS_2$:In_2S_3/g-C_3N_4 dual S-scheme heterojunction nanosheets. Carbon,2023 215, 118441. https://doi.org/10.1016/j.carbon.2023.118441.

[100] Zetian He, Che Qian, Daimei Chen, Kang Xu, Weichang Hao. Design of ultrathin CoAl-LDHs/$ZnIn_2S_4$ with strong interfacial bonding and rich oxygen vacancies for highly efficient

hydrogen evolution activity. Journal of Colloid and Interface Science,2023 651, 138-148. https://doi.org/10.1016/j.jcis.2023.07.179.

[101] Xiao-chen Bai, Greg Mcmullan, Sjorshw Scheres. How cryo-EM is revolutionizing structural biology. Trends in Biochemical Sciences,2015 40 (1), 49-57. https://doi.org/10.1016/j.tibs.2014.10.005.

[102] Zheng Meng, Jianjun Zhang, Haoyu Long, Hermenegildo García, Liuyang Zhang, Bicheng Zhu, Jiaguo Yu. Kelvin Probe Force Microscopy Reveals Spatially Resolved Charge-Transfer Mechanism in CdS/BiOBr S-scheme Heterojunction Photocatalyst. Angewandte Chemie International Edition,2025 64, e202505456. https://doi.org/10.1002/anie.202505456.

[103] Ricardo Garcia. Nanomechanical Mapping of Soft Materials with the Atomic Force Microscope: Methods, Theory and Applications. Chemical Society Reviews,2020. https://doi.org/10.1039/d0cs00318b.

[104] U Zerweck, C Loppacher, T Otto, S Grafstrom, Lm Eng. Accuracy and Resolution Limits of Kelvin Probe Force Microscopy. Physical Review B,2005 71. https://doi.org/10.1103/physrevb.71.125424.

[105] Xiaoyang Yue, Lei Cheng, Jiajie Fan, Quanjun Xiang. 2D/2D $BiVO_4$/$CsPbBr_3$ S-scheme heterojunction for photocatalytic CO_2 reduction: Insights into structure regulation and Fermi level modulation. Applied Catalysis B: Environmental,2022 304, 120979. https://doi.org/10.1016/j.apcatb.2021.120979.

[106] Jing Wang, Zhongliao Wang, Kai Dai, Jinfeng Zhang. Review on inorganic–organic S-scheme photocatalysts. Journal of Materials Science & Technology,2023 165, 187-218. https://doi.org/10.1016/j.jmst.2023.03.067.

[107] Shuaiqi Gong, Xue Teng, Yanli Niu, Xuan Liu, Mingze Xu, Chen Xu, Lvlv Ji, Zuofeng Chen. Construction of S-scheme 0D/2D heterostructures for enhanced visible-light-driven CO_2 reduction. Applied Catalysis B: Environmental,2021 298, 120521. https://doi.org/10.1016/j.apcatb.2021.120521.

[108] Wangyang Ma, Dewen Zheng, Yuxi Xian, Xianhai Hu, Qian Zhang, Shanyu Wang, Congliang Cheng, Jin Liu, Ping Wang. Efficient Hydrogen Evolution under Visible Light by Bimetallic Phosphide NiCoP Combined with g-C_3N_4 /CdS S-Scheme Heterojunction. ChemCatChem,2021 13 (20), 4403-4410. https://doi.org/10.1002/cctc.202100833.

[109] Abulikemu Abulizi, Tao Zhang, Kuerbangnisha Kadeer, Yalkunjan Tursun, Dilinuer Talifur. Designing effective and stable S-scheme RGO/$AgVO_3$ /AgBr hybrid with enhanced photocatalytic performance. Journal of the American Ceramic Society,2021 104 (8), 4095-4108.

https://doi.org/10.1111/jace.17801.

[110] Guangmin Ren, Zixuan Wei, Zizhen Li, Xiaochao Zhang, Xiangchao Meng. Fabrication of S-scheme hollow TiO_2@Bi_2MoO_6 composite for efficiently photocatalytic CO_2 reduction. Materials Today Chemistry,2023 27, 101260. https://doi.org/10.1016/j.mtchem.2022.101260.

[111] Azin Khamesan, Mohammadmehdi Esfahani, Jahanb Ghasemi, Faezeh Farzin, Anita Parsaei-Khomami, Mitra Mousavi. Graphitic-C_3N_4/ZnCr-layered double hydroxide 2D/2D nanosheet heterojunction: Mesoporous photocatalyst for advanced oxidation of azo dyes with in situ produced H_2O_2. Advanced Powder Technology,2022 33 (11), 103777. https://doi.org/10.1016/j.apt.2022.103777.

[112] Hongji Li, Dandan Wang, Chun Miao, Fengwu Xia, Yubo Wang, Yutong Wang, Chunbo Liu, Guangbo Che. g-C_3N_4/BiOI S-scheme heterojunction: A 2D/2D model platform for visible-light-driven photocatalytic CO_2 reduction and pollutant degradation. Journal of Environmental Chemical Engineering,2022 10 (4), 108201. https://doi.org/10.1016/j.jece.2022.108201.

[113] Antonio Bauzá, Antonio Frontera. Halogen and Chalcogen Bond Energies Evaluated Using Electron Density Properties. Chemphyschem : A European Journal of Chemical Physics and Physical Chemistry,2020 21 (1), 26-31. https://doi.org/10.1002/cphc.201901001.

[114] Jianjun Zhang, Liuyang Zhang, Wang Wang, Jiaguo Yu. In Situ Irradiated X-ray Photoelectron Spectroscopy Investigation on Electron Transfer Mechanism in S-Scheme Photocatalyst. The Journal of Physical Chemistry Letters,2022 13 (36), 8462-8469. https://doi.org/10.1021/acs.jpclett.2c02125.

[115] Thomas Hackl, Georg Schitter, Patrick Mesquida. AC Kelvin Probe Force Microscopy Enables Charge Mapping in Water. ACS Nano,2022 16 (11), 17982-17990. https://doi.org/10.1021/acsnano.2c07121.

[116] Bingquan Xia, Bowen He, Jianjun Zhang, Laiquan Li, Yanzhao Zhang, Jiaguo Yu, Jingrun Ran, Shizhang Qiao. TiO_2 /$FePS_3$ S-Scheme Heterojunction for Greatly Raised Photocatalytic Hydrogen Evolution. Advanced Energy Materials,2022 12 (46), 2201449. https://doi.org/10.1002/aenm.202201449.

[117] Ruiqi Gao, Rongchen Shen, Can Huang, Kaihui Huang, Guijie Liang, Peng Zhang, Xin Li. 2D/2D Hydrogen-Bonded Organic Frameworks/Covalent Organic Frameworks S-Scheme Heterojunctions for Photocatalytic Hydrogen Evolution. Angewandte Chemie International Edition,2025 64 (2), e202414229. https://doi.org/10.1002/anie.202414229.

[118] Xiang Zhao, Shujuan Xiao, Bingming Yao, Yifu Chen, Shouwu Yu. DFT-Based Mechanistic Exploration and Application in Photocatalytic Heterojunctions. Journal of Chemical Theory and

Computation,2024 20 (22), 9770-9786. https://doi.org/10.1021/acs.jctc.4c01051.

[119] Markus Bursch, Janmichael Mewes, Andreas Hansen, Stefan Grimme. Best-Practice DFT Protocols for Basic Molecular Computational Chemistry. Angewandte Chemie International Edition,2022 61 (42). https://doi.org/10.1002/anie.202205735.

[120] Yang Wu, Hong-xia Yu, Chun-hua Yang, He-na Zhang, Liang-hui Zhu, Yanming Ma, Xiao-chun Wang, Seanxiao-an Zhang. Essential effect of proton coupled electron sequent transfer on photocatalytic water complete dissociation: A DFT study. International Journal of Hydrogen Energy,2021 46 (69), 34216-34228. https://doi.org/10.1016/j.ijhydene.2021.07.223.

[121] Yang Liu, Meng Li, Tao Liu, Zhen Wu, Liuyang Zhang. Enhanced charge carrier transport in TiO_2/COF S-scheme heterojunction for efficient photocatalytic H_2O_2 production. Journal of Materials Science & Technology,2025 233, 201-209. https://doi.org/10.1016/j.jmst.2025.03.005.

[122] Libo Wang, Bei Cheng, Liuyang Zhang, Jiaguo Yu. In situ Irradiated XPS Investigation on S-Scheme TiO_2 @$ZnIn_2S_4$ Photocatalyst for Efficient Photocatalytic CO_2 Reduction. Small,2021 17 (41), 2103447. https://doi.org/10.1002/smll.202103447.

[123] Bingquan Xia, Bowen He, Jianjun Zhang, Laiquan Li, Yanzhao Zhang, Jiaguo Yu, Jingrun Ran, Shizhang Qiao. TiO_2/$FePS_3$ S-Scheme Heterojunction for Greatly Raised Photocatalytic Hydrogen Evolution. Advanced Energy Materials,2022 12 (46). https://doi.org/10.1002/aenm.202201449.

[124] Huili Ran, Xue Liu, Langhuan Ye, Jiajie Fan, Bicheng Zhu, Quanlong Xu, Yuechang Wei. Construction of CYAN–COF/$ZnIn_2S_4$ S-scheme heterojunction for boosted photocatalytic hydrogen generation. Journal of Materials Science & Technology,2025 234, 24-30. https://doi.org/10.1016/j.jmst.2024.12.089.

[125] Chunguang Chen, Zhongliao Wang, Jinfeng Zhang, Kai Dai, Jianjun Zhang, Liuyang Zhang. Multi-Energy-State Covalent Organic Framework/Sulfur-Vacancy-Engineered $Mn_{0.2}Cd_{0.8}S$ S-Scheme Photocatalyst for Enhanced Light Harvesting and H_2O_2 Generation. Advanced Materials,2026, e73326. https://doi.org/10.1002/adma.73326.

[126] Entian Cui, Yulian Lu, Zhaoxia Li, Zhilei Chen, Chengyan Ge, Jizhou Jiang. Interfacial B-O bonding modulated S-scheme B-doped N-deficient C_3N_4/O-doped-C_3N_5 for efficient photocatalytic overall water splitting. Chinese Chemical Letters,2025 36 (1), 110288. https://doi.org/10.1016/j.cclet.2024.110288.

[127] Bingbing Luan, Xiaoyu Chu, Ya Wang, Xiu Qiao, Yanxia Jiang, Fengming Zhang. Construction of COF/COF Organic S-Scheme Heterostructure for Enhanced Overall Water Splitting. Advanced Materials,2024 36 (49), 2412653. https://doi.org/10.1002/adma.202412653.

[128] Mahmoud Sayed, Bicheng Zhu, Panyong Kuang, Xiangyu Liu, Bei Cheng, Ahmedabdullahal Ghamdi, Swelm Wageh, Liuyang Zhang, Jiaguo Yu. EPR Investigation on Electron Transfer of 2D/3D g-C_3N_4/ZnO S-Scheme Heterojunction for Enhanced CO_2 Photoreduction. Advanced Sustainable Systems,2021 6 (1). https://doi.org/10.1002/adsu.202100264.

[129] Chang Cheng, Jianjun Zhang, Bicheng Zhu, Guijie Liang, Liuyang Zhang, Jiaguo Yu. Verifying the Charge-Transfer Mechanism in S-Scheme Heterojunctions Using Femtosecond Transient Absorption Spectroscopy. Angewandte Chemie International Edition,2023 62 (8). https://doi.org/10.1002/anie.202218688.

[130] Juntao Yan, Jianjun Zhang. Charge transfer kinetic analysis of S-scheme heterojunction by femtosecond transient absorption spectrum. Journal of Materials Science & Technology,2024 193, 18-21. https://doi.org/10.1016/j.jmst.2023.12.054.

[131] Jianjun Zhang, Bicheng Zhu, Liuyang Zhang, Jiaguo Yu. Femtosecond transient absorption spectroscopy investigation into the electron transfer mechanism in photocatalysis. Chemical Communications,2023 59 (6), 688-699. https://doi.org/10.1039/d2cc06300j.

[132] Bowen Liu, Kai Meng, Bei Cheng, Lei Wang, Guijie Liang, Yuanbiao Bie. Prolonging charge carrier lifetime in S-scheme heterojunctions via ligand-to-metal charge transfer of Ni-MOF for photocatalytic H_2 production and simultaneous phenylamine coupling. Journal of Materials Science &Amp; Technology,2025 214, 286-295. https://doi.org/10.1016/j.jmst.2025.02.013.

[133] Zhenkun Li, Yongxian Zhang, Youlin Wu, Bolin Yang, Zhengyu Zhou, Zhiliang Jin. In situ XPS evidence of fully conjugated COF and C_3N_4 construct S-scheme heterojunction boosting photogenerated carriers transfer and separate for efficiently photocatalytic hydrogen evolution. Journal of Materials Science & Technology,2025 233, 48-57. https://doi.org/10.1016/j.jmst.2025.01.040.

[134] Yulin Cheng, Jinchan He, Ping Yang. Construction of layered SnS_2 and g-C_3N_4 nanoarchitectonics towards pollution degradation and H_2 generation. Colloids and Surfaces a: Physicochemical and Engineering Aspects,2024 680, 132678. https://doi.org/10.1016/j.colsurfa.2023.132678.

[135] Junxian Bai, Rongchen Shen, Weilin Chen, Jun Xie, Peng Zhang, Zhimin Jiang, Xin Li. Enhanced photocatalytic H2 evolution based on a Ti_3C_2/$Zn_{0.7}Cd_{0.3}S$/Fe_2O_3 Ohmic/S-scheme hybrid heterojunction with cascade 2D coupling interfaces. Chemical Engineering Journal,2022 429, 132587. https://doi.org/10.1016/j.cej.2021.132587.

[136] Fei He, Bicheng Zhu, Bei Cheng, Jiaguo Yu, Wingkei Ho, Wojciech Macyk. 2D/2D/0D TiO_2/C_3N_4/Ti_3C_2 MXene composite S-scheme photocatalyst with enhanced CO_2 reduction activity.

Applied Catalysis B: Environmental,2020 272, 119006. https://doi.org/10.1016/j.apcatb.2020.119006.

[137] Mingwang Liu, Jing Wen, Runshi Xiao, Rong Tan, Ying Qin, Jinli Li, Yuxuan Bai, Mengzhen Xi, Wenhong Yang, Qie Fang, Liuyong Hu, Wenling Gu, Chengzhou Zhu. Improving Interface Matching in MOF-on-MOF S-Scheme Heterojunction through π–π Conjugation for Boosting Photoelectric Response. Nano Letters,2023 23 (11), 5358-5366. https://doi.org/10.1021/acs.nanolett.3c01650.

[138] Mengchi Liu, Peng Ye, Men Wang, Lele Wang, Chao Wu, Jing Xu, Yuanping Chen. 2D/2D Bi-MOF-derived BiOCl/MoS_2 nanosheets S-scheme heterojunction for effective photocatalytic degradation. Journal of Environmental Chemical Engineering,2022 10 (5), 108436. https://doi.org/10.1016/j.jece.2022.108436.

[139] Miaomiao Yang, Chihao Cao, Limeili Tian, Yangyang Huang, Jing Wang, Qingqiang Meng, Aiping Wu, Ying Zhang. 2D/2D P-Doped G-C_3N_4/$BiOCl_{0.75}I_{0.25}$ S-Scheme Van der Waals Heterojunction Photocatalysts for Boosting Tetracycline Hydrochloride Degradation. Small,2025. https://doi.org/10.1002/smll.202504672.

[140] Mingming Gao, Zhiyong Li, Xiaojiang Su, Xinyi Zhang, Jin Chang, Di Geng, Yinpeng Lu, Hexin Zhang, Tong Wei, Jing Feng. 2D/2D MgO/g-C_3N_4 S-scheme heterogeneous tight with Mg–N bonds for efficient photo-Fenton degradation: Enhancing both oxygen vacancy and charge migration. Chemosphere,2023 343, 140285. https://doi.org/10.1016/j.chemosphere.2023.140285.

[141] Bicheng Zhu, Haiyan Tan, Jiajie Fan, Bei Cheng, Jiaguo Yu, Wingkei Ho. Tuning the strength of built-in electric field in 2D/2D g-C_3N_4/SnS_2 and g-C_3N_4/ZrS_2 S-scheme heterojunctions by nonmetal doping. Journal of Materiomics,2021 7 (5), 988-997. https://doi.org/10.1016/j.jmat.2021.02.015.

[142] Chunxue Li, Xiaoteng Liu, Guixiang Ding, Pengwei Huo, Yan Yan, Yongsheng Yan, Guangfu Liao. Interior and Surface Synergistic Modifications Modulate the $SnNb_2O_6$/Ni-Doped $ZnIn_2S_4$ S-Scheme Heterojunction for Efficient Photocatalytic H_2 Evolution. Inorganic Chemistry,2022 61 (11), 4681-4689. https://doi.org/10.1021/acs.inorgchem.1c03936.

[143] Haopeng Jiang, Weikang Wang, Lijuan Sun, Tingting Kong, Zhongxi Lu, Hua Tang, Lele Wang, Qinqin Liu. Boosting photocatalytic CO_2 reduction by tuning photogenerated carrier kinetics in two-dimensional WO_x/BiOCl S-scheme heterojunction with oxygen vacancies. Journal of Catalysis,2022 416, 1-10. https://doi.org/10.1016/j.jcat.2022.10.015.

[144] Pengfei Tan, Mingyuan Zhang, Lu Yang, Ruifeng Ren, Huanhuan Zhai, Hele Liu, Jiaoyang Chen, Jun Pan. Modulated band structure in 2D/2D $ZnIn_2S_4$/B-C_3N_4 S-scheme heterojunction for

photocatalytic hydrogen evolution. Diamond and Related Materials,2023 140, 110456. https://doi.org/10.1016/j.diamond.2023.110456.

[145] Biao Zhou, Xin Xu, Mingjie Li, Liqin Wu, Shuang Xu, Ligang Yuan, Yanan Chong, Weiguang Xie, Pengyi Liu, Daiqi Ye, Geoffreyin Waterhouse, Yongcai Qiu, Guangxu Chen, Tingting Shi, Keyou Yan. Synergistic effects of heterointerface and surface Br vacancies in ultrathin 2D/2D $H_2WO_4/Cs_2AgBiBr_6$ for efficient CO_2 photoreduction to CH_4. Chemical Engineering Journal,2023 468, 143754. https://doi.org/10.1016/j.cej.2023.143754.

[146] Ying Tian, Kunfeng Zhang, Haoran Zhao, Bo Peng, Jinxia Liang, Hongxia Chen, Runfeng Huang, Yuanyuan Wei, Hanyu Chen. Synergetic promotional effect of dual oxygen vacancies and 2D/2D TiO_2/BiOBr S-scheme heterostructure for boosted photocatalytic oxytetracycline removal. Colloids and Surfaces a: Physicochemical and Engineering Aspects,2025 715, 136636. https://doi.org/10.1016/j.colsurfa.2025.136636.

[147] Qiaoqiao Li, Wenli Zhao, Zicheng Zhai, Kaixu Ren, Tingyu Wang, Hao Guan, Haifeng Shi. 2D/2D Bi_2MoO_6/g-C_3N_4 S-scheme heterojunction photocatalyst with enhanced visible-light activity by Au loading. Journal of Materials Science & Technology,2020 56, 216-226. https://doi.org/10.1016/j.jmst.2020.03.038.

[148] Yue Hu, Xiaohui Yu, Qinqin Liu, Lele Wang, Hua Tang. Highly metallic Co-doped MoS_2 nanosheets as an efficient cocatalyst to boost photoredox dual-reaction for H_2 production and benzyl alcohol oxidation. Carbon,2022 188, 70-80. https://doi.org/10.1016/j.carbon.2021.11.050.

[149] Akhila Amaregowda, Sneha Yadav, Rageshnath R, Udayakumara H, Snehanarayan Kulkarni, Harikaranahalli Puttaiah Shivaraju, Nk Lokanath. Synergistic visible-light photocatalytic degradation of amoxicillin and ciprofloxacin using Ag/AgO-integrated 2D/2D g-$C_3N_4/Ni_3V_2O_8$ S-scheme heterostructure. Materials Today Sustainability,2024 28, 101017. https://doi.org/10.1016/j.mtsust.2024.101017.

[150] Lina Zhao, Ji Bian, Xianfa Zhang, Linlu Bai, Linyao Xu, Yang Qu, Zhijun Li, Yuxin Li, Liqiang Jing. Construction of Ultrathin S-Scheme Heterojunctions of Single Ni Atom Immobilized Ti-MOF and $BiVO_4$ for CO_2 Photoconversion of nearly 100% to CO by Pure Water. Advanced Materials,2022 34 (41), 2205303. https://doi.org/10.1002/adma.202205303.

[151] Rose Amal, Carolina Belver, Wang Yong. Synergistic dual-vacancies and La single-atom engineering over S-Scheme WS_{2-x}/La1-$WO_{2.9}$ heterojunction for efficient N_2-to-NH_3 photosynthesis. Applied Catalysis B Environment and Energy,2023 343, 123593. https://doi.org/10.1016/j.apcatb.2025.125441.

[152] Yingxuan Miao, Yunxuan Zhao, Shuai Zhang, Run Shi, Tierui Zhang. Strain Engineering: A

Boosting Strategy for Photocatalysis. Advanced Materials,2022 34 (29). https://doi.org/10.1002/adma.202200868.

[153] Junhao Zhu, Zhengdong Sun, Jiaxin Ma, Yifei Shen, Xiao Wang, Meng Zhang. Strain-engineered Ga_2SSe/SnS_2 van der Waals heterojunction as an efficient S-scheme photocatalyst for solar water splitting. Surfaces and Interfaces,2025 74, 107637. https://doi.org/10.1016/j.surfin.2025.107637.

[154] Zhuojun Jiang, Xiu Gong, Yilin Feng, Hui Shen, Gui-lin Yin, Guohao Wang, Xiaoqing Xiao, Xiaosi Qi, Peng Chen. Interfacial Stress-Activated S-Scheme Heterojunction for Highly Selective Photothermal CO_2 Reduction with Low-Concentration. Applied Catalysis B: Environment and Energy,2026, 126931. https://doi.org/10.1016/j.apcatb.2026.126931.

[155] Chadawan Khamdang, Sirisak Singsen, Apinya Ngoipala, Ittipon Fongkaew, Anchalee Junkaew, Suwit Suthirakun. Computational Design of a Strain-Induced 2D/2D g-C_3N_4/ZnO S-Scheme Heterostructured Photocatalyst for Water Splitting. ACS Applied Energy Materials,2022 5 (11), 13997-14007. https://doi.org/10.1021/acsaem.2c02600.

[156] Yang Yang, Zisheng Du, Hongyuan Yang, Debabrata Bagchi, Guotao Yang, Prashanthw Menezes, Sugang Meng. Facet-Engineered S-Scheme Heterostructure with Enhanced Active Sites for Efficient Photocatalytic Degradation of Organic Contaminants. Advanced Functional Materials,2026. https://doi.org/10.1002/adfm.202525191.

[157] Xiuli Wang, Can Li. Roles of Phase Junction in Photocatalysis and Photoelectrocatalysis. The Journal of Physical Chemistry C,2018 122 (37), 21083-21096. https://doi.org/10.1021/acs.jpcc.8b06039.

[158] Yamin Xi, Wenbin Chen, Wenrou Dong, Zhixin Fan, Kefeng Wang, Yue Shen, Gaomei Tu, Shuxian Zhong, Song Bai. Engineering an Interfacial Facet of S-Scheme Heterojunction for Improved Photocatalytic Hydrogen Evolution by Modulating the Internal Electric Field. ACS Applied Materials & Interfaces,2021 13 (33), 39491-39500. https://doi.org/10.1021/acsami.1c11233.

[159] Xiaoqiang An, Jiyong Bian, Kai Zhu, Ruiping Liu, Huijuan Liu, Jiuhui Qu. Facet-dependent activity of TiO_2/covalent organic framework S-scheme heterostructures for CO_2 photoreduction. Chemical Engineering Journal,2022 442, 135279. https://doi.org/10.1016/j.cej.2022.135279.

[160] Irshad Ahmad, Yanhong Zou, Jiaying Yan, Yuyu Liu, Shazia Shukrullah, Muhammadyasin Naz, Humaira Hussain, Waheedqamar Khan, Nr Khalid. Semiconductor photocatalysts: A critical review highlighting the various strategies to boost the photocatalytic performances for diverse applications. Advances in Colloid and Interface Science,2023 311, 102830. https://doi.org/10.1016/j.cis.2022.102830.

[161] Amit Kumar, Atul Khosla, Sunilkumar Sharma, Pooja Dhiman, Gaurav Sharma, Lalitha Gnanasekaran, Mu. Naushad, Florianj Stadler. A review on S-scheme and dual S-scheme heterojunctions for photocatalytic hydrogen evolution, water detoxification and CO_2 reduction. Fuel,2023 333, 126267. https://doi.org/10.1016/j.fuel.2022.126267.

[162] Areen Sherryna, Muhammad Tahir, Zakiyamani Zakaria. *T*rimetallic $Ni_xCo_yAl_z$ LDH-Modified g-C_3N_4 with Influential Effects of M^{2+} /M^{3+} (Ni/Co) Active Centers for Stimulating Photocatalytic Hydrogen Production. ACS Applied Energy Materials,2024 7 (15), 6289-6311. https://doi.org/10.1021/acsaem.4c00895.

[163] Yanhong Wang, Hui Wang, Xuan Li, Le Gao, Yawen Li, Jiaqi Huo, Weiwei Kang, Chunxiao Zou, Lishan Jia. Oxygen vacancy-mediated direct solid phase integration of interfacial chemical bond reinforced $LaNiO_3$/RGO/g-C_3N_4 heterojunction for improving hydrogen production. Applied Surface Science,2023 616, 156501. https://doi.org/10.1016/j.apsusc.2023.156501.

[164] Junnan Tao, Xiaohui Yu, Qinqin Liu, Guiwu Liu, Hua Tang. Internal electric field induced S–scheme heterojunction MoS_2/CoAl LDH for enhanced photocatalytic hydrogen evolution. Journal of Colloid and Interface Science,2021 585, 470-479. https://doi.org/10.1016/j.jcis.2020.10.028.

[165] Qiqi Zhang, Xue Bai, Xiaoyun Hu, Jun Fan, Enzhou Liu. Efficient photocatalytic H2 evolution over 2D/2D S-scheme NiTe$_2$/g-C_3N_4 heterojunction with superhydrophilic surface. Applied Surface Science,2021 579, 152224. https://doi.org/10.1016/j.apsusc.2021.152224.

[166] Junxian Bai, Weijin Chen, Rongchen Shen, Zhimin Jiang, Peng Zhang, Wei Liu, Xin Li. Regulating interfacial morphology and charge-carrier utilization of Ti_3C_2 modified all-sulfide CdS/$ZnIn_2S_4$ S-scheme heterojunctions for effective photocatalytic H_2 evolution. Journal of Materials Science &Amp; Technology,2022 112, 85-95. https://doi.org/10.1016/j.jmst.2021.11.003.

[167] Lele Wang, Tao Yang, Lijie Peng, Qiqi Zhang, Xilin She, Hua Tang, Qinqin Liu. Dual transfer channels of photo-carriers in 2D/2D/2D sandwich-like $ZnIn_2S_4$/g-C_3N_4/Ti_3C_2 MXene S-scheme/Schottky heterojunction for boosting photocatalytic H_2 evolution. Chinese Journal of Catalysis,2022 43 (10), 2720-2731. https://doi.org/10.1016/s1872-2067(22)64133-0.

[168] Wen-ou Bai, Ke Wu, Chunlei Wu, Ning Li, Yangqin Gao, Lei Ge. Interfacial engineering to construct 2D-2D NiCo-LDH/g-C_3N_4 heterojunctions for enhanced photocatalytic hydrogen production performance. International Journal of Hydrogen Energy,2023 48 (44), 16704-16714. https://doi.org/10.1016/j.ijhydene.2023.01.153.

[169] Wendi Liu, Ya Xiong, Qian Liu, Xiao Chang, Jian Tian. The construction of S-scheme heterostructure in ultrathin WS_2/$Zn_3In_2S_6$ nanosheets for enhanced photocatalytic hydrogen evolution. Journal of Colloid and Interface Science,2023 651, 633-644.

https://doi.org/10.1016/j.jcis.2023.07.200.

[170] Xiaoyan Ding, Yanjun Xue, Jingjing Wang, Jian Tian. Semimetal 1T' phase molybdenum sulfide decorated on zinc indium sulfide with S-scheme heterojunction for enhanced photocatalytic hydrogen evolution. Journal of Colloid and Interface Science,2024 659, 225-234. https://doi.org/10.1016/j.jcis.2023.12.161.

[171] Haijun Hu, Xinyu Zhang, Kailai Zhang, Yali Ma, Haitang Wang, Hui Li, Hongwei Huang, Xiaodong Sun, Tianyi Ma. Construction of a 2D/2D Crystalline Porous Materials Based S-Scheme Heterojunction for Efficient Photocatalytic H_2 Production. Advanced Energy Materials,2024 14 (11). https://doi.org/10.1002/aenm.202303638.

[172] Xiaoyan Ding, Xinxin Xu, Jiahui Wang, Yanjun Xue, Jingjing Wang, Yingying Qin, Jian Tian. Construction of two-dimensional zinc indium sulfide/bismuth titanate nanoplate with S-scheme heterojunction for enhanced photocatalytic hydrogen evolution. Journal of Colloid and Interface Science,2024 662, 727-737. https://doi.org/10.1016/j.jcis.2024.02.124.

[173] Rabia Nawaz, Muhammad Saad, Ali Bahadur, Shahid Iqbal, Sajid Mahmood, Ammar Zidan, Muhammadshuaib Khan, Rabia Liaquat, Manzar Sohail, Mohamed Abdt Alotaibi. Designing an innovative 2D/2D step scheme α-Fe_2O_3/BiOBr/MoS_2 ternary integrated heterojunction with unparalleled visible-light-induced remarkable photocatalytic H_2 evolution. International Journal of Hydrogen Energy,2025 99, 112-122. https://doi.org/10.1016/j.ijhydene.2024.12.201.

[174] Xiaoya Ren, Kaihui Huang, Yixin Wei, Meng Cai, Mengjie Li, Rongchen Shen, Xin Li, Guosheng Shao, Fujun Miao. 2D/2D COF/MOF S-Scheme heterojunction boosts photocatalytic H_2 evolution. Journal of Materials Science &Amp; Technology,2025. https://doi.org/10.1016/j.jmst.2025.09.038.

[175] Jintao Jiang, Qisong Shi, Shurui Yin, Xueting Lv, Xiang Li, Qi Wang, Chuantao Wang, Jun Wan, Chunming Yang. Formation of hierarchical 2D/2D BP/$Mn_xCd_{1-x}S$ heterojunction boosting efficient photocatalytic hydrogen evolution. International Journal of Hydrogen Energy,2025 184, 151956. https://doi.org/10.1016/j.ijhydene.2025.151956.

[176] Liezhen Zhu, Jing Liu, Lin Liu, Youliang Shen, Lingfang Qiu, Xun Xu, Jiangbo Xi, Ping Li, Shuwang Duo. 3D $Zn_3In_2S_6$/TiO_2 S-scheme heterojunctions with strong 2D/2D hetero-interface interaction enable highly efficient photocatalytic H_2 production simultaneous with TC degradation. International Journal of Hydrogen Energy,2025 125, 254-265. https://doi.org/10.1016/j.ijhydene.2025.04.079.

[177] Xiaohui Li, Zhiqi Su, Shiting Wu, Lingxia Zheng, Huajun Zheng, Liang Mao, Xiaowei Shi. Synergistic Interactions of Bulk Polarization and Built-In Electric Field Inducing 2D/2D S-Scheme

Homojunction Toward Enhanced Photocatalytic Performance. Small,2024 20 (50), 2406485. https://doi.org/10.1002/smll.202406485.

[178] Hongzhao Deng, Xingang Fei, Yi Yang, Jiajie Fan, Jiaguo Yu, Bei Cheng, Liuyang Zhang. S-scheme heterojunction based on p-type $ZnMn_2O_4$ and n-type ZnO with improved photocatalytic CO_2 reduction activity. Chemical Engineering Journal,2021 409, 127377. https://doi.org/10.1016/j.cej.2020.127377.

[179] Aiyun Meng, Bei Cheng, Haiyan Tan, Jiajie Fan, Chenliang Su, Jiaguo Yu. TiO_2/polydopamine S-scheme heterojunction photocatalyst with enhanced CO_2-reduction selectivity. Applied Catalysis B: Environmental,2021 289, 120039. https://doi.org/10.1016/j.apcatb.2021.120039.

[180] Bo Yu, Yuxuan Wu, Fanming Meng, Qian Wang, Xueqiang Jia, Muhammadwasim Khan, Caimei Huang, Shuyi Zhang, Li Yang, Hao Wu. Formation of hierarchical Bi_2MoO_6/In_2S_3 S-scheme heterojunction with rich oxygen vacancies for boosting photocatalytic CO_2 reduction. Chemical Engineering Journal,2022 429, 132456. https://doi.org/10.1016/j.cej.2021.132456.

[181] Azmat Ali Khan, Muhammad Tahir. Constructing S-Scheme Heterojunction of CoAlLa-LDH/g-C_3N_4 through Monolayer Ti_3C_2 -MXene to Promote Photocatalytic CO_2 Re-forming of Methane to Solar Fuels. ACS Applied Energy Materials,2021 5 (1), 784-806. https://doi.org/10.1021/acsaem.1c03266.

[182] Cao Chen, Xindi Hu, Xiaoyang Yang, Xingyu Yang, Jiafu Qu, Chunxian Guo, Changming Li. Ambient-Stable Black Phosphorus-Based 2D/2D S-Scheme Heterojunction for Efficient Photocatalytic CO_2 Reduction to Syngas. ACS Applied Materials &Amp; Interfaces,2021 13 (17), 20162-20173. https://doi.org/10.1021/acsami.1c03482.

[183] Kai Wang, Xuezhen Feng, Yangzi Shangguan, Xiaoyong Wu, Hong Chen. Selective CO_2 photoreduction to CH_4 mediated by dimension-matched 2D/2D Bi_3NbO_7/g-C_3N_4 S-scheme heterojunction. Chinese Journal of Catalysis,2022 43 (2), 246-254. https://doi.org/10.1016/s1872-2067(21)63819-6.

[184] Zhenlong Zhao, Ji Bian, Lina Zhao, Hongjun Wu, Shuai Xu, Lei Sun, Zhijun Li, Ziqing Zhang, Liqiang Jing. Construction of 2D Zn-MOF/$BiVO_4$ S-scheme heterojunction for efficient photocatalytic CO_2 conversion under visible light irradiation. Chinese Journal of Catalysis,2022 43 (5), 1331-1340. https://doi.org/10.1016/s1872-2067(21)64005-6.

[185] Zhongliao Wang, Bei Cheng, Liuyang Zhang, Jiaguo Yu, Youji Li, S Wageh, Ahmeda Al-Ghamdi. S-Scheme 2D/2D Bi_2MoO_6/BiOI van der Waals heterojunction for CO_2 photoreduction. Chinese Journal of Catalysis,2022 43 (7), 1657-1666. https://doi.org/10.1016/s1872-

2067(21)64010-x.

[186] Minghui Zhang, Yuyin Mao, Xiaolei Bao, Guangyao Zhai, Difei Xiao, Dong Liu, Peng Wang, Hefeng Cheng, Yuanyuan Liu, Zhaoke Zheng, Ying Dai, Yuchen Fan, Zeyan Wang, Baibiao Huang. Coupling Benzylamine Oxidation with CO_2 Photoconversion to Ethanol over a Black Phosphorus and Bismuth Tungstate S-Scheme Heterojunction. Angewandte Chemie International Edition,2023 62 (36). https://doi.org/10.1002/anie.202302919.

[187] Shiping Li, Najmul Hasan, Fuchun Zhang, Jong-seong Bae, Chunli Liu. 2D $Bi_2MoO_6/Zn_3V_2O_8$ heterojunction photocatalyst for efficient photocatalytic reduction of CO_2 to CO and CH_4. Journal of Colloid and Interface Science,2023 652, 1533-1544. https://doi.org/10.1016/j.jcis.2023.08.189.

[188] Baoji Miao, Yange Cao, Imran Khan, Qiuling Chen, Salman Khan, Amir Zada, Muhammad Shahyan, Sharafat Ali, Rizwan Ullah, Jinbo Bai, Muhammad Rizwan, Abdullahms Alhuthali. Innovative dual-active sites in interfacially engineered interfaces for high-performance S-scheme solar-driven CO_2 photoreduction. Journal of Colloid and Interface Science,2024 661, 544-563. https://doi.org/10.1016/j.jcis.2024.01.168.

[189] Na Xu, Jiaming Li, Yujia Wang, Muhammad Yasir Akram, Bo Hu, Hongjun Dong. Adjustment of charge transfer behavior for layered photocatalysts through fabricating face-to-face 2D/2D S-scheme heterojunction toward efficient CO_2 reduction. Separation and Purification Technology,2025 354, 129528. https://doi.org/10.1016/j.seppur.2024.129518.

[190] Liting Wu, Dingyi Yang, Yalin Dong, Ze Wang, Yu Zhang, Tingting Wang, Liang Cheng, Yong Wang, Yizhang Wu. Enhanced CO_2 Reduction via S-Scheme Heterojunction of Amorphous/Crystalline Metal-free Carbon Nitride Photocatalysts. Chemical Engineering Journal,2024 500, 156777. https://doi.org/10.1016/j.cej.2024.156777.

[191] Yanan Chen, Wenzhuo Xiang, Zizhong Zhang, Tao Ji, Wenyue Su. Enhanced CO_2 conversion to CO using an S-scheme 2D/2D $WO_3/InVO_4$ photocatalysts. Chemical Engineering Journal,2025 508, 160993. https://doi.org/10.1016/j.cej.2025.160993.

[192] Zichen Wang, Baowei Cao, Rong Li, Baiquan Jing, Xiaolong Cai, Jinbo Cao, Dachuan He, Yunhua Xu. Constructing 2D/2D $BiOI/Bi_2O_2CO_3$ S-scheme heterojunction for boosted CO_2 photoreduction. Journal of Alloys and Compounds,2025 1037, 182207. https://doi.org/10.1016/j.jallcom.2025.182207.

[193] Su-xian Yuan, Ke Su, Meng-ran Zhang, Guang-xing Dong, You-xiang Feng, Min Zhang, Tong-bu Lu. Ultrathin 2D In-MOF nanosheet based 2D/2D heterojunction toward nearly exclusive CO_2-to-methanol photoreduction. Applied Catalysis B: Environment and Energy,2026, 126807.

https://doi.org/10.1016/j.apcatb.2026.126807.

[194] Yilin Cui, Zhongfu Li, Weikun Zhang, Yu Gao, Zhichao Dong, Conghua Liu. Sulfur vacancies boosting C_2H_4 selectivity of 2D/2D $In_{2.77}S_4/CuInS_2$ S-scheme heterojunction for CO_2 photoreduction. Acta Physico-Chimica Sinica,2026, 100274. https://doi.org/10.1016/j.actphy.2026.100274.

[195] Dong-eun Lee, Mv Jyothirmai, Naresh Mameda, Wan-kuen Jo, Surendar Tonda. Highly selective CO_2-to-CH_4 conversion via an interfacial charge transfer-optimized 2D/2D $Bi_2MoO_6/ZnIn_2S_4$ S-scheme heterophotocatalyst under visible light illumination. Journal of Environmental Chemical Engineering,2025 13 (5), 118452. https://doi.org/10.1016/j.jece.2025.118452.

[196] Qiaozhen Xu, Wenhao Liu, Tao Lv, Hong Liu. Plasmonic CuSe/CuTCPP S-scheme heterojunction for efficient CO_2 photoreduction under visible-near-infrared light. Journal of Catalysis,2025 448, 116188. https://doi.org/10.1016/j.jcat.2025.116188.

[197] Lei Li, Xinyan Dai, Kangjie Gao, Hangjing Yu, Fang Chen, Wentao Wang, Jiqiang Ning, Yong Hu. Customized interfacial electronic interactions in protonated g-C_3N_4/$ZnIn_2S_4$ S-scheme 2D/2D edge-to-face heterostructures for boosted CO_2 photoconversion. Chemical Engineering Journal,2025 514, 163193. https://doi.org/10.1016/j.cej.2025.163193.

[198] Paria Hemmati-Eslamlu, Aziz Habibi-Yangjeh. A review on impressive Z- and S-scheme photocatalysts composed of g-C_3N_4 for detoxification of antibiotics. FlatChem,2024 43, 100597. https://doi.org/10.1016/j.flatc.2023.100597.

[199] Wang Wang, Bei Cheng, Guoqiang Luo, Jiaguo Yu, Shaowen Cao. S-scheme heterojunction photocatalysts based on 2D materials. Materials Today,2024 81, 137-158. https://doi.org/10.1016/j.mattod.2024.10.006.

[200] Jiajia Liu, Yaodi Fu, Guoliang Chu, Ke Wen, Lingfang Qiu, Ping Li, Lihong Cheng, Banpeng Cao, Yi Tang, Xiangshu Chen, Hidetoshi Kita, Shuwang Duo. S-scheme 2D/2D B-doped N-deficient g-C_3N_4/$ZnIn_2S_4$ heterojunction for efficient H_2 production intergrated with tertracycline degradation under visible-light illumination. Process Safety and Environmental Protection,2024 191, 883-896. https://doi.org/10.1016/j.psep.2024.09.040.

[201] Meng-zhu Qin, Wen-xin Fu, Hai Guo, Cheng-gang Niu, Da-wei Huang, Chao Liang, Ya-ya Yang, Hui-yun Liu, Ning Tang, Qian-qian Fan. 2D/2D Heterojunction systems for the removal of organic pollutants: A review. Advances in Colloid and Interface Science,2021 297, 102540. https://doi.org/10.1016/j.cis.2021.102540.

[202] Yangyang Huang, Miaomiao Yang, Limeili Tian, Chihao Cao, Jian Zhao, Qingqiang Meng, Jing Wang, Aiping Wu. A novel $Bi_2MoO_6/BiOCl_{0.7}I_{0.3}$ 2D/2D S-scheme photocatalyst with triple-

driven charge separation for enhanced tetracycline hydrochloride degradation. Journal of Environmental Chemical Engineering,2025 13 (5), 118429. https://doi.org/10.1016/j.jece.2025.118429.

[203] Tao Pan, Dongdong Chen, Weicheng Xu, Jianzhang Fang, Shuxing Wu, Zhang Liu, Kun Wu, Zhanqiang Fang. Anionic polyacrylamide-assisted construction of thin 2D-2D WO_3/g-C_3N_4 Step-scheme heterojunction for enhanced tetracycline degradation under visible light irradiation. Journal of Hazardous Materials,2020 393, 122366. https://doi.org/10.1016/j.jhazmat.2020.122366.

[204] Wenliang Wang, Wenli Zhao, Haochun Zhang, Xincheng Dou, Haifeng Shi. 2D/2D step-scheme α-Fe_2O_3/Bi_2WO_6 photocatalyst with efficient charge transfer for enhanced photo-Fenton catalytic activity. Chinese Journal of Catalysis,2021 42 (1), 97-106. https://doi.org/10.1016/s1872-2067(20)63602-6.

[205] Caijian Zhang, Meiying Jia, Zhengyong Xu, Weiping Xiong, Zhaohui Yang, Jiao Cao, Haihao Peng, Haiyin Xu, Yinping Xiang, Ying Jing. Constructing 2D/2D N-ZnO/g-C_3N_4 S-scheme heterojunction: Efficient photocatalytic performance for norfloxacin degradation. Chemical Engineering Journal,2022 430, 132652. https://doi.org/10.1016/j.cej.2021.132652.

[206] Xiaoyan Lian, Suhang Chen, Fangyuan He, Shuai Dong, Bizhou Lin, Hui Li, Kangzhen Xu. Photocatalytic degradation of ammonium dinitramide over novel S-scheme g-C_3N_4/BiOBr heterostructure nanosheets. Separation and Purification Technology,2022 286, 120449. https://doi.org/10.1016/j.seppur.2021.120449.

[207] Karunamoorthy Saravanakumar, Velusamy Maheskumar, Yeonji Yea, Yeomin Yoon, Velluchamy Muthuraj, Changmin Park. 2D/2D nitrogen-rich graphitic carbon nitride coupled Bi_2WO_6 S-scheme heterojunction for boosting photodegradation of tetracycline: Influencing factors, intermediates, and insights into the mechanism. Composites Part B: Engineering,2022 234, 109726. https://doi.org/10.1016/j.compositesb.2022.109726.

[208] Sethumathavan Vadivel, Manabu Fujii, Saravanan Rajendran. Novel S-scheme 2D/2D $Bi_4O_5Br_2$ nanoplatelets/g-C_3N_5 heterojunctions with enhanced photocatalytic activity towards organic pollutants removal. Environmental Research,2022 213, 113736. https://doi.org/10.1016/j.envres.2022.113736.

[209] Qi Zhou, Luhong Zhang, Longfei Zhang, Bin Jiang, Yongli Sun. In-situ constructed 2D/2D $ZnIn2S_4$/$Bi_4Ti_3O_{12}$ S-scheme heterojunction for degradation of tetracycline: Performance and mechanism insights. Journal of Hazardous Materials,2022 438, 129438. https://doi.org/10.1016/j.jhazmat.2022.129438.

[210] Sivakumar Vigneshwaran, Do-gun Kim, Seok-oh Ko. Tuning of interfacial HGO@CLS nanohybrid S-scheme heterojunction with improved carrier separation and photocatalytic activity towards RhB degradation. Chemosphere,2023 340, 139914. https://doi.org/10.1016/j.chemosphere.2023.139914.

[211] Jiaxin Zhou, Huiling Tang, Chunxia Yao, Weiguo Song, Chengbin Liu, Wei Song, Zhijie Zhang. 2D/2D Ni-MOF/BiOCl S-scheme heterojunction with boosted charge transfer and photocatalytic degradation of tetracycline. Sustainable Materials and Technologies,2024 39, e00825. https://doi.org/10.1016/j.susmat.2024.e00825.

[212] Yang Wang, Dong Xu, Xuan Yang, Jing-hui He. Novel 2D/2D S-scheme heterojunction photocatalyst for peroxymonosulfate activation enables ciprofloxacin ultrafast degradation: High-efficiency photogenerated carrier transport. Chemical Engineering Journal,2024 488, 150844. https://doi.org/10.1016/j.cej.2024.150844.

[213] Shengyu Jing, Jing Ren, Anhu Wang, Ruolin Cheng, Huagen Liang, Hai Liu, Fu Chen, Panagiotis Tsiakaras. An efficient photo-Fenton In_2O_3@$FeIn_2S_4$ composite catalyst for tetracycline degradation. Chemical Engineering Journal,2024 491, 151549. https://doi.org/10.1016/j.cej.2024.151549.

[214] Zhiang Hou, Jinzhu Yue, Hao Chen, Jinnan Wang, Aimin Li, Philippe François-xavier Corvini. Bi atom sharing Co$Bi_2O_2C_3$/BiO$_3$ S-scheme induced singlet oxygen-dominated photocatalytic oxidation system. Chemical Engineering Journal,2024 502, 157963. https://doi.org/10.1016/j.cej.2024.157963.

[215] Baofei Hao, Younes Ahmadi, Tianhao Zhang, Changqi Chen, Zhansheng Lu, Huizhong Ma, Ki-hyun Kim. Ultrathin K-doped g-C_3N_4/BiOBr heterojunctions with S-scheme charge transfer for efficient photodegradation of tetracycline. Journal of Environmental Management,2025 391, 126677. https://doi.org/10.1016/j.jenvman.2025.126677.

[216] Wanxin Hu, Yan Shi, Junxia Yu, Haiyang Shi, Yingping Huang, Ruiping Li. Engineering 2D/2D FeOOH/BiOCl S-scheme heterojunction toward efficient and stable tetracycline photodegradation. Chinese Journal of Structural Chemistry,2025, 100832. https://doi.org/10.1016/j.cjsc.2025.100832.

[217] Linhong Xia, Kaisheng Zhang, Xudong Wang, Qi Guo, Yuning Wu, Yujie Du, Lixue Zhang, Jianfei Xia, Hua Tang, Xia Zhang, Yanhua Peng, Zhuo Li, Xiaolong Yang. 0D/2D Schottky junction synergies with 2D/2D S-scheme heterojunction strategy to achieve uniform separation of carriers in 0D/2D/2D quasi CNQDs/TCN/$ZnIn_2S_4$ towards photocatalytic remediating petroleum hydrocarbons polluted marine. Applied Catalysis B: Environmental,2023 325, 122387.

https://doi.org/10.1016/j.apcatb.2023.122387.

[218] Linxi Wang, Jian Sun, Bei Cheng, Rongan He, Jiaguo Yu. S-Scheme Heterojunction Photocatalysts for H_2O_2 Production. The Journal of Physical Chemistry Letters,2023 14 (20), 4803-4814. https://doi.org/10.1021/acs.jpclett.3c00811.

[219] Keyu Zhang, Yunfeng Li, Shidan Yuan, Luohong Zhang, Qian Wang. Review of S-Scheme Heterojunction Photocatalyst for H_2O_2 Production. Acta Phys. -Chim,2023, 2212010. https://doi.org/10.3866/PKU.WHXB202212010.

[220] Azin Khamesan, Mohammadmehdi Esfahani, Jahanb Ghasemi, Faezeh Farzin, Anita Parsaei-Khomami, Mitra Mousavi. Graphitic-C_3N_4/ZnCr-layered double hydroxide 2D/2D nanosheet heterojunction: Mesoporous photocatalyst for advanced oxidation of azo dyes with in situ produced H_2O_2. Advanced Powder Technology,2022 33 (11), 103777. https://doi.org/10.1016/j.apt.2022.103777.

[221] Lang Shi, Ziyang Chang, Yuhong Wu, Xin Tang, Pen Jiang, Yan Hua, Qianqian Shi, Jin-qi Xie. Photocatalytic production of hydrogen peroxide facilitated by Homogeneously Distributed 2D/2D S-scheme SCN/VS-SnS_2 heterojunction. Chemical Engineering Journal,2025 507, 160563. https://doi.org/10.1016/j.cej.2025.160563.